University of Alberta

Towards Molecular Quantum Computing: Laser Pulse Shaping of Quantum Logic Gates on Diatomic Molecules

by

Ryan Ryad Zaari

A thesis submitted to the Faculty of Graduate Studies and Research in partial fulfillment of the requirements for the degree of

Doctor of Philosophy

Department of Chemistry

Fall 2012
Edmonton, Alberta

dedicated to my parents who have provided infinite encouragement and continued support throughout my life

Abstract

The intent of this study is to determine the feasibility of diatomics as molecular quantum computing candidates and shed insight into the use of such experimental laser pulse shaping methods to represent quantum logic gates. Four appropriate rovibrational states of model diatomic molecules are encoded as the qubit states. A set of 2-qubit quantum logic gates (ACNOT, CNOT, NOT, Hadamard) are represented by amplitude and phase shaped laser pulses. The combinations of amplitudes and phases that produce the *optimal* laser pulse representation, for each quantum logic gate, are determined by a Genetic Algorithm optimization routine. The theoretical laser pulse shaping is analogous to current experimental frequency-domain pulse shaping apparatus with amplitude and phase control at individual frequencies.

A model set of diatomics is sampled in order to determine a relationship between optimal laser pulse shaping and the choice of diatomic molecule. We show that the choice of diatomic molecule greatly influences the ability to produce optimal laser pulse shapes to represent quantum logic gates. Tuneable parameters specific to laser pulse shaping instruments are varied to determine their effect on optimal pulse production. They include varying the number of amplitude and phase components, adjusting the number of frequency components, and altering the frequency resolution which is synonymous with altering the laser pulse duration. A time domain analytic form of the original frequency

domain laser pulse function is derived, providing a useful means to infer the laser pulse dependencies on these parameters. Initially, we show that the appropriate choice of rovibrational state qubits of carbon monoxide ($^{12}C^{16}O$) and the use of simple shaped binary pulses, 2 amplitude and 2 phase components, can provide significant control for specific quantum gates. Further amplitude variation at each frequency component is shown to be a crucial requirement for optimal laser pulse shaping, whereas phase variation provides minimal contribution. We show that the generation of optimal laser pulse shapes is highly dependent upon the frequency resolution and increasing the number of frequency components provides incremental improvements to optimal laser pulses.

Acknowledgements

I would like to express my gratitude to my supervisor, Dr. Alex Brown, who has provided me with an unimaginable experience as an undergraduate and graduate student. Much of the knowledge, success and growth I have obtained in this short time are reflections of his conscious drive to provide the best for his students. He is someone I truly respect and admire. Alex, I wish you all the best!

I graciously thank all of my friends, every single one, for your ability to distract me from the stresses of graduate school, provide an outlet to ground myself and continue to push me forward. I also thank those individuals within academia that i have encountered whom have provided me with useful knowledge both towards my Ph.D. and aiding towards my goals in life. Special thanks to *M.C-S* for her understanding in my academic endeavours and empathy in times of worry.

A huge hug goes out to my parents. I thank them for accepting my passions and entrusting in my long academic journey. From all their years of laborious struggles they have given me the opportunity to do what I love and be able to strive for my dreams. I love them both for that.

Lastly, to my brother. I envy all those amazing qualities you have that I lack and I know you will continue to give me inspiration.

Table of Contents

List of Tables

List of Figures

List of Abbreviations

ACNOT	*Alternative Controlled-NOT quantum logic gate*
CNOT	*Controlled-NOT quantum logic gate*
FWHM	*Full Width at Half Maximum*
GA	*Genetic Algorithm*
Had	*Hadamard quantum logic gate*
IR	*Infrared*
LC-SLM	*Liquid Crystal Spatial Light Modulator*
NMR	*Nuclear Magnetic Resonance*
OCT	*Optimal Control Theory*
Qubit	*Quantum Bit*
TDSE	*Time Dependent Schrödinger Equation*
TL	*Transform Limited*

Chapter 1

Introduction

1.1 Context

The use of laser fields to control quantum dynamics has been a topic of much theoretical and experimental interest over the last 25 years, see the reviews [1–7] and references therein. Current pulse shaping hardware can control the phase, amplitude and polarization of individual frequency components of a laser pulse over time durations on the femtosecond timescale [8–10]. Along with the complexity of pulse shape variability came optimization strategies to determine optimal pulse designs. The development of *closed-loop feed-back* optimization[11] allowed for laser pulses to be shaped and control to be achieved without a priori knowledge of the molecular system [12–15]. In experimental methods for control, a Genetic Algorithm (GA) is typically used in a closed loop feed-back setup to perform the laser pulse shaping. A metric that describes the ability of the current laser pulse to carry out the required operation or experiment, termed the *fidelity*, is fed back to the GA. In turn, adjustments are then made to the applied laser pulse parameters to improve the desired experimental outcome. This cycle continues over a desired number of repetitions, hence the laser pulse is shaped via a closed loop feedback. This type of experimental setup was first suggested by Judson and Rabitz[11] in 1992. The majority of theoretical pulse shaping optimizations are posed in the form of Optimal Control Theory (OCT)[16–18] or Genetic Algorithm (GA)[11]

optimization. OCT is a monotonically convergent iterative technique, whereas the GA is a heuristic search space optimization algorithm based upon biological rules of natural selection and survival of the fittest. Due to these relatively recent advances in pulse shaping methods and technologies, the number and variety of examples of quantum control has increased with these techniques now being applied to molecular quantum computing.

It was Richard Feynman who in 1982 initially proposed the idea of a quantum simulator[19] and a few years later in 1985 David Deutsch extended this idea to a universal quantum computer[20]. The former quantum simulator describes a quantum computer that is built to solve a specific problem whereas the latter universal quantum computer refers to the quantum analogue of our current conventional classical computers. It was initially misunderstood that a quantum computer would always outperform a classical computer. It has been determined that a quantum computer would perform significantly better than a classical computer on a select number of problems[21], the most common being Shor's algorithm[22] for prime number factorization as used in cryptography. Examples of some relevant scientific applications which provide motivation for the development of a quantum computer include solutions to systems of linear equations[23], quantum Fourier transforms[22], eigenvalue/eigenvector problems[24] and within chemistry, simulating chemical dynamics[25] and, the determination of molecular properties and geometry optimizations[26].

The two main techniques within chemistry that have been already successful at carrying out simple benchmark quantum computations are Nuclear Magnetic Resonance (NMR)[27–29]and ion traps[30, 31]. In 2002, Tesch and de Vivie-Riedle proposed an alternative approach by using a molecule's vibrational modes for quantum computation[32] and demonstrated the utility on a model of acetylene using OCT to find optimal laser pulses required to implement the quantum gates studied. Concurrently, the work of Apkarian and co-workers appeared[33, 34] suggesting the manipulation of ro-vibronic states for quantum computing applications using time-frequency-resolved coherent

anti-Stokes Raman scattering or four-wave mixing. Around the same time an experimental implementation by Vala et al. [35] showed that the Deutsch-Jozsa quantum algorithm could be realized on the rovibrational states of Li_2. Within theoretical molecular quantum computing using OCT, various studies on polyatomics emerged incorporating: (i) quantum gates [32, 36–41], (ii) quantum algorithms [42, 43] and experimental limitations of OCT concerned with (iii) frequency constraints[44–46] and (iv) mask functions[41]. The common difficulty in using polyatomic systems in order to carry out specific quantum computing operations resides in the difficulty in controlling the excitation to reside within a single mode while coupling of vibrational modes within the molecule exists. Another possibility is to use a diatomic molecule. A diatomic molecule satisfies the five criteria proposed by DiVincenzo and Loss [47] that are necessary for a system to be considered viable for quantum computation (see Section 1.2.7). A theoretical implementation for laser pulse shaping towards quantum computation on diatomic molecules using the GA was initially investigated for carbon monoxide ($^{12}C^{16}O$) by Tsubouchi and Momose[48].

1.2 Overview

For more general details, we refer the reader to an introduction to quantum computation[49] and also a recent review of the use of quantum computation to solve chemistry problems[50]. In this overview we provide a brief summary of the method and structure of theoretical GA optimized closed loop feedback with application towards quantum computation, as applied in this thesis. The details of each individual topic are covered more specifically within Chapters 2-4. Fig. 1.1 conceptualizes the general framework of a closed-loop feedback setup using a GA. Initially a random set of laser pulses, experimental or theoretical (see Section 1.2.4), are input into the quantum dynamics procedure (Fig. 1.1; lower box) in order to start the algorithm. The upper box is the GA routine (see Section 1.2.6), constituting the laser pulse optimization. In

the theoretical case, the quantum dynamics is determined by solving the time-dependent Schrödinger equation (TDSE) for the applied laser pulse, from an initial state Ψ_i, over the laser pulse duration, to a final state Ψ_f (see Section 1.2.5). A value for the Fidelity (see Section 1.2.3), between 0 and 1, is computed which describes the effectiveness of the specific laser pulse at carrying out the required quantum gate operation (see Section 1.2.2) over the chosen rovibrational state qubits (see Section 1.2.1). This is repeated for all laser pulses of that generation. The Fidelity is fed back into the GA so that it can rank the laser pulses and determine the appropriate optimization through tournament selection and uniform cross-over (see Section 1.2.6). A new set of laser pulses are produced which constitute the next generation. This process is continued for n generations. Both the GA and quantum dynamics are connected in a closed loop, providing feedback to each other in order to produce an optimal pulse for the quantum gate operation of interest.

1.2.1 Quantum Bits (Qubits)

The quantum bits or *qubits* are the chosen molecular states in which the quantum logic gate (Section 1.2.2) operations occur. They are analogous to the *bits*, 0 or 1, of a classical computer. Unlike a classical bit that exists in a definite state of 0 or 1, a qubit with its foundations in quantum mechanics can be in a superposition state. The most important superposition state with respects to quantum computing is entanglement[51]. In the cases studied herein the rovibrational states of a diatomic molecule, (ν J), are used to represent the 2-qubit state, $|q_1 q_2\rangle$. We are interested in 2-qubit operations and thus we have 4 qubit variations: $|00\rangle$,$|01\rangle$, $|10\rangle$ and $|11\rangle$. The choice of rovibrational states to represent the qubits is arbitrary. We choose a set of low energy rovibrational states, shown in Figure 1.2, that are connected via 1-photon excitations: $|00\rangle \equiv (1,2)$, $|01\rangle \equiv (0,1)$, $|10\rangle \equiv (2,1)$, $|11\rangle \equiv (1,0)$. It is this set of qubits that undergoes transformations according to the required quantum gate operation.

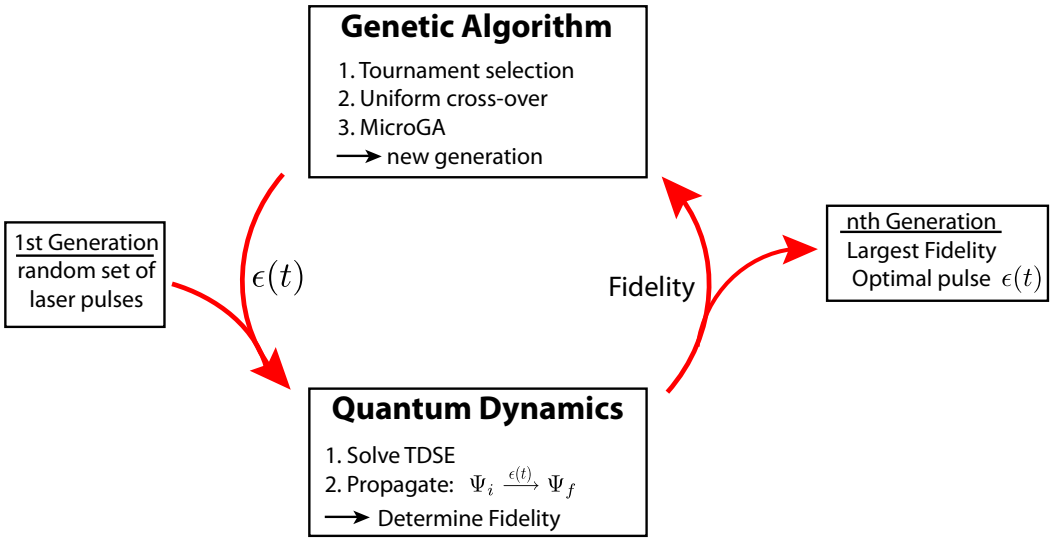

Figure 1.1: Illustration of theoretical shaped laser pulse optimization using a genetic algorithm (GA). The first generation of laser pulses is randomly generated. The time-dependent Schrödinger equation (TDSE) for the model diatomic is solved for each input laser pulse. The system is propagated from an initial state Ψ_i to a final state Ψ_f, at which point the fidelity is calculated based upon how close the laser pulse brings the system to the desired final state. The fidelity associated with each laser pulse is used to determine the GA optimization through tournament selection and uniform cross-over. The GA produces a new generation of laser pulses related to the previous ones. The cycle is repeated for n generations; the optimal laser pulse being produced in the nth generation.

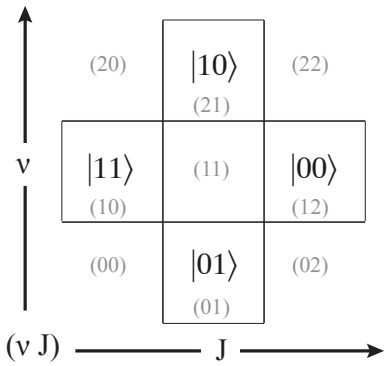

Figure 1.2: The set of diatomic rovibrational states (ν J) chosen to represent the qubits $|q_1 q_2\rangle$. Increasing vibrational states occur along the vertical and increasing rotational states along the horizontal.

1.2.2 Quantum Logic Gates

There are two types of implementations for quantum computation. The quantum algorithms constituting the computation could be determined and implemented directly, termed *problem-specific* quantum computing. This is synonymous to a quantum simulator [52] and has been experimentally applied to determine the eigenvalues of molecular hydrogen [53]. The approach of interest in this study is general and can in theory reproduce any quantum algorithm, and thus is termed *universal* quantum computing[35]. A universal quantum computer is comprised of a set of universal quantum logic gates, analogous to logic gates in classical computation (e.g., NOT, AND, OR). An example set of universal quantum logic gates is the Hadamard, CNOT and phase gate. The application of a series of quantum logic gates comprises a quantum algorithm. Quantum logic gates are reversible Unitary Hermitian matrix operators. The 2-qubit Hadamard, CNOT, ACNOT and NOT quantum logic gates are examined in this thesis and their operations are shown in Table 1.1. In order for a quantum logic gate operation to be applied to the molecular rovibrational state qubits, it is encoded into the laser pulse. Each quantum logic gate is represented by a specifically shaped laser pulse. Subsequent application of the laser pulse to the diatomic molecule implements the quantum gate operation on the qubits and carries out the transformation independent of the initial qubit state. An example is the ability for the ACNOT_1 laser pulse to cause no transformation if the qubit is initially $|10\rangle$ or $|11\rangle$, and to cause an excitation between $|00\rangle$ or $|01\rangle$ if initially in either of these states. Thus one laser pulse must be constructed in order to produce, at maximum, 4 independent transitions between the qubit states.

The goal of producing quantum gates is to apply them in a specific order to implement a quantum algorithm. Besides causing the required qubit excitations, there is an extra requirement imposed on the laser pulse quantum gate operation. That is, the quantum gate operation must also align the relative

phases of all the qubits together, by the end of the laser pulse interaction. This is termed *global phase alignment*[43, 54]. Thus subsequent application of quantum gates will impose the appropriate qubit transformation, since the qubits will all be in phase.

NOT_1 :	$\|00\rangle \leftrightarrow \|10\rangle$ $\|01\rangle \leftrightarrow \|11\rangle$	NOT_2 :	$\|00\rangle \leftrightarrow \|01\rangle$ $\|10\rangle \leftrightarrow \|11\rangle$
Had_1 :	$\|00\rangle \leftrightarrow \frac{1}{\sqrt{2}}(\|00\rangle + \|10\rangle)$ $\|01\rangle \leftrightarrow \frac{1}{\sqrt{2}}(\|01\rangle + \|11\rangle)$ $\|10\rangle \leftrightarrow \frac{1}{\sqrt{2}}(\|00\rangle - \|10\rangle)$ $\|11\rangle \leftrightarrow \frac{1}{\sqrt{2}}(\|01\rangle - \|11\rangle)$	Had_2 :	$\|00\rangle \leftrightarrow \frac{1}{\sqrt{2}}(\|00\rangle + \|01\rangle)$ $\|01\rangle \leftrightarrow \frac{1}{\sqrt{2}}(\|00\rangle - \|01\rangle)$ $\|10\rangle \leftrightarrow \frac{1}{\sqrt{2}}(\|10\rangle + \|11\rangle)$ $\|11\rangle \leftrightarrow \frac{1}{\sqrt{2}}(\|10\rangle - \|11\rangle)$
CNOT_1 :	$\|00\rangle \rightarrow \|00\rangle$ $\|01\rangle \rightarrow \|01\rangle$ $\|10\rangle \leftrightarrow \|11\rangle$	CNOT_2 :	$\|00\rangle \rightarrow \|00\rangle$ $\|10\rangle \rightarrow \|10\rangle$ $\|01\rangle \leftrightarrow \|11\rangle$
ACNOT_1 :	$\|10\rangle \rightarrow \|10\rangle$ $\|11\rangle \rightarrow \|11\rangle$ $\|00\rangle \leftrightarrow \|01\rangle$	ACNOT_2 :	$\|01\rangle \rightarrow \|01\rangle$ $\|11\rangle \rightarrow \|11\rangle$ $\|00\rangle \leftrightarrow \|10\rangle$

Table 1.1: The quantum gate operations studied, with the aim at representing each operation by a shaped laser pulse. NOT/ Hadamard: The number following the gate name refers to which qubit the gate operates on. CNOT/ACNOT: The number following the gate name refers to which qubit is the control qubit.

1.2.3 Fidelity and Average Population

The degree to which the shaped laser pulse represents the quantum logic gate operation of interest is stated by a metric. Initial theoretical studies which had not yet perceived the necessity of global phase alignment, used the average population $\bar{P}$, as this metric,

$$\bar{P} = \frac{1}{N} \sum_{k=1}^{N} |\langle \Psi_k(T) | \Phi_k \rangle|^2 , \tag{1.1}$$

where $\Psi_k(T)$ is the resulting wavefunction after the laser pulse of duration T has been applied and Φ_k is the target wavefunction. The wavefunctions are summed over the number of qubit transformations N, which in the case of 2-qubit operations as shown in Table 1.1 is $N = 4$. There is clearly no phase information contained in the average population function. Population transfer, along with global phase alignment, can be included in the required constraints for shaped laser pulses within the GA by using instead the fidelity function, F,

$$F = \frac{1}{N^2} \left| \sum_{k=1}^{N} \langle \Psi_k(T) | \Phi_k \rangle \right|^2 . \tag{1.2}$$

For an alternative expression of the fidelity showing average population and global phase alignment explicitly, see Equation 5.1. The fidelity is a number between 0 and 1. F=0 implies no excitation to the resultant qubit state(i.e., an incomplete quantum gate operation), while F=1 implies a 100% complete quantum gate operation on the qubits. Though the average population is a useful value to determine the extent of overall population transfer between the qubits, it is strictly the fidelity function that is used within the GA optimization procedure.

1.2.4 Laser field

In general, a laser field (electromagnetic radiation) is modelled classically as a combination of perpendicular oscillating electric and magnetic fields. The electric field interaction with the electric dipole moment is "five orders-of-magnitude"[56] or 10^5 times larger than the magnetic field interaction of the magnetic dipole. The magnetic field and subsequent magnetic dipole interaction of the diatomic molecule is minute. Therefore, its effects are omitted and only the electric field/electric dipole moment interaction is considered.

As stated by Milonni [57],"An arbitrarily large number n of 'photons' may occupy the same state, and when this situation obtains, it is accurate to regard the photon wave function as defining a classical field distribution." Thus

the quantum electrodynamic view of radiation for intense laser fields can be described classically. Overall, the light-matter interaction is treated semi-classically where the diatomic molecule is quantum mechanical and the laser pulse is classical in nature. The electric dipole approximation[58] is also used which reduces the form of the electric field due to the comparative size of the electric field wavelength compared to the molecule. The classical description of the laser field, $E(r,t)$, can be written in complex form according to,

$$E(r,t) = \epsilon_0 \cos(\omega t - \vec{k}\cdot\vec{r}) = \epsilon_0 \Re\left[e^{i\omega t} e^{-i\vec{k}\cdot\vec{r}}\right]. \tag{1.3}$$

It is a continuous laser field of single-frequency (ω) with peak field strength (ϵ_0) being a function of space and time. The norm of the wave vector ($\vec{k}$) is related to the frequency of the laser field by $k = \frac{\omega}{c}$, and thus is on the order of $10^{-6}\mathring{A}^{-1}$ for the mid-infrared frequencies used in this study. The value of k describes the number of oscillations of the electric field in space. In this case one oscillation occurs approximately every $10^6\mathring{A}$, which is much larger than the space occupied by the diatomic molecule. Consequently the resulting value of $\vec{k}\cdot\vec{r}$ is small and the Taylor series expansion for the electric field of the laser can be truncated to the first term, (i.e. unity):

$$e^{-ik\vec{n}\cdot\vec{r}} = 1 - \left[i\vec{k}\cdot\vec{r}\right] + \frac{1}{2}\left[-i\vec{k}\cdot\vec{r}\right]^2 + \cdots \approx 1. \tag{1.4}$$

The electric field can now be written strictly in terms of time,

$$E(r,t) = \epsilon_0 \Re\left[e^{i\omega t}\right] = \epsilon_0 \cos(2\pi\nu t). \tag{1.5}$$

For the optimized laser pulses studied herein, only the amplitude and phase were shaped (no polarization). This shaping occurs in the frequency domain which can be readily connected to the more familiar time-domain expression for the laser field. The form of the laser pulse for the described discretized frequency spectrum with amplitude and phase variation is[48]:

$$\epsilon(\nu_j) = \epsilon_0 \sqrt{A(\nu_j)} \exp\left[-2\ln 2\left(\frac{\nu_j - \nu_0}{\Delta\nu}\right)^2\right] \exp\left[i\phi(\nu_j)\right], \tag{1.6}$$

where ϵ_0 is the peak field strength, ν_0 is the central frequency and ν_j represents the discrete frequencies at which the field is shaped. A full width at half-maximum (FWHM) pulse width of $\Delta\nu$=100 cm^{-1}[48] with an overall Gaussian shaped envelope is used. The amplitude and phase range from $0 \leq A(\nu_j) \leq 1$ and $0 \leq \phi(\nu_j) \leq 2\pi$, respectively. A binary laser pulse is the specific restriction of $A(\nu_j)$=0 or 1, and $\phi(\nu_j)$=0 or π. A transformed-limited (TL) pulse is the case when $A(\nu_j)$=1 and $\phi(\nu_j)$=0. The familiar time-dependent form of the laser pulse can be determined by a Fourier transform or alternatively using the analytic form for the time-dependent field (see Appendix 4.5):

$$\epsilon(t) = \frac{\sin(\pi t d\nu)}{\pi t} \sum_{j=0}^{n} \epsilon_0 \sqrt{A_j} \exp\left[-2\ln 2 \left(\frac{\nu_j - \nu_0}{\Delta\nu}\right)^2\right] \cos(2\pi\nu_j t + \phi_j), \quad (1.7)$$

with frequency resolution $d\nu$. The frequency domain laser pulse shaping used in these studies is closely related to experimental Spatial Light Modulators using Liquid Crystal pixelated grids (LC-SLM). This requires diffraction of the incident laser pulse onto the LC-SLM, in which each pixel will be illuminated by a specific frequency band. At each pixel there is simultaneous control over the amount of light transmitted (amplitude) and the phase of that light passing through. Once each frequency band passes through and is affected by the LC-SLM, the light is recombined to form a new pulse shape depending on the alterations imposed by the shaper. Thus, there are numerous pulse shapes that can be generated by varying for instance: the number of frequency bands (ν_j), the resolution of the frequency bands illuminating each pixel ($d\nu$), and the variation in amplitude and phase. The task of the GA is to determine the optimal laser pulse within the vast pool of total pulse shape combinations.

In order to maintain a constant laser pulse energy during the conversion between the frequency domain and time domain (numerically or analytically), Parseval's equation is employed:

$$\int |\epsilon(\nu)|^2 \, d\nu = \beta^2 \int |\epsilon(t)|^2 \, dt. \quad (1.8)$$

The factor β ensures the appropriate laser pulse intensities within the time-

domain. The total laser pulse energy (E) and peak intensity (I; $\frac{TW}{cm^2}$) are related to the laser pulse by the following equations:

$$\frac{E}{A} \propto c\varepsilon_0 \int |\epsilon(\nu)|^2 \, d\nu, \tag{1.9}$$

$$I(t) \propto \frac{c\varepsilon_0 |\epsilon(t)|^2}{2}. \tag{1.10}$$

where c is the speed of light, ε_0 is the permittivity of free space, and A=50 μm is the area illuminated by the laser field [48]. The total laser pulse energy (E) is variable and in this study is between 5 $\mu J \leq E \leq 100 \mu J$, which reflects upper values of laser pulse energies experimentally available.

1.2.5 Quantum Dynamics

The diatomic-laser pulse interaction is determined by solving the time-dependent Schrödinger equation (TDSE),

$$i\hbar \frac{d\Psi(t)}{dt} = \hat{H}\Psi(t). \tag{1.11}$$

The semi-classical Hamiltonian, $\hat{H}$, composed of a time-independent operator $\hat{H}_0$, describing the natural evolution of the diatomic, combined with the time-dependent term describing the interaction of the electric field, $\epsilon(t)$, with the molecular dipole moment, $\mu(r)$, is given by,

$$\hat{H} = \hat{H}_0 - \vec{\mu}(r) \cdot \vec{\epsilon}(t) = \mu(r)\epsilon(t)\cos\theta. \tag{1.12}$$

The wavefunction, $\Psi(t)$, composed of a linear combination of time-dependent coefficients, $c_{\nu J}(t)$, with rovibrational state eigenvectors $|\nu J\rangle$ is described by,

$$\Psi(t) = \sum_{\nu J} c_{\nu J}(t)|\nu J\rangle. \tag{1.13}$$

The magnetic quantum number M is equal to zero for the closed shell diatomic molecules and linear electric field polarizations considered in our studies.

Solving the TDSE for the time-dependent coefficients in vector notation, $\underline{c}(t)$, results in,

$$\dot{\underline{c}}(t) = -\frac{i}{\hbar}\left[\underline{\underline{E}} - \epsilon(t)\underline{\underline{\mu}}\right]\underline{c}(t). \tag{1.14}$$

Each time step along the laser pulse duration is solved using Runge-Kutta fourth order integration. The time steps are chosen to be much smaller than the oscillatory period of the laser pulse such that the resulting integration error is also small. The diagonal rovibrational state energy matrix, $\underline{\underline{E}}$, is

$$\underline{\underline{E}} = \begin{pmatrix} E_{0,0} & 0 & \cdots & 0 \\ 0 & E_{0,1} & \cdots & 0 \\ \vdots & \vdots & \ddots & \vdots \\ 0 & 0 & \cdots & E_{6,8} \end{pmatrix} \tag{1.15}$$

The energies are determined from linear fits of diatomic molecular constants as calculated by Mantz et al. [59]; see details for specific problems discussed in Chapters 2-4. The rovibrational states used within the calculations constitute a reduced set of the total states available. Vibrational states vary from $0 \leq \nu \leq 6$ and rotational states vary from $0 \leq J \leq 8$, where the highest energy rovibrational state is (ν=6,J=8) denoted by $E_{6,8}$. The energies available within the laser pulses provide very little excitation to states with ν=6 or J=8, and thus there is insignificant population losses due to the rovibrational state truncation. The transition dipole moment matrix, $\underline{\underline{\mu}}$

$$\underline{\underline{\mu}} = \mu_{\nu,J}^{\nu',J'} = \begin{pmatrix} 0 & \mu_{0,J}^{1,J'} & 0 & & 0 & 0 & 0 \\ \mu_{1,J}^{0,J'} & 0 & \mu_{1,J}^{2,J'} & \cdots & & 0 & 0 \\ 0 & \mu_{2,J}^{1,J'} & 0 & & & & 0 \\ & \vdots & & \ddots & & \vdots & \\ 0 & & & & & \mu_{4,J}^{5,J'} & 0 \\ 0 & 0 & & \cdots & \mu_{5,J}^{4,J'} & 0 & \mu_{5,J}^{6,J'} \\ 0 & 0 & 0 & & 0 & \mu_{6,J}^{5,J'} & 0 \end{pmatrix} \tag{1.16}$$

is tridiagonal with zeroes along the diagonal and structured so that excitations occur via simultaneous $\Delta\nu = \pm 1$ and $\Delta J = \pm 1$ transitions. The notation for $\underline{\underline{\mu}}$ is given by initial states (ν,J) as a subscript and the final state excitation, (ν',J'), as a superscript. Equation 1.16 shows the structure for vibrational transitions and Equation 1.17 shows the rotational transition substructure of

the sample cell at $\mu_{0,J}^{1,J'}$.

$$\mu_{0,J}^{1,J'} = \begin{pmatrix} 0 & \mu_{0,0}^{1,1} & 0 & & 0 & 0 & 0 \\ \mu_{1,1}^{0,0} & 0 & \mu_{0,1}^{1,2} & \cdots & & 0 & 0 \\ 0 & \mu_{1,2}^{0,1} & 0 & & & & 0 \\ & \vdots & & \ddots & & \vdots & \\ 0 & & & & & \mu_{0,6}^{1,7} & 0 \\ 0 & 0 & & \cdots & \mu_{1,7}^{0,6} & 0 & \mu_{0,7}^{1,8} \\ 0 & 0 & 0 & & 0 & \mu_{1,8}^{0,7} & 0 \end{pmatrix} \tag{1.17}$$

Data for the transition dipole moments were taken from polynomial fits as a function of the angular momentum quantum number as calculated by Goorvitch and Chackerian[60].

1.2.6 Optimization with the Genetic Algorithm (GA)

The GA is a common optimization routine that has been used within optimal control, both experimentally and theoretically. Other theoretical optimization methods that have been tested include Ant Colony Optimization[61] and Simulated Annealing[62]. We use the GA routine developed by Carroll[63]. The general idea behind the GA is to use ideas of evolution and survival of the fittest, as is used in nature to produce suitable offspring, to find an optimal solution. Fig. 1.3 illustrates the general procedure for GA optimization. The algorithm begins by populating the first generation using a random set of individuals (i.e., laser pulses described by specific amplitude and phase parameters for a fixed pulse energy; Equation 1.6). For simplicity, the illustration makes use of 5 frequency components (ν_1 to ν_5) of trivial amplitude and phase, in which ν_3 is the central frequency. Each frequency is composed of amplitude (A) and phase (ϕ) parameters (Fig. 1.3-2.). The fitness or ability for the laser pulse to perform the required quantum logic gate operation, defined by the Fidelity function, is determined. Each individual can be represented as a binary string of bits (0s and 1s), which resembles a 'chromosome', for the set of parameters describing the amplitude and phase at each frequency component (Fig. 1.3-3). A tournament selection decides which laser pulses will become

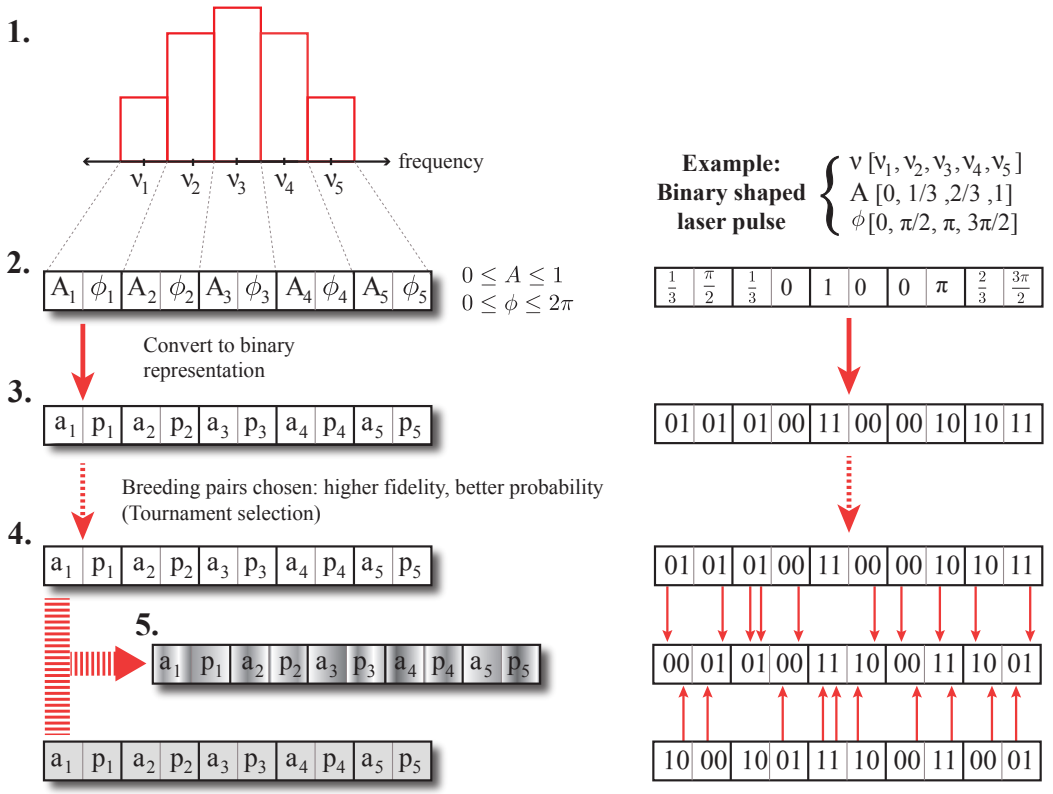

Figure 1.3: An illustration of the genetic algorithm procedure using only 5 frequency components (ν_1 to ν_5). A set of random laser pulses is used for the first generation. The rectangular row of boxes represents a laser pulse. **1.** Discretized frequency spectrum denoting the laser pulse shape. **2.** Amplitude (A) and phase (ϕ) parameters at each frequency. **3.** Binary representation. Discretization of the range of amplitude and phase values allows for this transformation. **4.** A tournament selection decides which laser pulses will breed (parents; white and grey). **5.** Breeding via uniform cross-over produces a child from parent1 and parent2. Tournament selection and uniform cross-over continue until a new generation of offspring is formed. An example is shown also using 5 frequencies with binary pulse shaping and an arbitrary choice of 4 amplitude and 4 phase components.

parents and breed. This occurs by selecting two laser pulses at random and the one with the highest fidelity is chosen as parent1 (Fig. 1.3-4; white box). Parent2 (Fig. 1.3-4; grey box) is determined similarly. Laser pulses associated with a larger fidelity have a greater chance of breeding. Breeding occurs via a uniform cross-over (Fig. 1.3-4.). Each bit from parent1 or parent2 has a 50% probability of being chosen to form the child. Thus the resulting child will have bit contributions from either parent (Fig. 1.3-5; mixed white/grey). The binary representation procedure is then reversed to obtain laser pulse parameters corresponding to the child. This child is then added to the next generation of laser pulses. This entire process is repeated until a new generation is produced consisting of the same number of children as the previous generation (i.e. the number of individuals in each generation is constant). Within this specific implementation of the GA we use a subroutine termed the microGA. The microGA replaces mutation with a form of interbreeding inhibitor. When a specific generation of individual pulse shapes becomes too similar to each other then the next generation is populated with the highest fidelity (*elite*) individual and the remaining individuals are randomly generated. Therefore, the microGA eliminates convergence to local minima.

1.2.7 Criteria for Quantum Computing

In order for a physical system to be a viable candidate for a quantum computer it must meet five criteria as proposed by DiVincenzo and Loss[47]. Diatomics can in general satisfy all five conditions accordingly:

1. Scalable system with well characterized qubits - rovibrational states as the qubits with scalability being satisfied through the inclusion of more rovibrational qubit states.

2. Initialization - rovibrational state preparation through current experimental techniques[35, 64], e.g., jet-cooling.

3. Long decoherence times - rovibrational states in diatomic molecules exhibit long decoherence times on the order of a thousand laser pulse (quantum gate) applications before significant information loss.

4. Universal set of quantum gates - Laser pulses are shaped to represent universal gates (e.g., Hadamard, phase, CNOT)

5. Measurement - rovibrational states can be projected onto other molecular states for computational read-out[35, 64].

1.3 Diatomic Quantum Computing using GA optimized Shaped Laser Pulses

In the present work, the focus is on quantum computing using the rovibrational states of a diatomic as the qubits and shaping laser pulses to represent quantum logic gates. Table 1.2 details the theoretical and experimental studies specifically concerning this type of *diatomic quantum computing*. There are only two experimental implementations and in both cases there was no feedback loop implemented. The majority of calculations done exploring molecular quantum computing implement the OCT algorithm to shape laser pulses, which in general does not reflect experimental pulse shaping conditions. Hosaka[64] proposed a setup based on available experimental techniques and explores its feasibility via numerical simulations. However, in general, there is a disconnect between computational simulations and experimental realization that needs to be bridged if further progress in molecular quantum computation is to be achieved. We suggest areas lacking in theoretical progress and attempt to provide useful insight into them with respect to diatomic quantum computing. These are covered in Chapters 2-4 and summarized in the following 3 sections. As a final synopsis, Chapter 5 will include a discussion of conclusions presented from the findings of the study, along with the current progress and future potential of molecular quantum computing using shaped laser pulses.

Table 1.2: Current list and key point summary of theoretical and experimental studies in diatomic quantum computing. The last two rows summarize the results of Chapters 2 and 3, respectively.

Molecular Model	**Optimization Method**	**Qubit States**	**Logic Gates/ Algorithm**	**Population or Phase Optimization**	**Ref**
$^{14}N^{16}O$	OCT	rovibrational	Deutsch-Jozsa	phase	[65]
$^{12}C^{16}O$	OCT	rovibrational	NOT,Had,$CNOT_1$	phase	[66]
$^{12}C^{16}O$	OCT	rovibrational	Deutsch-Jozsa	phase	[67]
$^{12}C^{16}O$	GA	rovibrational	NOT,Had,$CNOT_1$	phase	[48]
I_2	none	vibronic	Deutsch-Jozsa	phase	[34]
Li_2	OCT	vibronic	Deutsch-Jozsa	phase	[68]
LiH	none	rovibrational	NOT,Had	population	[69]
Na_2	none	rovibronic	NOT,$\frac{\pi}{8}$,Had	population	[70]
Na_2 / Li_2	OCT	vibronic	Deutsch-Jozsa	phase	[71]
NaX-NaY[a]	OCT	rotational	Deutsch-Jozsa	phase	[72]
NaCs	GA/OCT	rovibronic	$CNOT_1$	phase	[73]
OH	OCT	vibrational	NOT,$\frac{\pi}{8}$,Had	phase	[74]
OH / D($\omega_e\chi_e$)[b]	OCT	vibrational	NOT,Had	population	[55]
ortho-N_2 -D_2	none	rovibrational	NOT,CNOT	population	[75]
I_2	none	vibrational	$CNOT_1$,QFT	population	[76]
I_2	OCT	vibronic	Grovers	phase	[77]
I_2	experiment	vibrational	QFT	-	[64]
Li_2	experiment	rovibrational	Deutsch-Jozsa	-	[35]
$^{12}C^{16}O$	GA	rovibrational	NOT,Had CNOT,ACNOT	phase	[78]
D($\omega_e\chi_e$,B_e)[c]	OCT/GA	rovibrational	$ACNOT_1$,NOT_2	phase	[79]

[a] X,Y=Cl or Br
[b] D($\omega_e\chi_e$): model diatomic using vibrational anharmonicity
[c] D($\omega_e\chi_e$,B_e): model diatomic using vibrational anharmonicity and rotational constant

1.3.1 Quantum gate operations using mid-infrared binary shaped pulses on the rovibrational states of carbon monoxide.

Binary laser pulses (A=0 or 1 and ϕ=0 or π) are shaped to represent 8 quantum gates using 4 rovibrational states of the diatomic carbon monoxide ($^{12}C^{16}O$) as the qubits. A similar methodology was previously reported by Tsubouchi and Momose[48] on $^{12}C^{16}O$ for shaped laser pulses consisting of 64 amplitude and 64 phase variations on rovibrational state qubits that required 2-photon transitions. Our results showed that optimal laser pulses of lesser energy and with larger fidelities can be produced using only 2 amplitude and phase variations (binary pulse shaping) with a qubit representation that connected qubit transitions via 1-photon excitations. It was concluded that with an appropriate choice of qubit representation simple binary shaped pulses could be used. For the quantum gates with large fidelities it can be suggested that binary pulse shapes constitute the majority of the qubit excitation and variations beyond binary shaping only cause small incremental improvements.

This work was published as: *R. R. Zaari, A. Brown, J. Chem. Phys.* ***132****, 014307/1-9 (2010)*

1.3.2 Effect of diatomic molecular properties on binary laser pulse optimizations of quantum gate operations.

The two highest order parameters (largest contributors) of the Taylor series expansion in energy for a model diatomic (oscillating rotor) are the vibrational anharmonicity and the rotational constant. A plot of these parameters for 85 diatomics showed a general linear trend. A scan along the line of linear fit allowed for various diatomics to be studied, subsequent laser pulses shaped and trends established. This was carried out using the GA; OCT optimizations were included as a comparison. Results indicate that the specific choice of diatomic molecule strongly influences the ability to produce high fidelity

shaped laser pulses for the $ACNOT_1$ and NOT_2 quantum gates. A qualitative agreement was observed for the laser pulse fidelities between the GA and OCT methods indicating that the results are not dependent upon the optimization method employed. It was also concluded that global phase alignment increases the difficulty of producing high fidelity shaped laser pulses, not observed with population transfer alone.

This work was published as: *R. R. Zaari, A. Brown, J. Chem. Phys.* ***135****, 044317/1-7 (2011)*

1.3.3 Effect of Laser Pulse Shaping Parameters on Laser Pulse Shaping of Quantum Gates.

To study the impact of the experimental limitations of pulse shaping on quantum gate fidelities, four parameters present in discretized frequency domain laser pulse shaping were varied and laser pulses shaped to represent three quantum logic gates ($ACNOT_1$, NOT_2, Had_2). These four parameters are (i) the frequency resolution, which in turn describes the total pulse duration, (ii) the number of amplitude and phase components and (iii) the number of frequency components. Simple trends were observed for optimal fidelities as a function of the total pulse duration for the $ACNOT_1$ and NOT_2 quantum gates, showing regular high fidelity zones. Complex and irregular trends result for analogous calculations for the Had_2 gate. The number of amplitude components has a greater effect on producing high fidelities for all three quantum gates studied, compared to variations in phase. Also variations in the number of frequency components greatly affects the fidelity in conjunction with amplitude variations. The central frequency/frequencies produce the majority of the resulting fidelity.

Bibliography

[1] T. Brixner, G. Gerber, Chem. Phys. Chem. **4**, 418 (2003)

[2] M. Dantus, V. V. Lozovoy, Chem. Rev. **104**, 1813 (2004)

[3] P. Brumer, M. Shapiro, Annu. Rev. Phys. Chem. **43**, 257 (1992)

[4] G. Balint-Kurti, S. Zou, A. Brown, Adv. Chem. Phys. **138**, 43 (2008)

[5] C. Brif, R. Chakrabarti, H. Rabitz, New J. Phys. **12**, 075008 (2010)

[6] Y. Silberberg, Annu. Rev. Phys. Chem. **60**, 277 (2009)

[7] M. Shapiro, P. Brumer, *Quantum Control of Molecular Processes, 2nd Rev Enl edition* (Wiley, 2012)

[8] M. M. Wefers, K. A. Nelson, Opt. Lett. **18**, 2032 (1993)

[9] T. Brixner, G. Gerber, Opt. Lett. **26**, 557 (2001)

[10] Z. Jiang, C. B. Huang, D. E. Leaird, A. M. Weiner, Nat. Photonics **1**, 463 (2007)

[11] R. Judson, H. Rabitz, Phys. Rev. Lett. **68**, 1500 (1992)

[12] T. Baumert, T. Brixner, V. Seyfried, M. Strehle, G. Gerber, App. Phys. B **65**, 779 (1997)

[13] C. Bardeen, V. Yakovlev, K. Wilson, S. Carpenter, P. Weber, W. Warren, Chem. Phys. Lett. **280**, 151 (1997)

[14] M. Bergt, T. Brixner, B. Kiefer, M. Strehle, G. Gerber, J. Phys. Chem. A **103**, 10381 (1999)

[15] S. Zhang, Z. Sun, X. Zhang, Y. Xu, Z. Wang, Z. Xu, R. Li, Chem. Phys. Lett. **415**, 346 (2005)

[16] A. P. Peirce, M. A. Dahleh, H. Rabitz, Phys. Rev. A **37**, 4950 (1988)

[17] W. Zhu, J. Botina, H. Rabitz, J. Chem. Phys. **108**, 1953 (1998)

[18] J. Werschnik, E. K. U. Gross, J. Phys. B: At. Mol. Phys. **40**, R175 (2007)

[19] R. Feynman, Int. J. Theor. Phys. **21**, 467 (1982)

[20] D. Deutsch, Proc. R. Soc. London, Ser. A **400**, 97 (1985)

[21] D. Deutsch, Phys. World **5**, 57 (1992)

[22] P. Shor, SIAM J. Comput. **26**, 1484 (1997)

[23] A. W. Harrow, A. Hassidim, S. Lloyd, Phys. Rev. Lett. **103**, 150502 (2009)

[24] D. S. Abrams, S. Lloyd, Phys. Rev. Lett. **83**, 5162 (1999)

[25] I. Kassal, S. P. Jordan, P. J. Love, M. Mohseni, A. Aspuru-Guzik, Proc. Natl. Acad. Sci. U.S.A. **105**, 18681 (2008)

[26] I. Kassal, A. Aspuru-Guzik, J. Chem. Phys. **131**, 224102 (2009)

[27] L. Vandersypen, M. Steffen, G. Breyta, C. Yannoni, M. Sherwood, I. Chuang, Nature **414**, 883 (2001)

[28] J. Jones, M. Mosca, J. Chem. Phys. **109**, 1648 (1998)

[29] I. Chuang, L. Vandersypen, X. Zhou, D. Leung, S. Lloyd, Nature **393**, 143 (1998)

[30] C. Sackett, D. Kielpinski, B. King, C. Langer, V. Meyer, C. Myatt, M. Rowe, Q. Turchette, W. Itano, D. Wineland, I. Monroe, Nature **404**, 256 (2000)

[31] S. Gulde, M. Riebe, G. Lancaster, C. Becher, J. Eschner, H. Haffner, F. Schmidt-Kaler, I. Chuang, R. Blatt, Nature **421**, 48 (2003)

[32] C. Tesch, L. Kurtz, R. de Vivie-Riedle, Chem. Phys. Lett. **343**, 633 (2001)

[33] R. Zadoyan, D. Kohen, D. A. Lidar, V. A. Apkarian, Chem. Phys. **266**, 323 (2001)

[34] Z. Bihary, D. R. Glenn, D. A. Lidar, V. A. Apkarian, Chem. Phys. Lett. **360**, 459 (2002)

[35] J. Vala, Z. Amitay, B. Zhang, S. R. Leone, R. Kosloff, Phys. Rev. A **66**, 062316 (2002)

[36] C. Tesch, R. de Vivie-Riedle, Phys. Rev. Lett. **89**, 157901 (2002)

[37] U. Troppmann, C. Tesch, R. de Vivie-Riedle, Chem. Phys. Lett. **378**, 273 (2003)

[38] S. Suzuki, K. Mishima, K. Yamashita, Chem. Phys. Lett. **410**, 358 (2005)

[39] M. Schroeder, A. Brown, J. Chem. Phys. **131**, 034101 (2009)

[40] B. M. R. Schneider, C. Gollub, K. L. Kompa, R. de Vivie-Riedle, Chem. Phys. **338**, 291 (2007)

[41] B. M. R. Korff, U. Troppman, R. de Vivie-Riedle, J. Chem. Phys. **123**, 244509 (2005)

[42] L. Bomble, D. Lauvergnat, F. Remacle, M. Desouter-Lecomte, Phys. Chem. Chem. Phys. **12**, 15628 (2010)

[43] C.M. Tesch, R. de Vivie-Riedle, J. Chem. Phys. **121**, 12158 (2004)

[44] C. Gollub, M. Kowalewski, R. de Vivie-Riedle, Phys. Rev. Lett. **101**, 073002 (2008)

[45] M. Schroeder, A. Brown, New J. Phys. **11**, 105031 (2009)

[46] M. Lapert, R. Tehini, G. Turinici, D. Sugny, Phys. Rev. A **79**, 063411 (2009)

[47] D. P. DiVincenzo, D. Loss, Superlattices Microstruct. **23**, 419 (1998)

[48] M. Tsubouchi, T. Momose, Phys. Rev. A **77**, 052326 (2008)

[49] M. A. Nielsen, I. L. Chuang, *Quantum Computation and Quantum Information* (Cambridge, 2000)

[50] I. Kassal, J. D. Whitfield, A. Perdomo-Ortiz, M. H. Yung, A. Aspuru-Guzik, Annu. Rev. Phys. Chem. **62**, 185 (2011)

[51] A. Ekert, R. Jozsa, Phil. Trans. R. Soc. Lond. A **356**, 1769 (1998)

[52] I. Buluta, F. Nori, Science **326**, 108 (2009)

[53] B. P. Lanyon, J. D. Whitfield, G. G. Gillett, M. E. Goggin, M. P. Almeida, I. Kassal, J. D. Biamonte, M. Mohseni, B. J. Powell, M. Barbieri, A. Aspuru-Guzik, A.G. White, Nat. Chem. **2**, 106 (2010)

[54] J. P. Palao, R. Kosloff, Phys. Rev. A **68**, 062308 (2003)

[55] D. Babikov, J. Chem. Phys. **121**, 7577 (2004)

[56] J. M. Brown, A. Carrington, *Rotational Spectroscopy of Diatomic Molecules* (Cambridge University Press, 2003)

[57] P. Milonni, Phys. Rep. **25**, 1 (1976)

[58] H. A. Bethe, E. E. Salpeter, *Quantum Mechanics of One- and Two-Electron Atoms* (Springer, 1957)

[59] A. Mantz, J. Maillard, W. Roh, K. Roa, J. Mol. Spectrosc. **57**, 155 (1975)

[60] D. Goorvitch, C. Chackerian, Astro. J. Supp. Ser. **91**, 483 (1994)

[61] C. Gollub, R. de Vivie-Riedle, Phys. Rev. A **79**,021401(R) (2009)

[62] B. Amstrup, J. D. Doll, R. A. Sauerbrey, G. Szabó, A. Lorincz, Phys. Rev. A **48**, 3830 (1993)

[63] D.L. Carroll, Genetic Algorithm driver **v1.7.0** (2004).

[64] K. Hosaka, H. Shimada, H. Chiba, H. Katsuki, Y. Teranishi, Y. Ohtsuki, K. Ohmori, Phys. Rev. Lett. **104**, 180501 (2010)

[65] K. Mishima, K. Yamashita, Chem. Phys. **367**, 63 (2010)

[66] J. L. Chen, C. M. Ling, C. C. Hwang, Y. H. Ho, J. Chem. Phys. **134**, 134103 (2011)

[67] K. Shioya, K. Mishima, K. Yamashita, Mol. Phys. **105**, 1283 (2007)

[68] Y. Ohtsuki, Chem. Phys. Lett. **404**, 126 (2005)

[69] W. Z. Cao, L. J. Tian, H. J. Jiang, C. Li, Int. J. Quant. Info. **6**, 1223 (2008)

[70] C. Menzel-Jones, M. Shapiro, Phys. Rev. A **75**, 052308 (2007)

[71] K. Mishima, K. Tokumo, K. Yamashita, Chem. Phys. **343**, 61 (2008)

[72] K. Mishima, K. Yamashita, Chem. Phys. **361**, 106 (2009)

[73] D. Sugny, L. Bomble, T. Ribeyre, O. Dulieu, M. Desouter-Lecomte, Phys. Rev. A **80**, 042325 (2009)

[74] M. Zhao, D. Babikov, J. Chem. Phys. **125**, 024105 (2006)

[75] E. A. Shapiro, I. Khavkine, M. Spanner, M. Y. Ivanov, Phys. Rev. A **67**, 013406 (2003)

[76] Y. Teranishi, Y. Ohtsuki, K. Hosaka, H. Chiba, H. Katsuki, K. Ohmori, J. Chem. Phys. **124**, 114110 (2006)

[77] Y. Ohtsuki, New J. Phys. **12**, 045002 (2010)

[78] R. R. Zaari, A. Brown, J. Chem. Phys. **132**, 014307 (2010)

[79] R. R. Zaari, A. Brown, J. Chem. Phys. **135**, 044317 (2011)

Chapter 2

Quantum gate operations using mid-infrared binary shaped pulses on the rovibrational states of carbon monoxide.†

2.1 Introduction

Laser control of molecules has seen its greatest development in the last two decades due to advancements in experimental laser sources and our theoretical understanding of the underlying principles of control. [1–5] These developments have opened the door to femtosecond and emerging attosecond science. The use of lasers allows for more specific control of molecules, from the individual nuclei in reaction dynamics [5] to the individual electrons of a molecule. [6–8] It has been proposed that laser control of molecular states could be used as a construct for quantum logic gates within quantum computing[9] and numerous studies have followed this suggestion, see for example Refs. [10–15]. A fully functioning quantum computer would allow for many applications and uses, but solving quantum mechanical problems exactly would be one of the most important. The full capability of outperforming a classical computer resides in a quantum computer's ability to create superposition states, something

† Reprinted with permission from Ryan R. Zaari and Alex Brown, Journal of Chemical Physics, **132**, 014307 (2010). Copyright 2010, American Institute of Physics.

that a classical computer cannot do.

Currently molecular quantum computing is seeing studies from all aspects such as controlling nuclear states using Nuclear Magnetic Resonance,[16, 17] electronic states in ion traps[18, 19] and the control of rovibrational states with shaped laser pulses[20] - the last of which is relevant here. Within rovibrational control, a laser field is used to manipulate the rovibrational states of a molecule in order to create a series of quantum logic gate operations from which quantum algorithms can be implemented. As there are classical logic operations in traditional boolean algebra, there is also a set of analogous quantum logic operations. Each laser field is designed to behave as a certain quantum logic gate and would act on chosen rovibrational states representing the qubits (quantum bits), inevitably executing a quantum algorithm. Currently there are two main theoretical methods to determine optimal laser fields (not limited to quantum logic gate operations): Optimal Control Theory (OCT)[3, 22] and the Genetic Algorithm (GA),[23] along with some other less common methods such as simulated annealing[24] and ant colony optimization.[25] OCT often relies on an iterative method which maximizes a functional, composed in part by a time dependent laser field term. The most desirable laser field is the one which produces the greatest value for the functional. Since in general there are no explicit restrictions on the possible laser fields produced by the OCT method, they can contain frequencies which are not attainable by current experimental pulse shaping techniques. OCT has been used to study quantum gate operations, using the vibrational states of OH[10] or the rovibrational states of CO.[11] In the case of using OCT on larger systems such as acetylene[12] and $MnBr(CO)_5$,[13] the vibrational modes were chosen to represent the qubits, while also using reduced dimensional models of the system. The GA has been used to optimize quantum gate operations using the rovibrational states of thiophosgene ($SCCl_2$) [14] and also CO. [15] The GA optimization which is implemented in this study selects desired properties of the laser field in the frequency domain and thus mimics experimental laser pulse shaping procedures

using a feedback loop. The GA searches for frequency dependent amplitude and phase components that construct laser pulses producing the greatest fidelity for the chosen quantum logic gate. For rovibrational state control, the range of frequencies available is in the mid-infrared (mid-IR) regime.

There are few aspects of molecular quantum computing using shaped mid-IR laser pulses that have been investigated to indicate strengths and weaknesses of such a procedure. There are many adjustable parameters of the pulse shaper that can affect the resulting quantum gate fidelity. These include the frequency resolution of the shaper, the central frequency, the bandwidth, the input laser pulse energy, and the range of amplitude and phase values. Alternatively, there are also intrinsic molecular properties that can dictate resulting quantum gate fidelities, such as the rovibrational state energies, transition dipole moments, available selection rules and the choice of qubit rovibrational state representaiton. A poor choice of the rovibrational states to represent the qubits may result in ineffective population transfer and thus lower the fidelity of the gate operation. In this paper, we investigate the effects of a restricted range of amplitude and phase values (binary pulse), as well as an alternative choice of rovibrational states to represent the qubits, on quantum gate fidelities. These results are compared to previous work on $^{12}C^{16}O$ by Tsubouchi and Momose.[15] In their study, they chose qubit representations of the rovibrational states that resulted in some 2-photon quantum gate operations. As will be shown here, all gates can be reduced to 1-photon transitions through judicious choice of the qubit states. The number of possible amplitude and phase values within a given range is another important factor. More values within the range means greater variation in the attributes of the resulting pulsed laser field. However, this puts a large burden on the GA optimization's ability to search efficiently through these values for the greatest fidelity. The simplest shaped laser pulse consists of a choice of two amplitude (0 or 1) and two phase values (0 or π) for each frequency component and this is denoted as a binary laser pulse. The GA optimization can then efficiently

find the greatest fidelity within this reduced, but still extremely large, search space. Moreover, all other possible shaped laser pulses which contain more than two values of amplitude and phase within this range will have search spaces that also contain the binary laser pulse as a possible solution. Thus, the binary laser pulse sets a lower bound on the possible fidelities that can be obtained with the GA optimization method for a specific quantum logic gate. In comparison, Tsubouchi and Momose[15] chose a range of 64 choices each for the amplitude and phase, thus producing an extremely large search space. In summary, binary laser pulses were optimized in the frequency domain using a GA procedure, to carry out common quantum gate operations. Specific rovibrational states of $^{12}C^{16}O$ were chosen to represent the qubits such that single photon transitions would result.

2.2 Theory

The model system chosen was the rovibrational states of carbon monoxide ($^{12}C^{16}O$), in its ground electronic state. Select rovibrational states of CO are chosen to represent the qubits and the quantum gate operations are carried out by shaped binary pulses. The projection quantum number J_z along the total angular momentum J is zero. The rovibrational states are represented with the vibrational quantum number ν and the rotational quantum number J, in the form (ν J). The CO model consists of 7 vibrational states ranging from ν=0 to 6, each containing 9 rotational states ranging from J=0 to 8. These energies were obtained by Mantz et al. [26] using a linear fit of the molecular constants to a power series in $(\nu+\frac{1}{2})$ of the sum of both rotational and vibrational term values. The accessible rovibrational states are $\Delta\nu=\pm1$ and $\Delta J=\pm1$ due to selection rules and the utilization of mid-IR pulses. It is important to point out that previous work by Shioya et al. [11] also on CO, but using iterative OCT, produced laser pulses that contained both microwave and infrared frequencies. This allowed them to have independent control of rotational or vibrational

states, which is not permitted here. Binary (two amplitude and two phase) laser field pulses with frequency domain optimization are chosen. Tsubouchi and Momose[15] chose to carry out similar calculations on CO also with GA optimization but using much larger 64 amplitude and 64 phase varied laser pulses and a different choice of states for the qubits. A comparison between our results and those of Tsubouchi and Momose[15] is made in the results, see Sec.2.3.1.

2.2.1 Quantum Mechanical System

In the present work, the objective is to determine a laser field which directs the system from an initial state to a final target state. Moreover in this study the laser pulses are designed to perform unitary quantum logic gate operations on the rovibrational state wavefunctions of CO, but in general this can extend beyond simple population control. The time-dependent Schrödinger equation (TDSE) with the Hamiltonian, $H(t)$, describing the laser pulse/molecular dipole interaction is:

$$i\hbar\frac{d\Psi(r,t)}{dt} = H(r,t)\Psi(r,t) = \left[H_0(r) - \epsilon(t)\mu(r)\right]\Psi(r,t), \tag{2.1}$$

where $H_0(r)$ is the time-independent rovibrational Hamiltonian, $\epsilon(t)$ is the electric field of the laser pulse and $\mu(r)$ is the molecular dipole moment.

The molecular wavefunction, $\Psi(r,t)$ is represented in the familiar linear time-dependent form as:

$$\Psi(r,t) = \sum_{\nu J} c_{\nu J}(t)\psi_{\nu J}(r) \tag{2.2}$$

where we have a linear combination of time-dependent rovibrational coefficients, $c_{\nu J}(t)$, and stationary states $\psi_{\nu J}(r)$.

Rewriting the TDSE in terms of the time-dependent coefficients $c_{\nu J}(t)$, in matrix notation, results in an equation of the form:

$$\dot{\underline{c}}(t) = -\frac{i}{\hbar}\left[\underline{\underline{E}} - \epsilon(t)\underline{\underline{\mu}}\right]\underline{c}(t). \tag{2.3}$$

The time-dependent coefficients are now contained in a rovibrational state vector, $\underline{c}(t)$ and the Hamiltonian consists of a square energy matrix ($\underline{\underline{E}}$) along with a square transition dipole matrix ($\underline{\underline{\mu}}$) with matrix elements based upon the allowed transitions of ν and J. The energies were obtained from the results of work by Mantz et al. [26] who used linear fits of the molecular constants. The transition dipole moments were obtained from the results of work by Goorvitch and Chackerian[27] who used polynomial fits relative to the angular momentum quantum number. The goal is to find the optimal electric field (laser pulse), $\epsilon(t)$, to cause the desired quantum gate operation. For a given electric field, the equation is integrated using the fourth-order Runge-Kutta method. The time step used in the integration is the ratio between the number of time points (2^{20}) and the total pulse duration (6.67 ps), which in this study results in dt= 0.0064 fs. This value is much smaller than the oscillation period.

2.2.2 Molecular Qubit Basis

A 'qubit' is the shorthand name given to a 'quantum bit,' which is analogous to the bit in classical computing. It is a representation of the state of the system and thus is written in the general form, $|q_1\ q_2\rangle$, where q_1 and q_2 are denoted the first and second qubits, respectively. The qubits can be represented in two different ways. The first case entails that each qubit is represented by a separate 2-level or quasi 2-level system, and then these n qubits are appropriately coupled.[16–19] Alternatively, and the choice used herein, n qubits can be represented by $N = 2^n$ combinations of N molecular states.[14, 20, 21] We have chosen four rovibrational states of CO to encode the 2-qubit basis using the latter representation. The proper choice of rovibrational states to represent the qubits is important when attempting to control quantum gates with a laser pulse. In the scenario where there is independent control of vibrational and rotational state transitions,[11] an obvious choice has been the rovibrational states (ν J)=(00), (01), (10) and (11) to represent the qubit states $|00\rangle$, $|01\rangle$, $|10\rangle$ and $|11\rangle$ qubits, respectively. The required excitations will

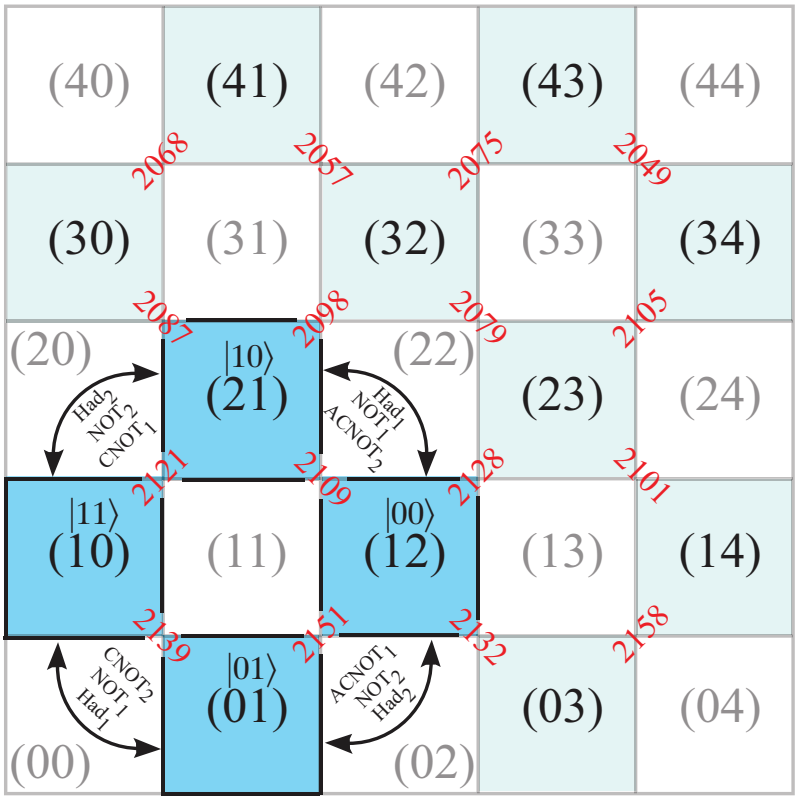

Figure 2.1: Illustration of the first 12 accessible rovibrational states, (shaded light blue boxes) of $^{12}C^{16}O$ labeled as (ν J). The chosen qubit representations (shaded dark blue boxes) are labeled as $|q_1 q_2\rangle$. Available transitions are governed by the following simultaneous vibrational and rotational transitions: $\Delta\nu$=$\pm$1 and ΔJ=$\pm$1 which are illustrated by states connected along a diagonal. Some rovibrational states are inaccessible (white boxes). Excitation frequencies (red text) are in cm^{-1} and lie between the accessible rovibrational states. The qubits ($|00\rangle$,$|01\rangle$,$|10\rangle$,$|11\rangle$) that undergo a state change (black arrows) during an applied quantum gate operation, according to Table 2.1, are labeled by the corresponding gate. Notice that the NOT and Hadamard gates require simultaneous control of 2 transitions.

involve 1-photon transitions, but will require frequencies both in the mid-IR and microwave regions. In the case studied here, where there must be simultaneous vibrational and rotational state transitions, due to the absorption of mid-IR radiation, the above choice of qubits would result in forbidden transitions according to the allowed transitions. Previous work by Tsubouchi and Momose[15] alluded to the idea that quantum gate operations which consist of 2-photon transitions seem to be poorly controlled with a shaped mid-IR laser pulse. Therefore, it would be ideal to have quantum gate operations which consist of 1-photon transitions. The qubit basis chosen in this work is shown in Figure 2.1. For the CNOT, ACNOT, NOT and Hadamard quantum gates, the transitions encountered all remain single photon and as a consequence the rovibrational state arrangement is cyclic.

2.2.3 Quantum Gates

A set of universal quantum gates is desirable because any quantum operation, in principle, can then be represented by a combination of this finite set. In the present study, the NOT, Hadamard (Had), Controlled-NOT (CNOT) and alternative Controlled-NOT (ACNOT) gates are studied, as shown in Table 2.1. The Hadamard gate, CNOT gate and the phase gate (not shown) comprise one such set of universal quantum gates. The NOT and Hadamard quantum gates are labelled such that the number following the gate name refers to whether the gate operates on the first or second qubit. In the case of the CNOT and ACNOT gates, the labelling refers to whether the control qubit is the first or second qubit.

If the vibrational and rotational states could be controlled independently then the NOT and Hadamard gates would be considered 1-qubit operations. This means that the 2-qubit state can be written as: $|q_1\ q_2\rangle = |q_1\rangle|q_2\rangle$, where qubit1 encodes the vibrational states and qubit2 encodes the rotational states.

NOT_1 :	$\|00\rangle \leftrightarrow \|10\rangle$ $\|01\rangle \leftrightarrow \|11\rangle$	NOT_2 :	$\|00\rangle \leftrightarrow \|01\rangle$ $\|10\rangle \leftrightarrow \|11\rangle$
Had_1 :	$\|00\rangle \leftrightarrow \frac{1}{\sqrt{2}}(\|00\rangle + \|10\rangle)$ $\|01\rangle \leftrightarrow \frac{1}{\sqrt{2}}(\|01\rangle + \|11\rangle)$ $\|10\rangle \leftrightarrow \frac{1}{\sqrt{2}}(\|00\rangle - \|10\rangle)$ $\|11\rangle \leftrightarrow \frac{1}{\sqrt{2}}(\|01\rangle - \|11\rangle)$	Had_2 :	$\|00\rangle \leftrightarrow \frac{1}{\sqrt{2}}(\|00\rangle + \|01\rangle)$ $\|01\rangle \leftrightarrow \frac{1}{\sqrt{2}}(\|00\rangle - \|01\rangle)$ $\|10\rangle \leftrightarrow \frac{1}{\sqrt{2}}(\|10\rangle + \|11\rangle)$ $\|11\rangle \leftrightarrow \frac{1}{\sqrt{2}}(\|10\rangle - \|11\rangle)$
CNOT_1 :	$\|00\rangle \rightarrow \|00\rangle$ $\|01\rangle \rightarrow \|01\rangle$ $\|10\rangle \leftrightarrow \|11\rangle$	CNOT_2 :	$\|00\rangle \rightarrow \|00\rangle$ $\|10\rangle \rightarrow \|10\rangle$ $\|01\rangle \leftrightarrow \|11\rangle$
ACNOT_1 :	$\|10\rangle \rightarrow \|10\rangle$ $\|11\rangle \rightarrow \|11\rangle$ $\|00\rangle \leftrightarrow \|01\rangle$	ACNOT_2 :	$\|01\rangle \rightarrow \|01\rangle$ $\|11\rangle \rightarrow \|11\rangle$ $\|00\rangle \leftrightarrow \|10\rangle$

Table 2.1: Quantum gate operations which are implemented by an optimized laser pulse. NOT/ Hadamard: The number following the gate name refers to which qubit the gate operates on. CNOT/ACNOT: The number following the gate name refers to which qubit is the control qubit.

The result is that either qubit1 or qubit2 will be independent upon the operation and the gate only needs to act on one of the qubits. Hence, it is called a 1-qubit operation. As pointed out previously, the laser pulses used in the current study are shaped using frequencies in the mid-infrared to induce simultaneous vibrational and rotational transitions. However, this qubit representation cannot treat qubit1 and qubit2 separately and so both the NOT and Hadamard quantum gate operations resemble 2-qubit operations.

The efficiency of a quantum gate operation is determined by the gate fidelity,[28, 29]

$$F = \frac{1}{N^2}\left|\sum_{k=1}^{N}\langle\Psi_k(T)|\Phi_k\rangle\right|^2, \tag{2.4}$$

where $\Psi_k(T)$ is the resulting wavefunction after the laser pulse of duration T has been applied and Φ_k is the target wavefunction. The wavefunctions are summed over the number of transitions N and then divided by a normalization factor N^2 to ensure the fidelity ranges between 0 and 1. A fidelity of 1 implies

complete population transfer within the quantum gate operation, as well as the target states being globally phase aligned, as described by,

$$|\Psi_{00}\rangle + |\Psi_{01}\rangle + |\Psi_{10}\rangle + |\Psi_{11}\rangle \longrightarrow (|\Psi_{00}\rangle' + |\Psi_{01}\rangle' + |\Psi_{10}\rangle' + |\Psi_{11}\rangle')\, e^{i\phi} \quad (2.5)$$

where $|\Psi\rangle$ is the state of the qubit initially, $|\Psi\rangle'$ is the state of the qubit after operation by a quantum gate and $e^{i\phi}$ is the acquired global phase.

The fidelity function enforces the global phase correction which is an important feature in order to apply quantum gates sequentially, as described by Tesch and de Vivie-Riedle.[29] If one uses an iterative OCT algorithm to determine the quantum gates, additional transitions to those shown in Table 2.1 must be optimized to ensure global phase alignment. However, for the GA procedure (or any other stochastic algorithm), the optimization of these additional transitions is not needed as the fidelity, Eq.(2.4), is used explicitly to judge the fitness of a particular laser pulse during the optimization.

The average final state population, which does not incorporate phase alignment is given by,

$$\bar{P} = \frac{1}{N} \sum_{k=1}^{N} |\langle \Psi_k(T) | \Phi_k \rangle|^2 . \quad (2.6)$$

Though not used within the optimization algorithm as a means to judge the fitness of the laser pulses, Eq.(2.6) does give an indication of the ability of the laser pulse to transfer population without global phase alignment.

2.2.4 Laser Pulse Optimization

The laser pulses used to carry out the individual quantum gate operations are constructed in the frequency domain. The shaped laser pulse, written in terms of the frequency components ν_j, is modeled by[15]

$$\epsilon(\nu_j) = \epsilon_0 \sqrt{A(\nu_j)} \exp\left[-2 \ln 2 \left(\frac{\nu_j - \nu_0}{\Delta\nu} \right)^2 \right] \exp\left[i\phi(\nu_j) \right], \quad (2.7)$$

where ϵ_0 is the peak field strength, ν_0 is the central frequency, and ν_j represents the discrete frequencies at which the field is shaped. The amplitude and phase

range from $0 \leq A(\nu_j) \leq 1$ and $0 \leq \phi(\nu_j) \leq 2\pi$, respectively. The transform limited (TL) pulse, which is the input pulse for experimental pulse shaping, defines the pulse structure which is to be shaped. The TL-pulse is defined by $A(\nu_j) = 1$ and $\phi(\nu_j) = 0$ in Eq.(2.7). The amplitude and phase components can be adjusted independently, producing a shaped pulse with defined amplitude and phase features. This shaped pulse is bound by the structure of the TL-pulse such as its bandwidth, amplitude and by the physical pulse shaper frequency discretization. The TL-pulse used has a Gaussian profile with a full width at half-maximum (FWHM) pulse width of $\Delta\nu$=100 cm^{-1}. The central frequency ν_0 is dependent upon the quantum gate operation being optimized and is chosen to be the average resonant frequency of the transition involved for the specific qubit change. The bandwidth of frequencies ranges from $\pm 250 cm^{-1}$ of the central frequency. The pulse shaper was arbitrarily chosen to contain 51 discrete amplitude, $A(\nu_j)$, and phase, $\phi(\nu_j)$, components, resulting in a frequency step of dν=10 cm^{-1}.

A result of having 51 discrete ν_j frequency components is that the spectrum contains step-like features. To our knowledge, other theoretical pulse shaping studies have not used discretized frequencies. [30–32] Rather, once the frequencies with associated amplitude and phase components (51 here) are chosen, they are cubic spline interpolated to produce a smooth spectrum. Cubic spline fitting, as seen in the other studies, can result in elements of $\epsilon(\nu)$ which extend beyond the limits initially set by the TL-pulse. In the present study, the frequency domain field, $\epsilon(\nu)$, is Fourier transformed (integrated) as a sum of rectangles rather than via a spline fit. In the time domain, the non-finite electric field, $\epsilon(t)$, is truncated at $\pm\frac{0.5n-1}{2T}$ of the central time, where n is the total number of parameters optimized (51×2=102) and T is the half the entire frequency range (250 cm^{-1}). This gives a total temporal pulse duration of 6.67 ps. The integrated laser pulse energy, E, is given as: [15]

$$\frac{E}{A} = c\varepsilon_0 \int |\epsilon(\nu)|^2 \, d\nu, \tag{2.8}$$

where c is the speed of light, ε_0 is the permittivity of free space, and A is the area illuminated by the laser field. In the results presented, the pulse area corresponds to a beam focused down a diameter of $50\mu m$. The energy and amplitude of the frequency domain TL-pulse is used as a reference to properly normalize and construct the correct time domain laser pulse intensity. Varying the total energy within the original TL-pulse dictates the fraction of this energy that will be part of the resulting optimized laser pulse energy and its corresponding intensity.

In the context of this study, the simplest amplitude and phase shaped laser pulse is studied, namely a binary pulse. This constitutes two choices for both the amplitude and phase, being 0 or 1, and 0 or π, respectively. Substitution of all four combinations of these binary amplitude and phase parameters into Eq.(2.7) yields unique values for $\sqrt{A(\nu_j)}\exp\left[i\phi(\nu_j)\right] = 0, \pm 1$. This results in a real valued three parameter choice for the total amplitude of $\epsilon(\nu)$ for each frequency value, ν_j. The binary pulse shape is important since all general pulse shaping experiments optimize in a search space in which the binary pulse shape is already a solution. For example, a pulse shaper with a choice of eight amplitude and phase components will by default also contain the amplitude parameters 0 and 1, and also the phase parameters 0 and π. Thus there is the possibility that the binary pulse could be chosen as the optimal pulse shape. Studying simple binary pulse shapes sets the lower bounds for the fidelity of the quantum gate operations, while allowing for a much simpler parameter search space. In the current study the parameter search space for a binary pulse consists of 3^{51} possible combinations of amplitude and phase, while a pulse shaper with eight independent amplitude and phase components would result in a parameter search space of $(8 \times 8 - 1)^{51} = 21^{51} \times 3^{51}$. The search space size has an effect on the ability for the optimization algorithm to find the optimal solution efficiently and the credibility of that solution.

Binary pulse optimization has other interesting characteristics that have been explored previously. Firstly, it will produce a laser pulse which is symmet-

ric in the time domain. Secondly, binary shaped laser pulses direct the target state populations of the individual gate transitions to phase-aligned solutions. Work by Schröder and Brown[33] demonstrated the use of temporally symmetric pulses for quantum gate operations using OCT with a filter function. Laser pulses symmetric in time occurred naturally as the most efficient means of control in other studies,[34, 35] while examining NOT gates optimized with (non-filtered) OCT. In experimental studies by Lozovoy et al.,[36] molecular fragmentation was selectively controlled using only binary phase shaped laser pulses.

In order to search through the combinations of amplitude and phase which produce the optimal pulse shape for the quantum gate operation being studied, the Genetic Algorithm (GA) optimization routine is utilized.[37] The GA uses the general ideas behind natural selection and survival of the fittest to logically determine the optimal pulse shape to cause the greatest fidelity, without having to evaluate all possible combinations of amplitude and phase. Within this particular GA we chose to use *elitism* and the *microGA* procedures rather than mutation. *Elitism* is when the highest fidelity individual from the previous generation is automatically included in the construction of the new generation. The *microGA* eliminates biological interbreeding by restarting the generation with the *elite* individual and randomly selected individuals, when the individuals (laser pulses) of a generation become too similar. The GA is chosen to produce 500 generations with 8 individuals in each. With these choices of GA parameters, minimal change in the fidelity (less than 0.2% and usually less than 0.05%) was observed for the elite individuals between generations 400 to 500 suggesting that the calculation was near the global maximum fidelity.

2.3 Results and Discussion

2.3.1 Optimal Quantum Gates

In order to determine the maximum fidelities of the quantum gates studied at the chosen central frequencies and frequency discretization, nine different total TL-pulse energies were chosen, i.e., [5, 7, 10, 15, 20, 25, 30, 35, 60μJ]. The optimal laser pulses which produce the greatest fidelity for each quantum gate are listed in Table 2.2, along with the associated central frequency, pulse energy and peak intensity. The total energy contained in the TL-pulse and optimized pulse were determined by Eq.(2.8). The central frequency ν_0 was chosen as the resonant frequency for gates involving a single transition (CNOT/ACNOT) or the average frequency if there were two resonant frequencies involved (NOT/Had). There is a distinct gap between the fidelities obtained for the CNOT and ACNOT gates, compared to the Hadamard and NOT gates. While all the fidelities from the CNOT and ACNOT pulses are greater than or equal to 0.80, the greatest fidelity obtained from the Hadamard and NOT pulses is 0.62 (Had_1). It also seems that the average population $\bar{P}$ for optimized laser fields for the Hadamard and NOT gates is also around 0.60. Not only do the optimized laser fields for the Hadamard and NOT gates have difficulty in producing a global phase, they also struggle at transferring population compared to the CNOT and ACNOT gates. As described previously, the Hadamard and NOT quantum gates here act as 2-qubit operations and are not explicitly 1-qubit, as they are usually treated. The poor fidelities obtained for the Hadamard and NOT gates may be due to the fact that these gates must control an extra transition compared to the CNOT and ACNOT gates (see Table 2.1 or Fig.2.1).

In Table 2.2, there is a comparison between the CNOT_1 and ACNOT_2 quantum gates studied by Tsubouchi and Momose,[15] who also used CO as a candidate molecule. The differences between their study and this one is that they smoothed their frequency domain field, $\epsilon(\nu)$, using cubic spline

Table 2.2: Optimal fidelities, F, for the quantum logic gates studied using the specified qubit representation (Fig.2.1) of the rovibrational states of $^{12}C^{16}O$. The associated central frequency, transform-limited and optimized pulse energies, peak intensity and average populations are also shown.

Quantum Gate	**Central Frequency** ν_0, **cm**$^{-1}$	**Pulse Energy (TL-pulse Energy)** μ**J**	**Peak Intensity** **TW/cm**^{2}	**Fidelity,** F **/ Avg. Population,** $\bar{P}$
$CNOT_1$	2121	2.20 (5)	0.0466	0.8113 / 0.9814
$CNOT_2$	2139	4.55 (10)	0.0896	0.7962 / 0.8241
$ACNOT_1$	2151	4.07 (10)	0.0901	0.9729 / 0.9904
$ACNOT_2$	2109	0.77 (5)	0.033	0.8416 / 0.9302
Had_1	2124	13.21 (30)	0.229	0.6172 / 0.6294
Had_2	2136	11.71 (25)	0.381	0.5075 / 0.6538
NOT_1	2124	10.72 (25)	0.264	0.4921 / 0.5053
NOT_2	2136	12.20 (20)	0.293	0.5118 / 0.6025
$CNOT_1$[15]	2115	NR (30)	0.592	0.6877 / 0.7249
$ACNOT_2$ [15]	2147	NR (20)	0.232	0.6374 / 0.8924

NR - Not reported

interpolation, chose different rovibrational states to represent the qubits and optimized laser pulses with a choice of 64 amplitude and phase components. As previously stated, their choice of qubits resulted in quantum gate operations which included 2-photon transitions. Our qubit representation is chosen such that all gate operations involve only 1-photon transitions. The importance of the choice of qubit states is apparent when comparing the fidelities and even the average final state populations from Tsubouchi and Momose[15] and the current study. They obtain fidelities which are at most 0.69, while we are able to produce fidelities that are greater than 0.80. Also compared to their study, we were able to utilize pulse energies and peak intensities that are much lower. Of course, these comparisons are not entirely fair due to the different choices of qubit states but it is interesting to note that the laser fields they generated are governed by independent choice of 64 amplitude and 64 phase components, which are then cubic spline fit. We use only two amplitude and two phase discretized binary laser fields to produce much higher fidelities. In the next sections, we discuss in more detail the dynamics for two quantum gates which when optimized produced a high fidelity ($ACNOT_1$) and low fidelity (NOT_2).

2.3.2 $ACNOT_1$ Quantum Gate

The $ACNOT_1$ quantum gate laser pulse produced the greatest fidelity (0.9729), see Table 2.2. The resulting frequency and time domain laser pulse is shown in Fig.2.2 and the resulting state populations during the pulse interaction in Fig.2.3. Fig.2.2(a) shows the frequency domain optimized pulse, $\epsilon(\nu)$, in black and the TL-pulse in red. They are discrete and the optimized laser pulse is composed of select frequencies bound by the TL-pulse Gaussian shape. Negative amplitudes depict phase values of π radians. The main features to notice within Fig. 2.2(a) are that the $ACNOT_1$ quantum gate is centered at ω_0=2151cm^{-1} and the GA chooses this frequency which is associated with the needed $|00\rangle \leftrightarrow |01\rangle$ transition, i.e., $(\nu J) = (01) \leftrightarrow (12)$. Frequencies the GA doesn't include are those associated with transitions between other

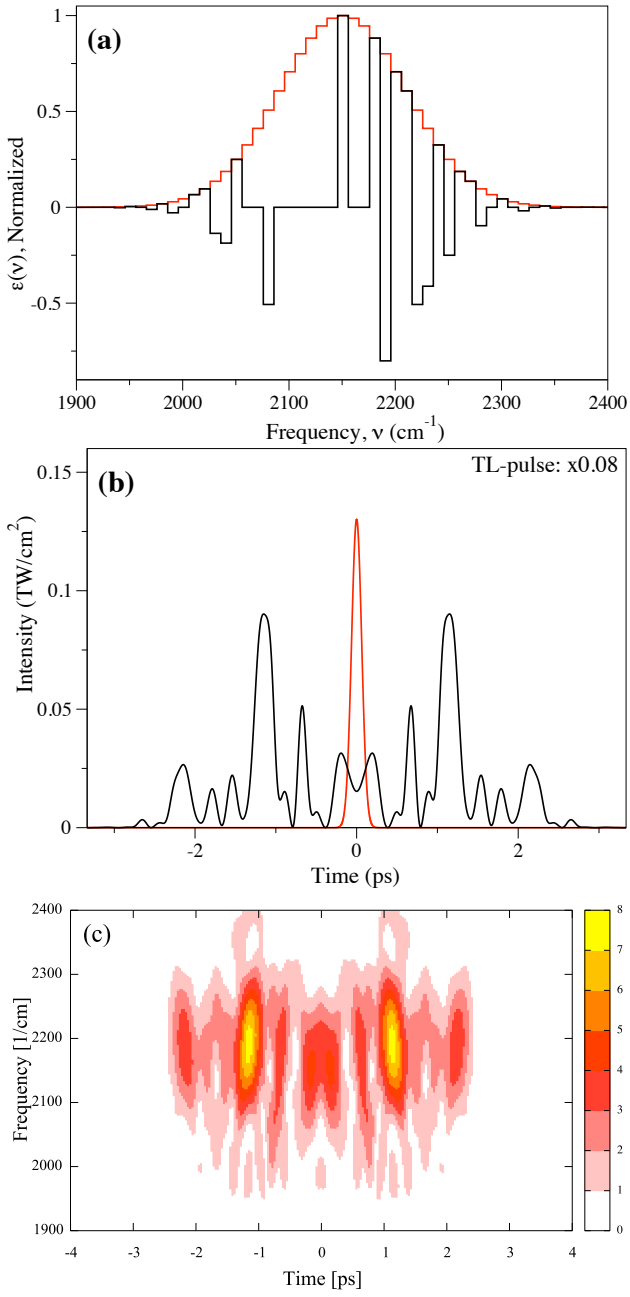

Figure 2.2: Resulting laser pulse for the optimized ACNOT$_1$ quantum gate at E$_{pulse}$=4.07μJ . a) Frequency domain $\epsilon(\nu)$, where negative values denote a phase $\phi(\nu) = \pi$. Red: TL-pulse, black: Optimized pulse. b) Time domain intensity, $|\epsilon(t)|^2$. Red: TL-pulse (intensity scaled by a factor of 0.08), black: optimized pulse. c) XFROG trace for the obtained optimal field.

qubits, namely the (10) $\leftrightarrow$ (01), (10) $\leftrightarrow$ (21) and (21) $\leftrightarrow$ (12) transitions, i.e., 2139cm^{-1}, 2121cm^{-1} and 2109cm^{-1}, respectively. These frequency components are located within the large zero amplitude region to the left of the central frequency. The square of the Fourier transform of this frequency domain field produces the time domain laser pulse intensity profile, Fig.2.2(b), when truncated to a maximum temporal width of 6.67ps, as specified previously. Shown in this figure are the optimized laser field (black) along with the TL-pulse (red) scaled down by a factor of 0.08. The TL-pulse has a peak intensity of 1.63 TW/cm^{-2}, while that of the optimized laser pulse is only 0.09 TW/cm^{-2}. Another feature is that the TL-pulse has a FWHM temporal width of Δt=147fs, while the optimized laser pulse has stretched to $\sim$5.5 ps. The optimized laser field also contains 4.07μJ of the total original 10μJ from the TL-pulse.

The state transitions that the ACNOT$_1$ gate must control, see Table 2.1, are shown in the state population graphs of Fig. 2.3(a)-2.3(d). Since the average population is relatively high at 0.9904, it is expected that all transitions are well controlled. The $|00\rangle \leftrightarrow |01\rangle$ transition according to Fig.2.3(a) and Fig.2.3(b) occurs via a complex 2-state transfer, with little excitation of outlying states. For the other qubit states of the ACNOT$_1$ gate operation, they must remain the same after the laser field interaction. The only change that must occur is that both qubits $|10\rangle$ and $|11\rangle$ must acquire a global phase change, as did the transition $|00\rangle \leftrightarrow |01\rangle$. For this to occur the states must undergo some population change and this is seen in Fig.2.3(c) and Fig.2.3(d). The resulting phase changes undergone in the qubit transformations $|00\rangle \leftrightarrow |01\rangle$, $|10\rangle \rightarrow |10\rangle$ and $|11\rangle \rightarrow |11\rangle$ are -1.055, -1.303 and -0.937 radians respectively. The phase change for the $|10\rangle \rightarrow |10\rangle$ transition is higher than that obtained for the other two qubit transformations. This could be due to some population being lost from the qubit state $|10\rangle$ by the end of the pulse interaction resulting in $P_{(21)}$=0.9739, compared to the final populations of the other states, $P_{(12)/(01)}$=0.9944 and $P_{(10)}$=0.9988.

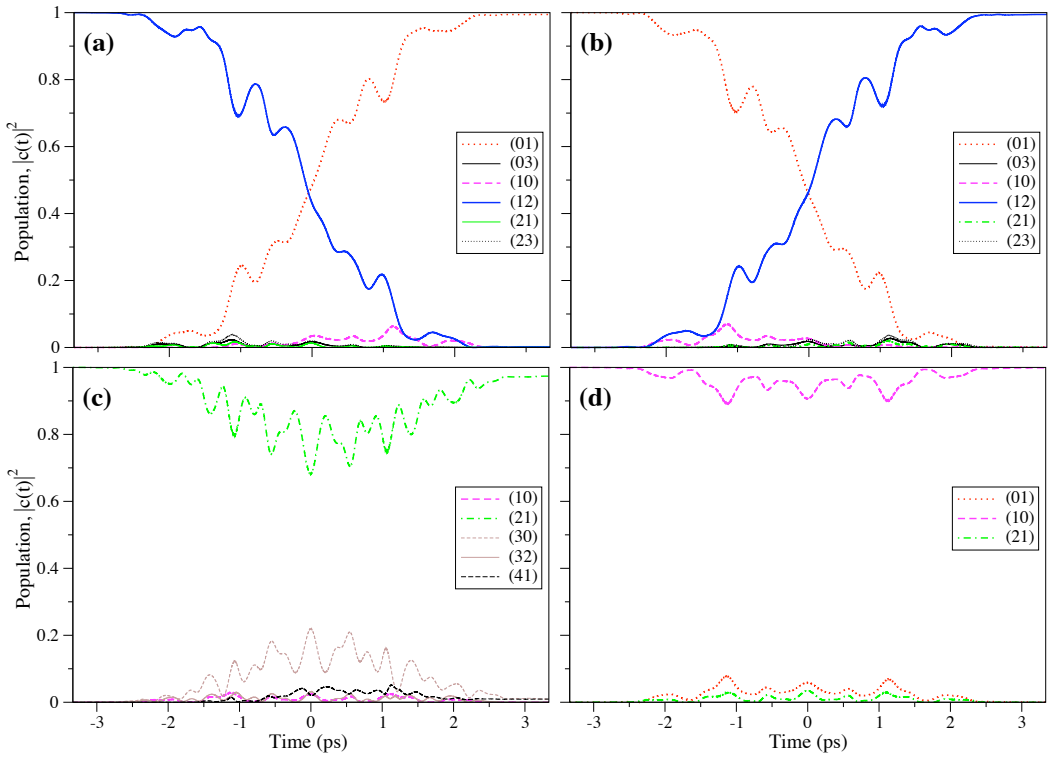

Figure 2.3: Resulting populations for the optimized ACNOT_1 quantum gate at E_{pulse}=4.07μJ . a)-d) Propagation of states with the ACNOT_1 optimized laser pulse over the pulse duration for transitions: a)$|00\rangle \rightarrow |01\rangle$, b)$|01\rangle \rightarrow |00\rangle$, c)$|10\rangle \rightarrow |10\rangle$ and d)$|11\rangle \rightarrow |11\rangle$. The most important contributing rovibrational states are shown.

2.3.3 NOT_2 Quantum Gate

The optimal NOT_2 quantum gate laser pulse is shown in Fig.2.4 in both the frequency and time domain. The resulting population transitions for the gate operation are in Fig.2.5. The optimal NOT_2 gate laser pulse has frequency components associated with the gate transitions, (21) $\leftrightarrow$ (10) and (12) $\leftrightarrow$ (01), 2121cm^{-1} and 2151cm^{-1} respectively , as well as 2139 cm^{-1} which is the (10) $\leftrightarrow$ (01) transition not required for the NOT_2 gate operation. The (21) $\leftrightarrow$ (12) transition frequency, 2109cm^{-1} is not present. The resulting intensity of the laser pulse in the time domain is shown in Fig.2.4(b), where the TL-pulse has been scaled down by a factor of 0.10. The TL-pulse this time has a peak intensity of 3.25 TW/cm^{-2}, while the optimized laser pulse has a peak of 0.29 TW/cm^{-2}. The TL-pulse has a temporal width of Δt=147fs, while the optimized laser pulse spans a length of $\sim$6ps and contains 12.20μJ of the total original 20μJ from the TL-pulse.

The average final population obtained for the optimal NOT_2 quantum gate is 0.6025, indicating that the laser pulse populates other accessible states. This is shown in Fig.2.5(a)-Fig.2.5(d), where there are many other states appreciably populated by the end of the pulse duration. Excitation to other non qubit states is seen for all optimal laser pulses obtained for the Hadamard and NOT gates.

The fidelities for the Hadamard and NOT gates are not as high as those obtained for the CNOT and ACNOT gates. The implications of this is that the qubit states under the quantum gate operation, which must acquire a global phase by the end of the pulse duration, are in fact not coherent. The phase changes undergone during the NOT_2 operation for example are -0.4817 and 0.3136 radians for the transitions, $|10\rangle \rightarrow |11\rangle$ and $|00\rangle \rightarrow |01\rangle$, respectively. The phase changes may be of similar magnitude but are different by a shift of over $\pi/4$ radians. Indeed the NOT_2 gate and other binary laser pulses optimized for the Hadamard and NOT quantum gates have difficulty in controlling

not only the average population but also the global phase.

2.4 Conclusion

It was shown in this study that simple binary shaped pulses can provide sufficiently good control for quantum gate operations with a proper choice of qubits represented by rovibrational states of $^{12}C^{16}O$. In some cases, as in the CNOT and ACNOT gates, remarkable control is achieved considering the simplicity of the binary pulse shape. The fidelities obtained further improve on previous work by Tsubouchi and Momose,[15] in which they used a variation of 64 amplitudes and 64 phases, along with a qubit representation that included 2-photon transitions. As a result, the optimal input pulse energies and peak intensities produced for the CNOT and ACNOT gates were much larger than those needed in our study. The optimized NOT and Hadamard gate laser pulses produced only moderate fidelities since the required 2-qubit operation consisted of controlling population and phase between all four qubits simultaneously. Current work is directed at investigating general properties of molecular systems and pulse shapers in order to deduce crucial requirements for control of molecular states with shaped laser pulses. Future work involves studying in more detail the underlying features of binary pulses which allows them to exhibit such good control.

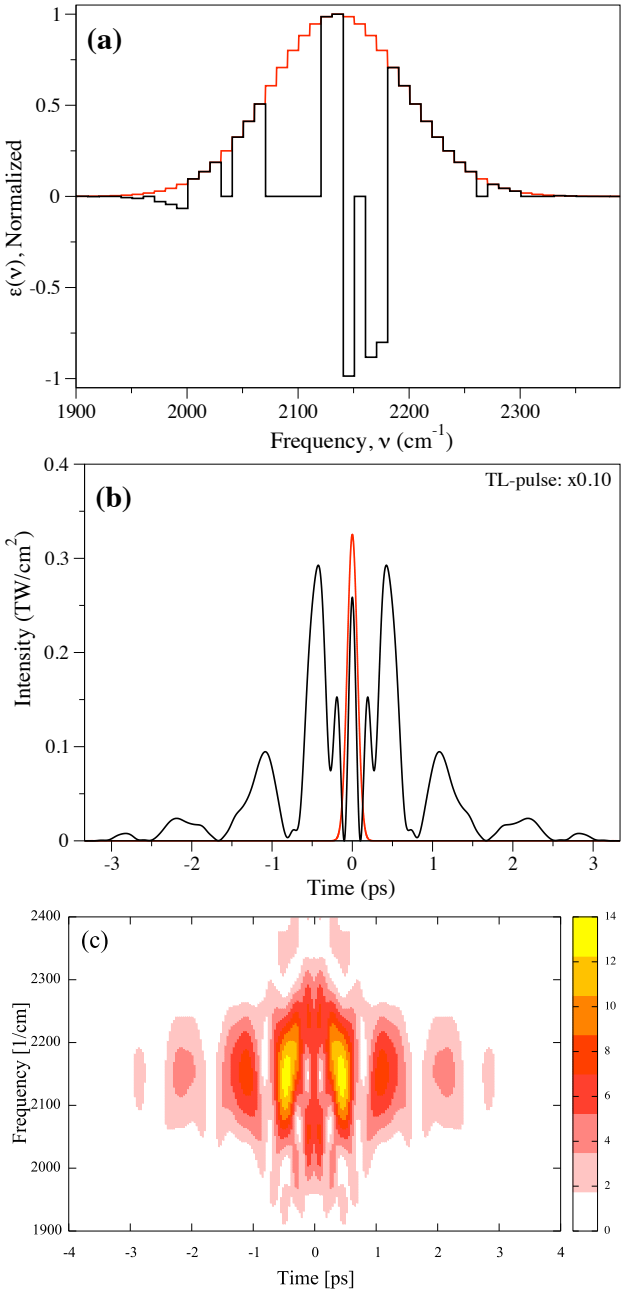

Figure 2.4: Resulting laser pulse for the optimized NOT_2 quantum gate at E_{pulse}=12.20μJ . a) Frequency domain $\epsilon(\nu)$, where negative values denote a phase $\phi(\nu) = \pi$ radians. Red: TL-pulse, black: Optimized pulse. b) Time domain intensity, $|\epsilon(t)|^2$. Red: TL-pulse (intensity scaled by a factor of 0.10), black: optimized pulse. c) XFROG trace for the obtained optimal field.

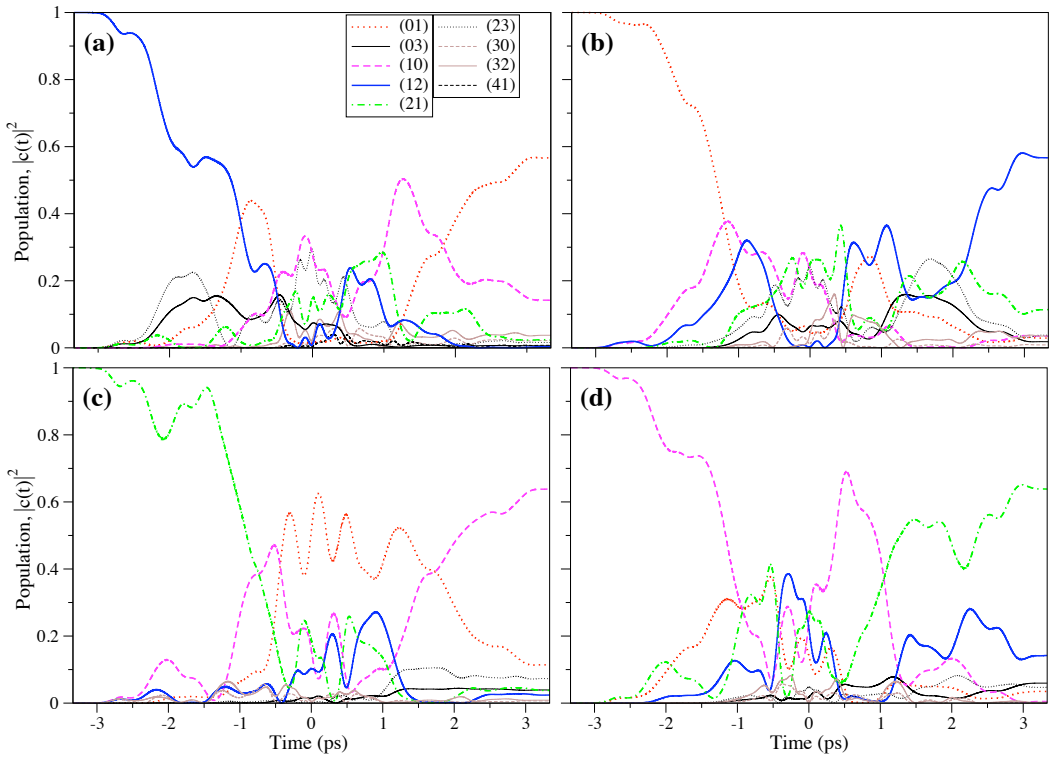

Figure 2.5: Resulting populations for the optimized NOT_2 quantum gate at E_{pulse}=12.20μJ . a)-d) Propagation of states with the NOT_2 optimized laser pulse over the pulse duration for transitions: a)$|00\rangle \rightarrow |01\rangle$, b)$|01\rangle \rightarrow |00\rangle$, c)$|10\rangle \rightarrow |11\rangle$ and d)$|11\rangle \rightarrow |10\rangle$. The most important contributing rovibrational states are shown.

Bibliography

[1] M. Shapiro, P. Brumer, *Principles of the Quantum Control of Molecular Processes*, (Wiley, 2003)

[2] S. Rice, M. Zhao,*Optical Control of Molecular Dynamics*, (Wiley, 2000).

[3] G. Balint-Kurti, S. Zou, A. Brown, Advances in Chemical Physics, **138**, 43 (2008)

[4] M. Dantus, V. Lozovoy, Chem. Rev. **104**, 1813 (2004)

[5] T. Brixner, G. Gerber, Chem. Phys. Chem. **4**, 418 (2003)

[6] I. Znakovskaya, P. von den Hoff, S. Zherebtsov, Phys. Rev. Lett. **103**, 103002 (2009)

[7] T. Zuo, A. Bandrauk, P. Corkum, Chem. Phys. Lett. **259**, 313 (1996)

[8] G. Yudin, A. Bandrauk, P. Corkum, Phys. Rev. Lett. **96**, 63002 (2006)

[9] C. Tesch, R. de Vivie-Riedle, Phys. Rev. Lett. **89**, 157901 (2002)

[10] D. Babikov, J. Chem. Phys. **121**, 7577 (2004)

[11] K. Shioya, K. Mishima, K. Yamashita, Molec. Phys. **105**, 1283 (2007)

[12] C. Tesch, L. Kurtz, R. de Vivie-Riedle, Chem. Phys. Lett. **343**, 633 (2001)

[13] B. Korff, U. Troppmann, K. Kompa, R. de Vivie-Riedle, J. Chem. Phys. **123**, 244509 (2005)

[14] D. Weidinger, M. Gruebele, Molec. Phys. **105**, 1999 (2007)

[15] M. Tsubouchi, T. Momose, Phys. Rev. A **77**, 052326 (2008)

[16] L. Vandersypen, M. Steffen, G. Breyta, C. Yannoni, M. Sherwood, I. Chuang, Nature **414**, 883 (2001)

[17] E. Knill, R. Laflamme, R. Martinez, C. H. Tseng, Nature **404**, 368 (2000).

[18] F. Schmidt-Kaler, H. Häffner, M. Riebe, S. Gulde, G. Lancaster, T. Deuschle, C. Becher, C. Roos, J. Eschner, R. Blatt, Nature **422**, 408 (2003)

[19] S. Gulde, M. Riebe, G. P. T. Lancaster, C. Becher, J. Eschner, H. Häffner, F. Schmidt-Kaler, I. L. Chuang, R. Blatt, Nature **421**, 48 (2003).

[20] J. Vala, Z. Amitay, B. Zhang, S. Leone, R. Kosloff, Phys. Rev. A **66**, 62316 (2002)

[21] J. Ahn, T. C. Weinacht, P. H. Bucksbaum, Science **287**, 463 (1994)

[22] W. Zhu, J. Botina, H. Rabitz, J. Chem. Phys. **108**, 1953 (1998)

[23] R. Judson, H. Rabitz, Phys. Rev. Lett. **68**, 1500 (1992)

[24] B. Amstrup, J. Doll, R. Sauerbrey, G. Szabo, A. Lorincz, Phys. Rev. A **48**, 3830 (1993)

[25] C. Gollub, R. de Vivie-Riedle, Phys. Rev. A **79**, 021401 (2009)

[26] A.W. Mantz, J.P. Maillard, W.B. Roh, K.N. Rao, J. Mol. Spec. **155**, 57 (1975)

[27] D. Goorvitch, C. Chackerian, Astrophys. J. Suppl. Ser. **91**, 483 (1994)

[28] J. Palao, R. Kosloff, Phys. Rev. A **68**, 62308 (2003)

[29] C. Tesch, R. de Vivie-Riedle, J. Chem. Phys. **121**, 12158 (2004)

[30] C. Gollub, R. de Vivie-Riedle, Phys. Rev. A **78**, 033424 (2008)

[31] M. Tsubouchi, A. Khramov, T. Momose, Phys. Rev. A **77**, 023405 (2008)

[32] F. Langhojer, D. Cardoza, M. Baertschy, T. Weinacht, J. Chem. Phys. **122**, 014102 (2005)

[33] M. Schröder, A. Brown, New J. Phys. **11** 105031 (2009)

[34] U. Troppmann, R. de Vivie-Riedle, J. Chem. Phys. **122**, 154105 (2005)

[35] B. Schneider, C. Gollub, K. Kompa, R. de Vivie-Riedle, Chem. Phys. **338**, 291 (2007)

[36] V. Lozovoy, T. Gunaratne, J. Shane, M. Dantus, Chem. Phys. Chem. **7**, 12 (2006)

[37] D.L. Carroll, Genetic Algorithm driver **v1.7.0** (2004).

Chapter 3

Effect of diatomic molecular properties on binary laser pulse optimizations of quantum gate operations.††

3.1 Introduction

Although in principle a molecule or ensemble of molecules could be used as a quantum computer, experimental control of such systems is difficult. Using nuclear states of an ensemble of perfluorobutadienyl iron complex[1], cytosine[2] or chloroform[3] in Nuclear Magnetic Resonance (NMR) or electronic states of $^{9}Be^{+}$ or $^{40}Ca^{+}$ ions in an electric field trap[4, 5], have been shown to be possible architectures for a quantum computer. Another proposal uses molecular states (electronic, vibrational and/or rotational) and a shaped laser pulse to manipulate them[6–8]. A set of molecular states is chosen to act as the quantum bits (qubits) and a laser pulse is shaped accordingly to act as a quantum logic gate on the chosen qubits. The qubit can be described as a 2-level state vector and is analogous to the classical bit. Molecular quantum

computing with shaped laser pulses also warrants the advantage of satisfying all five of DiVincenzo's criteria[9], which define feasible quantum computers. Furthermore, diatomic molecules exhibit very long decoherence times, allowing for many laser pulse interactions before substantial information loss. Shaping laser sources in the mid-IR, corresponding to ro-vibrational state transition frequencies, was an initial limitation but this has been overcome[10]. Despite the theoretical interest in this approach, there has been few experimental implementations utilizing shaped laser pulses for molecular quantum computing [11].

The many theoretical contributions include, (i) studying molecular systems: modes of acetylene[6, 12, 13], ammonia[14, 15] and thiophosgene[16], vibrational/ro-vibrational excitations within diatomics[17–25] and of dipole-dipole coupled diatomics[26], and (ii) investigating experimental issues[10, 27, 28]. Many of the theoretical studies were based on iterative optimal control theory[29] (OCT) and the resulting pulses were inaccessible to present experiments, e.g., shaped in both the mid-IR and microwave frequency regimes. A more appropriate theoretical method, and one which attempts to mimic experimental implementation, is to both shape in the frequency domain and use a Genetic Algorithm[30] (GA) to optimize the laser pulse. Some diatomic molecules studied using OCT include CO[19], NO[20], OH[21, 25], Na_2 and Li_2[22],NaCs[23], I_2[24] and those which incorporate laser pulse shaping in the frequency domain using the GA is CO[17, 18]. The small number of diatomics studied using frequency shaped GA optimized laser pulses encouraged this current study. Within theoretical laser molecular control, there are two obvious options in determining optimal control either by: (i) varying the experimental laser pulse parameters or (ii) varying the intrinsic molecular properties. In our previous analysis[18], good control was exhibited by binary laser pulse shaping on a set of universal quantum logic gates for the diatomic $^{12}C^{16}O$. Binary shaped laser pulses, which consist of two amplitude and two phase variation, are the easiest to shape experimentally and are also used in this study.

We currently investigate the effect of varying the intrinsic molecular parameters of ro-vibrational state energy on the ability to control specific quantum logic gates ($ACNOT_1$ and NOT_2). By varying the vibrational anharmonicity and rotational constants systematically, diatomics that exhibit properties allowing them to be well controlled by a binary shaped laser pulse can be determined. The $ACNOT_1$ quantum gate exhibited the best control using binary pulse shaping in our previous work on $^{12}C^{16}O$[18]. Optimization was initially implemented using a GA to determine optimally shaped laser pulses as discussed in our previous work. In order to ensure that the obtained fidelities are due to the intrinsic molecular properties and not the optimization algorithm, we carried out further optimizations using a cubic spline fit GA procedure[17, 28] and also using the popular iterative OCT optimization[29]. The optimization comparison was carried out on a set of diatomics for the $ACNOT_1$ gate. Binary pulse GA optimizations for the $ACNOT_1$ and NOT_2 quantum logic gates were carried out on a larger set of diatomics.

3.2 Theory

An investigation of a variety of diatomics and their ability to be used for molecular quantum computing, using shaped laser pulses, is of interest to experimental pursuits. Laser pulses were constructed, by optimization using a discretized GA routine, to represent the $ACNOT_1$ and NOT_2 quantum gate operations. Other popular optimization techniques, the cubic spline fit GA and OCT, were used to test, verify and compare the resulting fidelities.

3.2.1 Model System

The ro-vibrational states (ν,J) of diatomics consisting of the lowest energy vibrational (ν) and rotational states (J), are used. Our calculations are relevant to diatomics with closed shell electron configurations in their ground electronic states. The projection of the total angular momentum (J_z) is zero.

Select rovibrational states of the diatomic are used to represent the qubits $|q_1 q_2\rangle$ for quantum gate operation, namely: $|00\rangle \equiv (1,2)$, $|01\rangle \equiv (0,1)$, $|10\rangle \equiv (2,1)$, $|11\rangle \equiv (1,0)$ in order to implement single photon transitions. The transition dipole moment values used are those calculated by Goorvitch et al.[31] for carbon monoxide. The choice of transition dipoles should have a modest effect on the resulting optimized laser pulses by only affecting the relative field intensities. The mid-IR pulses are optimized to cause simultaneous rotational and vibrational state transitions according to $\Delta J = \pm 1$ and $\Delta \nu = \pm 1$. A more detailed explanation of the quantum mechanical system, choice of molecular qubit basis and quantum gates, and structure of the laser pulse can be obtained from our previous study[18].

The general time-dependent Schrödinger equation (TDSE) can be written as a vector of time-dependent coefficients $\underline{c}(t)$, ro-vibrational state energy matrix $\underline{\underline{E}}$, transition dipole moment matrix $\underline{\underline{\mu}}$ and the electric field of the laser pulse $\epsilon(t)$:

$$\dot{\underline{c}}(t) = -\frac{i}{\hbar}\left[\underline{\underline{E}} - \epsilon(t)\underline{\underline{\mu}}\right]\underline{c}(t). \tag{3.1}$$

The task is to determine the structure of the electric field of the laser pulse such that it induces transitions from the chosen initial state $\underline{c}(0)$ to the chosen final state $\underline{c}(T)$ with ideally 100% success. The TDSE was solved at every time step by using the fourth-order Runge-Kutta method. The time steps (6×10^{-6}ps for the GA and 1×10^{-4}ps for OCT) were chosen to be much smaller than the oscillation period of the laser pulse having a total time duration of T=6.67 ps.

The ability to produce optimal laser pulses to carry out quantum gate operations on various diatomics was tested by varying the ro-vibrational state energies. The energy values were obtained by using the Taylor series expansion

in energy for an oscillating rotator (i.e. model diatomic)[32]:

$$\begin{aligned} E_{\nu J} &= \omega_e(\nu+1/2) - \omega_e\chi_e(\nu+1/2)^2 + ... - \omega_e b_e(\nu+1/2)^6 + \\ & J(J+1)[B_e - \alpha_e(\nu+1/2) + \gamma_e(\nu+1/2)^2 - \delta_e(\nu+1/2)^3] - (3.2) \\ & J^2(J+1)^2[D_e - \beta_e(\nu+1/2) + \pi_e(\nu+1/2)^2] + \\ & J^3(J+1)^3[H_e - \eta_e(\nu+1/2)] \end{aligned}$$

The anharmonicity ($\omega_e\chi_e$) and rotational constant (B_e) are the largest contributors to changes in the ro-vibrational state transition energies and subsequently values for these parameters were varied. The remaining 13 coefficients of Eq.3.2 were taken from work done by Mantz et al. for carbon monoxide[32]. A plot of the anharmonicity and rotational constants of some 42 common heteronuclear diatomic species[33] are shown in Fig.3.1. The values shown in Fig.3.1 exclude diatomics containing hydrogen and/or deuterium which lie in a separate region of the graph. A linear fit to the plotted values (Fig.3.1, solid line) is represented by the equation of the middle line, $B_e = 0.136\omega_e\chi_e - 0.06$. The values studied along this line range from $4.19 < \omega_e\chi_e < 16.60$ and $0.51 < B_e < 2.20$. Also studied were values for the anharmonicity and rotational constants taken from an upper line parallel to the linear fit (Fig.3.1, dashed line) and represented by the equation, $B_e = 0.136\omega_e\chi_e + 0.099$. This upper line extends from $7.79 < \omega_e\chi_e < 15.42$ and $1.16 < B_e < 2.2$, nearly crossing the values for carbon monoxide at $\omega_e\chi_e$=13.288 and B_e=1.93. Initially, binary pulse GA optimizations were carried out on the upper line for the ACNOT$_1$ gate. The ACNOT$_1$ gate produced the greatest fidelity in our previous studies[18]. Subsequent spline-GA and OCT optimizations were carried out along this line to further verify the resulting trends of the fidelities as a function of $\omega_e\chi_e$ and B_e. Population only GA optimizations were also carried out along this upper line to compare to analogous phase optimized fidelities (see Eq.3.4 in Sec.3.2.3). Further binary pulse GA optimizations were carried out on the line of linear fit for both the ACNOT$_1$ and NOT$_2$ gates with and without global phase alignment. The NOT$_2$ quantum gate was cho-

sen because in previous work it produced low fidelities and shares a common transition with $ACNOT_2$.

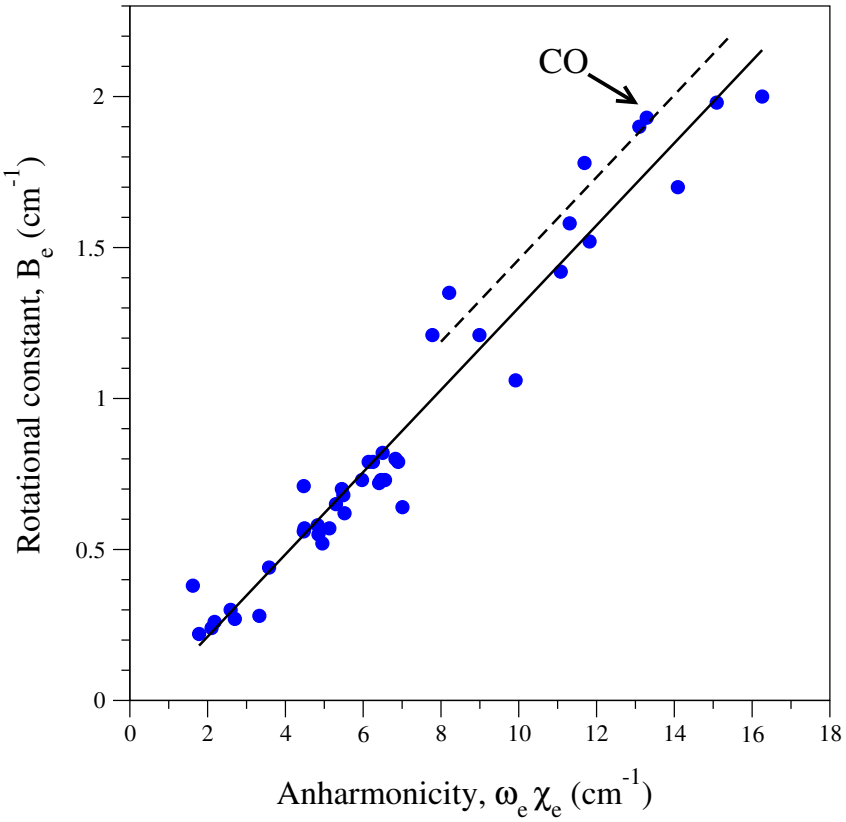

Figure 3.1: (Color online) Anharmonicities ($\omega_e\chi_e$) plotted against rotational constants (B_e) for a variety of diatomic molecules[33]. A linear fit to these values (solid line) and an upper line (dashed line) with the same slope as the linear fit are shown. The position of carbon monoxide (CO) is indicated.

3.2.2 Quantum Logic Gates

A more detailed explanation of the $ACNOT_1$ and NOT_2 quantum logic gates can be found in previous work[18]. The $ACNOT_1$ and NOT_2 gates are selected from a set of universal quantum logic gates that would be required in a quantum algorithm. In previous work[18], also using binary shaped laser pulse optimization but on $^{12}C^{16}O$, the $ACNOT_1$ gate produced the best optimized laser pulse compared to the other seven gates studied, while the NOT_2

gate produced one of the lowest fidelities. The ACNOT_1 and NOT_2 gates also share a common transition, $|00\rangle \leftrightarrow |01\rangle$, as shown in Table.3.1. In this current study we choose to further optimize laser pulses representing the ACNOT_1 and NOT_2 gates but for a range of diatomic species as detailed in Sec.3.2.1.

The ACNOT_1 and NOT_2 gates manipulate the ro-vibrational state qubits, with an acquired phase $e^{i\theta_n}$, as shown in Table 3.1.

ACNOT_1	NOT_2
$\|00\rangle \rightarrow \|01\rangle e^{i\theta_1}$	$\|00\rangle \rightarrow \|01\rangle e^{i\theta'_1}$
$\|01\rangle \rightarrow \|00\rangle e^{i\theta_2}$	$\|01\rangle \rightarrow \|00\rangle e^{i\theta'_2}$
$\|10\rangle \rightarrow \|10\rangle e^{i\theta_3}$	$\|10\rangle \rightarrow \|11\rangle e^{i\theta'_3}$
$\|11\rangle \rightarrow \|11\rangle e^{i\theta_4}$	$\|11\rangle \rightarrow \|10\rangle e^{i\theta'_4}$

Table 3.1: Two quantum gate operations which are implemented by an optimized laser pulse. Each gate operation on each qubit acquires an arbitrary phase, $e^{i\theta_n}$.

3.2.3 Laser Pulse Optimization

In order to optimize laser pulses for control of specific quantum gate transitions, an optimization routine is implemented. In this study both the Genetic Algorithm (GA), a heuristic algorithm, and optimal control theory (OCT), an iterative optimization routine, are used. The GA optimizes the combination of parameters (amplitude and phase; Eq.3.3 in Sec.3.2.3) associated with each frequency to produce an optimal laser pulse. Alternatively, the iterative OCT algorithm offers the greatest laser pulse flexibility, in frequency composition and electric field amplitude, with optimization occurring in the time domain. It is also a monotonically convergent algorithm, whereas the GA being a heuristic search space optimization, relies on appropriate sampling of the search space to obtain suitable solutions. Within the context of laser pulse shaping, the discretized frequency domain optimization is used because the fields constructed resemble those that are designed experimentally.

In order to determine if the resulting fidelities of the upper line (Fig.3.1; dashed line) were due to intrinsic molecular properties, alternative methods were also carried out, namely: (i) cubic spline interpolated GA optimization, (ii) OCT using a Transform Limited (TL) pulse as an initial guess, and (iii) OCT using the resultant discrete GA optimized laser pulse as an initial guess.

Genetic Algorithm (GA)

The GA is an evolutionary optimization algorithm and incorporates aspects of biology such as mutation, cross-over and survival of the fittest. For a thorough explanation of the GA algorithm incorporated in this study see work by Carroll [30]. The GA optimizes a laser pulse field in the frequency domain with discretized frequencies ν_j. The laser pulse has a Gaussian profile, with amplitude A(ν_j) and phase $\phi(\nu_j)$, of the following form:

$$\epsilon(\nu_j) = \epsilon_0 \sqrt{A(\nu_j)} \exp\left[-2\ln 2\left(\frac{\nu_j - \nu_0}{\Delta\nu}\right)^2\right] \exp\left[i\phi(\nu_j)\right], \qquad (3.3)$$

The laser pulse spectrum has a full width half-maximum (FWHM) of $\Delta\nu$=100 cm^{-1}, peak field strength ϵ_0 and frequency range of $\pm$ 250 cm^{-1} from the central frequency ν_0. The central frequency is chosen, for the ACNOT$_1$ gate, to be the transition from $|00\rangle \rightarrow |01\rangle$. For the NOT$_2$ gate it is the average of the $|00\rangle \rightarrow |01\rangle$ and $|10\rangle \rightarrow |11\rangle$ transitions. The maximum energy attainable by an ACNOT$_1$ quantum gate shaped laser pulse is 10μJ and for the NOT$_2$ gate is 20μJ. Though the amplitude and phase can range from $0 \leq A(\nu_j) \leq 1$ and $0 \leq \phi(\nu_j) \leq 2\pi$, we restrict ourselves to binary laser pulse shaping and thus $A(\nu_j)$=0 or 1 and $\phi(\nu_j)$=0 or π. Each of the 51 frequency components has an associated amplitude and phase, each with a spectral width of dν=10 cm^{-1}. The pulse duration of T=6.67ps is the zero crossing for the pulse envelope of a discretized frequency spectrum, according to T=2/dν. The task of the GA is to search the parameter space of amplitudes and phases at each frequency (ν_j) in a manner that requires evaluating only a small number of combinations. In this case there are 4^{51} total combinations of amplitude and

phase for all frequencies, to produce laser pulses. The GA shows little change between generations after evaluating only 8000 laser pulse combinations (500 generations each with 16 individuals per generation).

When a laser pulse spectrum, $\epsilon(\nu)$ is produced, it must be transformed to the time domain in order to solve the TDSE. This is carried out by either: (i) Fourier transforming the discretized frequency spectrum, $\epsilon(\nu_j)$, directly or (ii) cubic spline interpolating the discretized frequency spectrum $\epsilon(\nu_j)$ followed by Fourier transforming. The two methods do not in general produce identical results since a spline interpolated frequency spectrum may not reflect the original discretized spectrum[17]. The cubic spline interpolates an extra 10 points between each frequency component to produce a curve consisting of 510 points.

During optimization the GA requires a value to weight the effectiveness of a laser pulse to carry out the required gate operation. This value is described by the fidelity function[34], F:

$$F = \frac{1}{N^2} \left| \sum_{k=1}^{N} \langle \Psi_k(T) | \Phi_k \rangle \right|^2 , \tag{3.4}$$

The summation of the overlap of the resulting state after laser pulse interaction, $\psi_k(T)$, to the target final state, ϕ_k, results not only in population control but also in global phase alignment. Global phase alignment is the task of inducing phase changes by the laser pulse on the qubits such that by the end of the pulse interaction the qubits are all phase aligned [21, 35]. This is equivalent to making the acquired phases (θ_1, θ_2, θ_3, θ_4) equal, see Table 3.1. Qubits which are not aligned appropriately within the group will undergo a different phase change when subsequent laser pulses are applied, leading to an ineffective quantum gate operation.

Within both types of GA optimization procedures the 7 lowest energy vibrational states are used each containing the 9 lowest energy rotational states were used.

Optimal Control Theory (OCT)

The alternative optimization routine implemented and the most widely used within laser molecular control is optimal control theory (OCT)[29]. It consists of maximizing an objective function that contains three terms. The first is an average population term, the second term consists of the field components and the last term satisfies the TDSE:

$$J = \sum_k \left|\left\langle \Psi_i^k(T)|\Phi_f^k\right\rangle\right|^2 - \int_0^T \frac{\alpha_0}{s(t)} \left|\epsilon(t)\right|^2 dt - \sum_k 2Re\left[\left\langle \Psi_i^k(T)|\Phi_f^k\right\rangle \int_0^T \left\langle \Psi_j^k(t)\left|i\left[H_0 - \mu\varepsilon(t)\right] + (\partial/\partial t)\right|\Psi_i^k(t)\right\rangle dt\right] \tag{3.5}$$

Ψ_i^k is the resulting wavefunction after interaction with the laser pulse field of the ith state for the kth qubit transformation for the specific quantum logic gate. Φ_f^k is the target state of the qubit transformation for the specific quantum logic gate. The electric field term in the objective function contains the electric field, $\epsilon(t)$, and the penalty parameter, α_0, which is an arbitrary constant that determines the weight of the field term on the resulting objective function, J. The penalty parameter is important for appropriate laser pulse optimization and chosen (based upon numerical experimentation) to be α_0=10. The objective functional is maximized to produce a laser pulse that acts as one of the quantum gate operations being studied (see Table 3.1). The OCT fields produced have the same pulse duration of T=6.67 ps as the GA calculations. The laser pulse envelope, *s(t)* with amplitude s_0, is defined by:

$$s(t) = s_0 \sin^2\left(\pi t/T\right). \tag{3.6}$$

As stated previously, the quantum gate operation being represented by the optimized laser pulse not only induces a change in population but must also induce a global phase alignment between the qubits. Within the GA this was accomplished through the fidelity function, F (Eq.3.4). The simplest process of including global phase alignment within OCT without altering the objective function, and thus subsequent maximization, is to include an auxiliary

transition to optimize[35]:

$$\begin{aligned}&\left[|\Psi_{00}\rangle + |\Psi_{01}\rangle + |\Psi_{10}\rangle + |\Psi_{11}\rangle\right]_{t=0} \quad \longrightarrow \\ &\left[(|\Psi_{00}\rangle + |\Psi_{01}\rangle + |\Psi_{10}\rangle + |\Psi_{11}\rangle)e^{i\theta_5}\right]_{t=T}\end{aligned} \tag{3.7}$$

This fifth stipulation on the requirement for the resultant optimized laser field is incorporated within the summation of the first term of the objective function. The qubits, after operation by the laser pulse, are then biased to shift by the same amount of phase, $e^{i\theta_5}$ (global phase alignment). Phase alignment is in general more difficult to optimize than population. To increase the weight of phase alignment within OCT, four instances of Eq.3.7 were included, along with the four transitions required for the ACNOT_1 gate, hence a summation of k in Eq.3.5 over 8 terms. This method for incorporating global phase alignment by including Eq.3.7 is not equivalent to the fidelity within the GA. During OCT optimizations the fidelity, though not used for OCT optimization, was also calculated in order to compare OCT to GA results.

Within the OCT algorithm, the lowest 4 vibrational state energies each containing the lowest 4 rotational state energies were used for the three diatomics that produced the greatest fidelities within the discretized GA, namely: $\omega_e\chi_e(B_e)$=8.087(1.20)cm^{-1}, 13.44(1.93)cm^{-1} and 14.69(2.10)cm^{-1}. All others diatomics using OCT were optimized using the 5 lowest energy vibrational states containing the 5 lowest energy rotational states. The validity of using these reduced sets was verified by propagating the OCT optimized laser pulses using 7 vibrational states each containing 9 rotational states, which was used in the GA optimizations. The error in the fidelity, i.e. the difference between the 7×9 model and the reduced set of ro-vibrational states, is at most $|\Delta\text{F}|=|0.04|$.

3.3 Results and Discussion

3.3.1 $ACNOT_1$ optimizations for diatomics along the upper line of Fig.3.1

Optimization methods comparison

The fidelities for laser pulses optimized using the four GA and OCT methods (described in Sec.3.2.3) for the $ACNOT_1$ gate of diatomics along the upper dashed line of Fig.3.1 are shown in Fig.3.2. The resulting fidelities of the cubic spline GA optimizations (hollow red dots/lines) are in good qualitative agreement with the discretized GA (solid black dots/lines), of Fig.3.2.

Laser pulses optimized with the OCT algorithm should provide the greatest variation to the electric field. Thus if possible OCT would produce optimized laser pulses with very complex features but producing near 100% fidelity. The results using OCT with a TL pulse guess field in Fig.3.2 (hollow blue squares), show some instances where there is a difficulty in producing sufficiently high fidelities. The OCT using a TL pulse as a guess field failed to find laser fields of comparable fidelity to the discretized GA, even though solutions were found when the discretized GA results were used as a guess field within OCT calculations (Fig.3.2, solid green squares). This could be due to a poor choice in guess field (i.e. a TL pulse), the enforced pulse envelope $s(t)$, or the choice of the penalty parameter α_0. In general the resulting fidelities for the OCT calculated laser fields follow the same qualitative structure as the fidelities for the discretized GA calculated laser fields. Overall the qualitative features in Fig.3.2 are observed independent of the laser pulse optimization procedure employed. These results imply that the relative arrangement of rovibrational state energy levels, in other words the choice of diatomic, has a great impact on the resulting fidelity and ability to shape laser pulses for specific quantum gate operations. Further discretized GA optimizations were carried out for diatomics along the linear fit of Fig.3.1 for the $ACNOT_1$ and NOT_2 quantum logic gates.

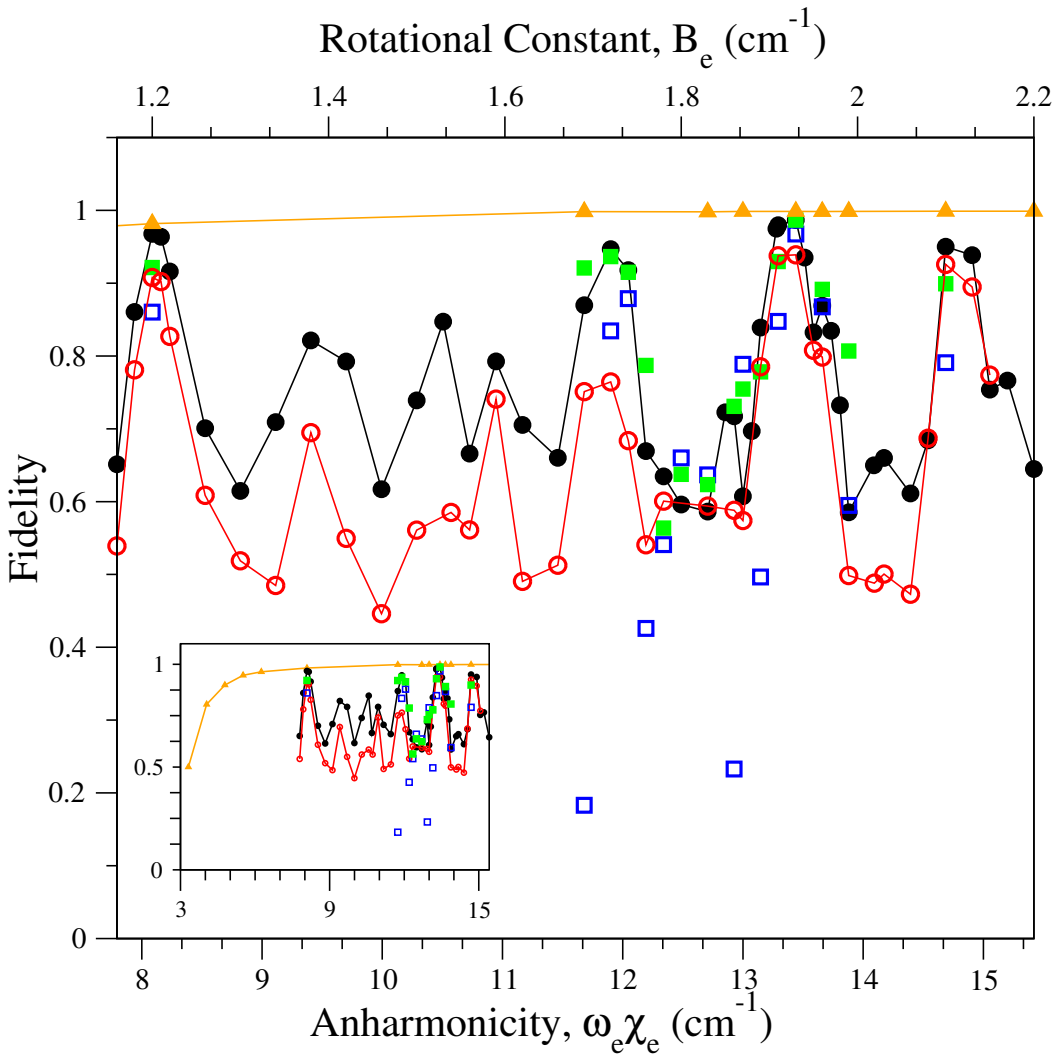

Figure 3.2: (Color online) Resulting fidelities of optimized laser pulses for the quantum logic gate $ACNOT_1$ for values of anharmonicity and rotational constants of the upper line (dashed line, Fig.3.1) using the following globally phase aligned methods: (i) discretized GA (solid black dots/lines), (ii) cubic spline interpolated GA (hollow red dots/lines), (iii) OCT with a TL pulse as a guess field (hollow blue squares), (iv) OCT with the discretized GA optimized laser pulse as an initial guess (solid green squares). Fidelities for discretized GA optimized laser pulses without global phase alignment (solid orange triangles/lines) were also calculated. The inset graph illustrates the effect of optimization without global phase alignment (population only) at a greater range of $\omega_e\chi_e$ and B_e values.

Also, as a means to show that global phase alignment limits the ability to produce high fidelity shaped laser pulses, optimizations without global phase alignment using the discretized GA method were implemented (Fig.3.2; solid orange triangles/lines). The results are similar to those obtained by Babikov[21] for qubits based purely upon vibrational states, optimizing different quantum gates but still without global phase alignment. In Fig.3.2, the optimizations without global phase alignment lacked any of the complex features obtained for the other methods that enforced global phase alignment. The smooth curve produced has high fidelities at large values of $\omega_e\chi_e/B_e$ and decreases substantially at lower $\omega_e\chi_e/B_e$ values (Fig.3.2 inset; solid orange triangles/lines) - though the required anharmonicities required in the rovibrational case are much smaller than those needed when only vibrational states are considered[21].

High fidelity diatomics using the discretized GA method

Plots of the optimal frequency spectrum (Eq.3.3) and resulting population dynamics for the four largest fidelity points of Fig.3.2 of the ACNOT_1 qubit operations are illustrated in Fig. 3.3. These four points correspond to the following diatomics with vibrational anharmonicity and rotational constants: $\omega_e\chi_e(B_e)$=8.087(1.20)cm^{-1}, 11.90(1.72)cm^{-1}, 13.44(1.93)cm^{-1} and 14.69(2.10)cm^{-1}. There does not seem to be a clear and simple connection between pulse spectrum properties (binary amplitude and phase) that leads to large ACNOT_1 gate fidelities. The choice of binary amplitude plays a role in ro-vibrational state population dynamics but the choice of binary phase has a critical role in the resultant global phase alignment. Both are required in order to produce a maximum fidelity. To illustrate this, a time-dependent propagation was performed using a pulse where the central frequency (ν_0) of width 10 cm^{-1} was the only frequency component included and either a phase of ϕ=0 or ϕ=π was used. This corresponds to a positive or negative amplitude for the frequency component at ν_0 within the frequency domain, respectively

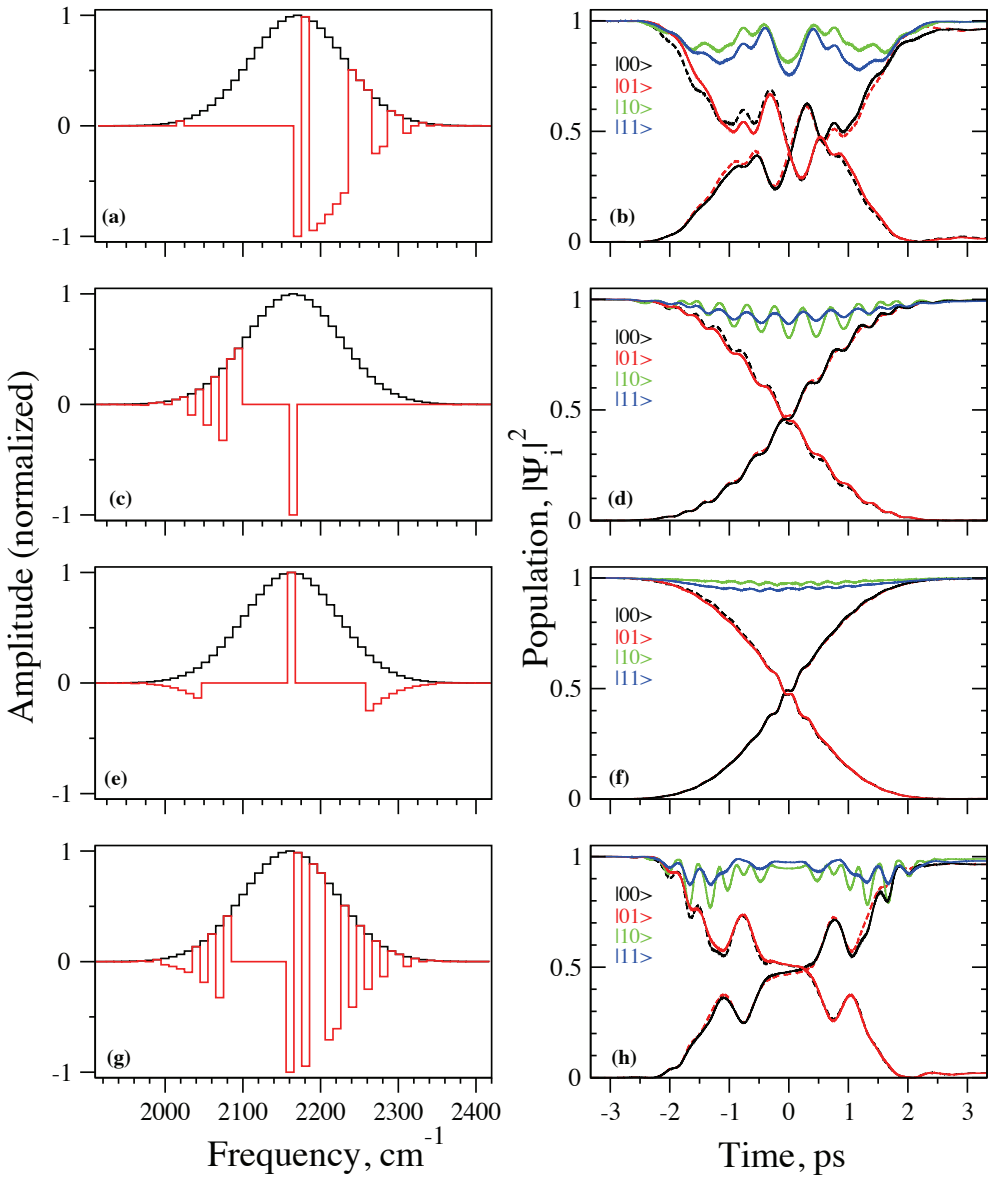

Figure 3.3: (Color online) Plots of the frequency spectrum Eq.3.3 (left column) and the corresponding qubit population for each operation within the ACNOT$_1$ gate (right column) for the 4 largest fidelity points of Fig.3.2 namely, (a,b): $\omega_e\chi_e(B_e)$=8.087(1.20)cm^{-1}, (c,d): $\omega_e\chi_e(B_e)$=11.90(1.72)cm^{-1}, (e,f): 13.44(1.93)cm^{-1}, (g,h): 14.69(2.10)cm^{-1}. Left column: (black) T-L pulse, (red) optimized pulse. Right column: (dotted black/red) $|00\rangle \rightarrow |01\rangle$, (solid red/black) $|01\rangle \rightarrow |00\rangle$, (green) $|10\rangle \rightarrow |10\rangle$, (blue) $|11\rangle \rightarrow |11\rangle$.

and a relative π-shift in phase between the two laser pulses in the time domain. Fidelities and average populations for the two pulses on each of the above four diatomics were then calculated and shown in Table 3.2.

Table 3.2: Resulting fidelities and average populations for the four highest fidelity diatomics within Fig.3.2 using only a single discretization containing the central frequency, ν_0. Also, the discretization at ν_0 is chosen to have a phase of ϕ=0 or π.

	$\boldsymbol{\phi = 0}$		$\boldsymbol{\phi = \pi}$	
$\omega_e\chi_e$ (B_e) $\mathbf{cm}^{-1}$	Fidelity F	Average Population	Fidelity F	Average Population
8.087 (1.20)	0.0662	0.9662	0.8998	0.9662
11.90 (1.72)	0.0345	0.9977	0.8999	0.9977
13.44 (1.93)	0.9865	0.9979	0.0111	0.9979
14.69 (2.10)	0.1318	0.9979	0.8478	0.9979

In all cases the choice of phase ϕ=0 or π had no effect on the population dynamics and thus the average population was the same. The choice of phase did have a dramatic effect on the fidelities though, resulting in either a high >80% or a low <14% fidelity. Moreover the arrangement of ro-vibrational states within these four high fidelity diatomics is such that much of the control, both population and global phase alignment, can be obtained by using only the one discretization of the central frequency using the current implemented spectral width, pulse energy and choice of qubits.

3.3.2 Discretized GA optimizations along the line of linear fit in Fig.3.1

$\mathbf{ACNOT_1}$ and $\mathbf{NOT_2}$ quantum gates

Laser pulse fields were optimized for the $ACNOT_1$ and NOT_2 quantum gates using the discretized GA method. Both $ACNOT_1$ and NOT_2 optimizations were implemented for diatomic species along the middle line of linear fit from Fig.3.1. The resulting fidelities produced by optimizations with global phase alignment (Eq.3.4) and without global phase alignment, along the line of linear fit, are shown in Fig.3.4.

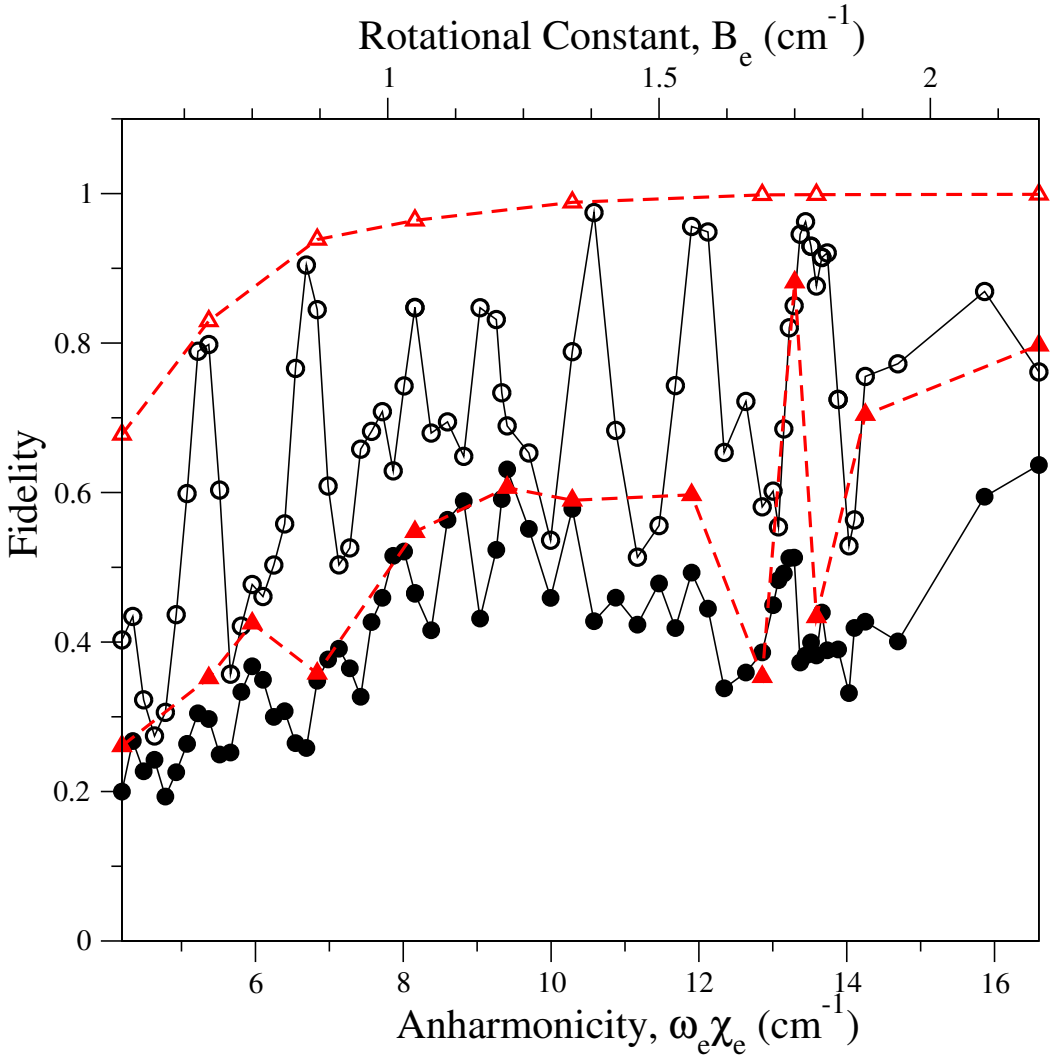

Figure 3.4: (Color online) Resulting fidelities of optimized laser pulses for the ACNOT$_1$ (hollow black dots/lines) and NOT$_2$ (solid black dots/lines) for values of anharmonicity ($\omega_e\chi_e$) and rotational constants (B_e) of the linear fit of Fig.3.1. Also plotted are respective optimizations without global phase alignment for the ACNOT$_1$ (hollow red triangles/dashed line) and NOT$_2$ (solid red triangles/dashed line) gates.

Acknowledging that the NOT_2 gate must carry out an extra transition compared to the $ACNOT_1$ may indicate why the $ACNOT_1$ gate has greater fidelities than the NOT_2 gate. In fact it is clear from further analysis (not shown here) that under the model conditions the NOT_2 gate optimization fails to control both population and phase alignment. From the regions studied and under the model conditions, there does not seem to be a diatomic that provides high fidelities for both the $ACNOT_1$ and NOT_2 gates; the NOT_2 gate being the limiting factor.

There is an interesting example in Fig.3.4 in which the transitions constituting the quantum gate operation cannot be globally phase aligned with sufficiently high fidelity. For the NOT_2 gate at points near $\omega_e\chi_e$=13.5 or B_e=1.8, the average population reaches 0.88 for optimizations without global phase alignment, but the fidelity only reaches 0.51 with global phase alignment. Thus, a binary laser pulse can be effectively optimized to carry out the NOT_2 gate operations but only if the qubit states do not need to be globally phase aligned, which is not the necessary requirement.

3.4 Conclusion

From the results presented there is an indication that the arrangement of the rovibrational state energies of a diatomic, in this case described by the anharmonicity and rotational constants, play an important role in the ability to produce binary shaped laser pulses to represent the $ACNOT_1$ and NOT_2 quantum gates. This was attributed to the intrinsic diatomic properties, and not the specific choice of optimization procedure, as investigated by repeating the calculations for differing Genetic Algorithm (discretization; cubic spline fit) and Optimal Control Theory (Transform Limited and Genetic Algorithm initial guesses) calculations. Overall there are specific regions (diatomics) in which the $ACNOT_1$ gate can be optimized to produce fidelities greater than 90% and also regions which produce moderate fidelities of 50%-60%. There is

no specific diatomic in which an efficient laser pulse was optimized to represent the NOT_2 gate operation. The maximum fidelity obtained was only 64% in this case, due to the lack of overall population transfer by NOT_2 gate laser pulse. Thus, for the model used, there was no diatomic that exhibited a high fidelity for both the $ACNOT_1$ and NOT_2 gate operations. It was also indirectly shown that the necessary requirement of global phase alignment makes it more difficult to optimize a laser pulse to carry out the $ACNOT_1$ or NOT_2 quantum gate operations.

Further investigations are needed to determine the reasons behind the only moderate control of the NOT_2 gate and how to establish high fidelities. This includes examining fidelities produced by optimizing a binary 2-pulse sequence or appropriate pulse energies for optimal control of the NOT_2 gate. Overall the conditions in order to enforce global phase alignment with high fidelities is not clearly understood. It may be necessary to increase the frequency resolution to values resolvable below a spectral width of 10 cm^{-1}. This will also result in a corresponding increase in the pulse duration since the the spectral width is inversely proportional to the pulse duration here and this effect on gate fidelities is currently being investigated. Increasing the number of amplitude and phase components beyond binary pulse shaping used in this and our previous studies, may also improve the fidelities. All of the suggestions noted require the GA to search a vastly larger parameter space than previously studied and thus there will be increased uncertainty in the GA's ability to find the correct optimally shaped laser pulse. Methods to avoid this problem in order to study the above mentioned conditions are currently being explored.

Bibliography

[1] L. Vandersypen, M. Steffen, G. Breyta, C. Yannoni, M. Sherwood, I. Chuang, Nature **414**, 883 (2001)

[2] J. Jones, M. Mosca, J. Chem. Phys. **109**, 1648 (1998)

[3] I. Chuang, L. Vandersypen, X. Zhou, D. Leung, S. Lloyd, Nature **393**, 143 (1998)

[4] C. Sackett, D. Kielpinski, B. King, C. Langer, V. Meyer, C. Myatt, M. Rowe, Q. Turchette, W. Itano, D. Wineland, I. Monroe, Nature **404**, 256 (2000)

[5] S. Gulde, M. Riebe, G. Lancaster, C. Becher, J. Eschner, H. Haffner, F. Schmidt-Kaler, I. Chuang, R. Blatt, Nature **421**, 48 (2003)

[6] C. Tesch, R.D. Vivie-Riedle, Phys. Rev. Lett. **89**, 157901 (2002)

[7] Z. Bihary, D. Glenn, D. Lidar, V.A. Apkarian, Chem. Phys. Lett. **360**, 459 (2002)

[8] R. Zadoyan, D. Kohen, D. Lidar, V. Apkarian, Chem. Phys. **266**, 323 (2001)

[9] D. P. DiVincenzo, D. Loss, Superlattices Microstruct. **23**, 419 (1998)

[10] M. Tsubouchi, T. Momose, J. Opt. Soc. Am. B **24**, 1886 (2007)

[11] J. Vala, Z. Amitay, B. Zhang, S. Leone, R. Kosloff, Phys. Rev. A **66**, 62316 (2002)

[12] C. Tesch, L. Kurtz, R. de Vivie-Riedle, Chem. Phys. Lett. **343**, 633 (2001)

[13] U. Troppmann, C. Tesch, R. de Vivie-Riedle, Chem. Phys. Lett. **378**, 273 (2003)

[14] S. Suzuki, K. Mishima, K. Yamashita, Chem. Phys. Lett. **410**, 358 (2005)

[15] M. Schröder, A. Brown, J. Chem. Phys. **131**, 034101 (2009)

[16] D. Weidinger, M. Gruebele, Mol. Phys. **105**, 1999 (2007)

[17] M. Tsubouchi, T. Momose, Phys. Rev. A **77**, 52326 (2008)

[18] R.R. Zaari, A. Brown, J. Chem. Phys. **132**, 014307 (2010)

[19] K. Shioya, K. Mishima, K. Yamashita, Mol. Phys. **105**, 1283 (2007)

[20] K. Mishima, K. Yamashita, Chem. Phys. **367**, 63 (2010)

[21] D. Babikov, J. Chem. Phys. **121**, 7577 (2004)

[22] K. Mishima, K. Tokumo, K. Yamashita, Chem. Phys. **343**, 61 (2008)

[23] L. Bomble, P. Pellegrini, P. Ghesquière, M. Desouter-Lecomte, Phys. Rev. A **82**, 062323 (2010)

[24] Y. Ohtsuki, Chem. Phys. Lett. **404**, 126 (2005)

[25] T. Cheng, A. Brown, J. Chem. Phys. **124**, 034111 (2006)

[26] K. Mishima, K. Yamashita, Chem. Phys. **361**, 106 (2009)

[27] T. Witte, D. Zeidler, D. Proch, K. Kompa, M. Motzkus, Opt. Lett. **27**, 131 (2002)

[28] C. Gollub, R. de Vivie-Riedle, Phys. Rev. A **78**, 033424 (2008)

[29] W. Zhu, J. Botina, H. Rabitz, J. Chem. Phys. **108**, 1953 (1998)

[30] D.L. Carroll, Genetic Algorithm driver **v1.7.0** (2004).

[31] D. Goorvitch, C. Chackerian, Astrophys. J. Suppl. Ser. **91**, 483 (1994)

[32] A.W. Mantz, J.P. Maillard, W.B. Roh, K.N. Rao, J. Mol. Spec. **155**, 57 (1975)

[33] K. Irikura, J. Phys. Chem. Ref. Data **36**, 389 (2007)

[34] J. Palao, R. Kosloff, Phys. Rev. A **68**, 62308 (2003)

[35] C. Tesch, R. de Vivie-Riedle, J. Chem. Phys. **121**, 12158 (2004)

Chapter 4

Effect of Laser Pulse Shaping Parameters on the Fidelity of Quantum Logic Gates.

4.1 Introduction

Promising experimental implementations of quantum algorithms, within the facet of chemistry, come in the form of nuclear magnetic resonance (NMR)[1–3] and ion traps[4, 5]. Within NMR an ensemble of molecules is excited via tuned laser pulses. Current linear ion trap quantum computer implementations use the shaped laser pulses to control individual atoms[6], although trapping approaches have been proposed and are currently being extended to molecules[7, 8]. Instead of exciting hyperfine states or atomic transitions, a complementary approach involves the control of the rovibrational states of a diatomic molecule (*diatomic quantum computing*) [9]. In this method, a mid-infrared laser pulse is shaped through a closed-loop feedback[10–12] mechanism to represent each specific quantum gate operation, through diatomic rovibrational state qubit excitations. Experimentally the use of internal degrees of freedom of diatomic molecules for quantum computing has not received much attention. Two possible implementations using Li_2[13] and I_2[14] have been presented and neither utilized a closed-loop feedback loop for optimization. The two experiments implemented the quantum algorithms directly, termed

problem-specific quantum computing, whereas the approach of interest in our studies is *universal* quantum computing, where in principle any quantum algorithm can be implemented [13]. In order for future closed-loop feedback experiments to be realized, further theoretical investigations on the requirements for experimental implementations will be useful.

The majority of theoretical studies within diatomic quantum computing, using shaped laser pulses, produce excellent qubit control but with laser pulses that are difficult, or perhaps impossible to realize experimentally and/or only show proof of principle applications on a particular choice of diatomic molecule [15–30]. In contrast we previously studied the performance of shaped laser pulses on a general model diatomic[31] and the ability to achieve high control with laser pulses having very few parameters (binary pulse shaping)[32]. The theoretical optimizing or shaping of laser pulses generally comes in two common forms: Optimal Control Theory (OCT)[33, 34] and Genetic Algorithm (GA)[11] optimization. Unless specific constraints are applied [35–37], OCT optimization can produce large intensities, a large range of frequency components (depending on the rotational, vibrational and/or electronic transitions available) and experimentally inaccessible pulse shapes. On the other hand, the GA can be incorporated into an experimental closed-loop feedback setup and thus theoretical implementation allows for an appropriate description of the possible laser pulses shapes. While the molecular structure is clearly important [31], it is also necessary to explore the limitations of the laser pulse shaping apparatus within the context of this specific application.

The aforementioned experimental implementations using Li_2 and I_2 had a laser pulse shaping setup that utilized a liquid crystal spatial light modulator (LC-SLM). A transform-limited (TL) pulse is incident upon a diffraction grating and the LC-SLM is illuminated by the resulting frequency spectrum. The output laser frequencies from the LC-SLM are recombined to form the shaped laser pulse. The LC-SLM contains a series of pixels that can independently control the amplitude and phase at each specific frequency resolution, and

thus provides a multitude of various laser pulse shapes. The GA is used to determine the optimal combination of amplitude and phase at each frequency component in order to implement the desired quantum gate operation. We have implemented an analogous theoretical framework, which was also used in our previous works[31, 32]. The object of the study detailed herein is to elucidate the importance of some important adjustable parameters within a typical LC-SLM, namely (i) the effect of varying the LC-SLM pixel frequency resolution ($d\nu$), (ii) effective variance of the amplitude (A_j) and (iii) phase (ϕ_J)at each pixel, and (iv) the effect of changing the number of pixels (n) included within the laser pulse shaping. Each of these four important parameters affects the total number of laser pulse combinations and thus the total size of the parameter space that needs to be explored to find the optimal laser pulse. It is important to have a parameter space of minimal size such that the GA can locate the optimal laser pulse with confidence and within an appropriate amount of computational time. A minimum parameter space requires a balance between the number of pulse shaping parameters and a maximum laser pulse fidelity, and hence the current study. In the present work, laser pulses are optimized to represent three common quantum gates ($\mathrm{ACNOT_1}$, $\mathrm{NOT_2}$, $\mathrm{Had_2}$) on the rovibrational state qubits of carbon monoxide ($^{12}\mathrm{C}^{16}\mathrm{O}$). Building from our [31] and others [18] previous work using GA laser pulse optimization on CO, we demonstrate the effect of laser pulse shaping parameters on the ability to produce optimal laser pulses.

4.2 Theory

A full explanation of the theoretical framework employed in this study is detailed in our previous work[31, 32] (see Sections 2.2 and 3.2, respectively). A brief overview of the theory along with the relevant details are given in this section.

The time-dependent Schrödinger equation (TDSE) can be written in ma-

trix notation with time-dependent coefficients $c_{\nu J}(t)$:

$$\dot{\underline{c}}(t) = -\frac{i}{\hbar}\left[\underline{\underline{E}} - \epsilon(t)\underline{\underline{\mu(r)}}\right]\underline{c}(t). \tag{4.1}$$

In Equation 4.1, $\underline{c}(t)$ is the column vector of time-dependent rovibrational state coefficients, $\underline{\underline{E}}$ is the rovibrational state energy matrix, $\epsilon(t)$ is the linearly polarized electric field of the laser pulse and $\underline{\underline{\mu(r)}}$ is the rovibrational transition dipole matrix. The TDSE is solved using the Runge-Kutta fourth order method with 2^{20}-2^{22} time points depending on the pulse duration. The number of time points chosen is determined by an incremental change until a convergence threshold is met, based upon the total population remaining after pulse interaction. There is a tradeoff between the selected convergence threshold and the computational time required for each calculation.

4.2.1 Model System

We restrict our study to the diatomic carbon monoxide ($^{12}C^{16}O$) with excitations occurring between rovibrational states according to vibrational excitation $\Delta\nu$=±1 and rotational excitation ΔJ=±1. The CO model consists of 7 vibrational states ($0 \leq \nu \leq 6$) each with 9 rotational states ($0 \leq$ J ≤ 8) for a total of 63 rovibrational states. With the energy contained in the laser pulses being optimized, rovibrational states higher than those used in the study were insignificantly populated and thus the reduced set used in this study is adequate. The four rovibrational states (ν,J) used to represent the qubits $|q_1 q_2\rangle$ are: $|00\rangle \equiv$ (1,2), $|01\rangle \equiv$ (0,1), $|10\rangle \equiv$ (2,1) and $|11\rangle \equiv$ (1,0). Refer to Figure 2.1 for an illustration containing the qubits, rovibrational states and transition frequencies involved. The rovibrational state energies were determined by Mantz et al. [38] and the transition dipole moments were taken from work of Goorvitch and Chackerian[39].

4.2.2 Quantum Logic Gates

In the present study three quantum logic gates were studied: the alternative Controlled-NOT (ACNOT_1) gate, NOT_2 gate and Hadamard 2 (Had_2) gate. The qubit operations for each gate are depicted in Table. 4.1. The subscript '1' of the ACNOT_1 gate is used to denote the control qubit, here q_1, and subsequent flip of the target qubit q_2 when q_1=0. In the case of the NOT_2 and Had_2 gates, the subscript '2' simply denotes a flip of qubit 2 (q_2). Laser pulses are to be shaped in order to implement the state transformations required for each quantum gate operation. Thus each quantum gate operation will have a unique laser pulse and each laser pulse will have an associated value describing its ability to perform the quantum gate operation, termed the *Fidelity* (see Section 4.2.3).

ACNOT_1 :	$\|10\rangle \rightarrow \|10\rangle$	NOT_2 :	$\|00\rangle \leftrightarrow \|01\rangle$	Had_2 :	$\|00\rangle \leftrightarrow \frac{1}{\sqrt{2}}(\|00\rangle + \|01\rangle)$
	$\|11\rangle \rightarrow \|11\rangle$		$\|10\rangle \leftrightarrow \|11\rangle$		$\|01\rangle \leftrightarrow \frac{1}{\sqrt{2}}(\|00\rangle - \|01\rangle)$
	$\|00\rangle \leftrightarrow \|01\rangle$				$\|10\rangle \leftrightarrow \frac{1}{\sqrt{2}}(\|10\rangle + \|11\rangle)$
					$\|11\rangle \leftrightarrow \frac{1}{\sqrt{2}}(\|10\rangle - \|11\rangle)$

Table 4.1: Quantum gate operations which are implemented by an optimized laser pulse in this study with qubit representation $|q_1 q_2\rangle$. NOT_2/ Had_2: The qubit flip occurs on qubit 2 (q_2). ACNOT_1: The control qubit is q_1 and the qubit flip occurs on the target qubit q_2 when q_1=0.

4.2.3 Laser Pulse Optimization

The present study investigates features of experimental pulse shaping using a LC-SLM where shaping occurs in the frequency domain. The LC-SLM produces a discretized frequency spectrum, $\epsilon(\nu_j)$, given by:

$$\epsilon(\nu_j) = \epsilon_0 \sqrt{A(\nu_j)} \exp\left[-2\ln 2 \left(\frac{\nu_j - \nu_0}{\Delta\nu}\right)^2\right] \exp\left[i\phi(\nu_j)\right], \qquad (4.2)$$

where ϵ_0 is the peak field strength, ν_0 is the central frequency, $\Delta\nu$=100 cm^{-1} is the full width at half-maximum (FWHM) pulse width and ν_j represents the discrete frequencies at which the field is shaped. The amplitude and phase range from $0 \leq A(\nu_j) \leq 1$ and $0 \leq \phi(\nu_j) \leq 2\pi$, respectively. In the case of binary pulse shaping (a choice of 2A and 2ϕ), A=0 or 1 and ϕ=0 or π. A transform limited (TL) pulse results when A=1 and ϕ=0 for all frequency components, ν_j, of Equation 4.2. Typically, in order to obtain the time-domain laser pulse from this frequency domain spectrum, a Fourier transform is used. An analytic form for the time-domain laser pulse, $\epsilon(t)$, has been derived from the discretized frequency spectrum, $\epsilon(\nu_j)$ (see Appendix 4.5):

$$\epsilon(t) = \mathrm{sinc}\,(\pi t d\nu) \sum_{j=0}^{n} A'_j \cos(2\pi\nu_j t + \phi_j), \tag{4.3}$$

where $A'_j = d\nu\epsilon_0\sqrt{A_j}e^{-2\ln 2\left(\frac{\nu_j-\nu_0}{\Delta\nu}\right)^2}$ and contains variables as described in Equation 4.2. The frequency resolution is labeled by $d\nu$ and the summation occurs over n discretized frequency components. The symmetry of resulting laser pulses can be deduced using Equation 4.3. The *sinc* function is symmetric along the pulse duration from $-\frac{T}{2} \leq t \leq \frac{T}{2}$. As long as the phase at each frequency component (ϕ_j) of the *cosine* function varies only by ϕ=0 or ϕ=π, where $\cos(2\pi\nu_j t + \pi) = -\cos(2\pi\nu_j t)$, then overall the resulting laser pulse shapes will be symmetric in time. Moreover, a symmetric pulse shape guarantees that the resulting phases of the set of two qubit transitions of the quantum gate operation will be the same. For example, a symmetric laser pulse being shaped to represent the ACNOT$_1$ gate will result in the qubits $|00\rangle$ and $|01\rangle$ being in phase. This effect of temporally symmetric laser pulses was originally documented by Schröder and Brown [35].

The frequency of transition between the two qubits of the ACNOT$_1$ gate shown in Table 4.1, was chosen as the central frequency (ν_0=2151 cm^{-1}). The NOT$_2$ and Had$_2$ gates shown in Table 4.1 include two transitions at 2121cm^{-1} and 2151cm^{-1} between respective qubits. In order for the laser pulse to be

centralized between these two frequencies, an average between the transitions involved was chosen as the central frequency, namely 2136 cm^{-1}. For the $ACNOT_1$a gate the sequential addition of further frequency components is shown in Figure 4.1. Also shown in Figure 4.1b is the method by which further frequency components are added for the NOT_2 and Had_2 gates.

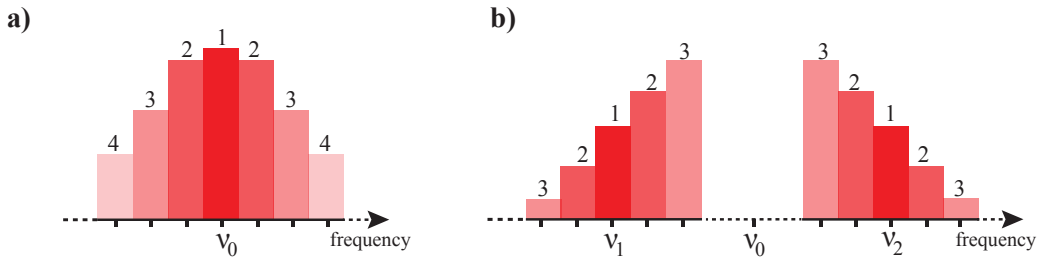

Figure 4.1: Illustration of the incremental addition of frequency components for the $ACNOT_1$, NOT_2 and Had_2 gates. (a) $ACNOT_1$ gate. One frequency component at '1', the central frequency ν_0. Three frequency components at '1' and '2'. Five frequency components at '1' ,'2' and '3'. Seven frequency components at '1' ,'2', '3' and '4'. The addition of more frequency components continues in this manner. (b) NOT_2 and Had_2 gates. Two frequency components at '1', the transition frequencies ν_1, ν_2. Six frequency components at '1' and '2'. Ten frequency components at '1' ,'2' and '3'. The addition of more frequency components continues in this manner.

With reference to Equation 4.3 the variables we are manipulating within this study are A_j (amplitude), ϕ_j (phase), n (number of frequency components) and $d\nu$ (frequency resolution). These four parameters will produce different laser pulse shapes and thus different rovibrational state qubit dynamics. In order to optimize a pulse shape for performing a particular quantum gate operation, a Genetic Algorithm (GA)[40] is utilized. The GA uses evolutionary strategies from biology such as natural selection and survival of the fittest to search the parameter space of possible laser pulse shapes and find the appropriate one, without having to sample all combinations. In the results reported here, we use between 25 and 1000 generations each consisting of 16 individuals and a micro-GA subroutine. The micro-GA eliminates *inbreeding*, which is the

case when individual laser pulses become too similar, by keeping the best individual and randomly selecting 15 new individuals to create a new generation. The chosen number of generations was determined based upon the relative size of the parameter space. For example, the $ACNOT_1$ gate with a parameter space consisting of a single frequency component (n=1) with 16 amplitude ($16A$) and 2 phase (2ϕ) choices would consist of $(16 \times 2)^1 = 32$ possible laser pulse combinations. If the same quantum gate had a parameter space consisting of 13 frequency components (n=13), $32A$ and 2ϕ, then it would produce $(32 \times 2)^{13} = 3.02 \times 10^{23}$ laser pulse combinations! A large number of generations would be required for the latter case to ensure appropriate sampling of the parameter space and to ensure confidence of the optimal solution being found.

In order for the GA to know how well an individual (laser pulse) performs the desired quantum gate operation, a fitness function is needed. The form of the fitness function, in this case termed the *fidelity* (F), used in the present work is,

$$F = \frac{1}{N^2} \left| \sum_{k=1}^{N} \langle \Psi_k(T) | \Phi_k \rangle \right|^2 , \tag{4.4}$$

where $\Psi_k(T)$ is the resulting wavefunction after the laser pulse has been applied, T is the total laser pulse duration and Φ_k is the target wavefunction. The wavefunctions are summed over the number of transitions required by the quantum gate, N, and then divided by a normalization factor, N^2, to ensure the fidelity ranges between 0 and 1. The fidelity is dependent upon the phase alignment of all the qubits, which can be explicitly viewed in an alternative representation of the fidelity,

$$F = \frac{1}{N^2} \left[\sum_{k}^{N} |r_k|^2 + 2 \sum_{k \neq k'}^{N} r_k r_{k'} \cos(\Delta\phi_{kk'}) \right] . \tag{4.5}$$

For simplicity, the time-dependent wavefunctions (Equation 4.4; $\Psi_k(T)$, Φ_k) are written in complex Euler notation, i.e. $\Psi_k = r_k e^{i\phi_k}$ and Φ_k are assumed to be real. The term r_k describes the magnitude of the time-dependent coef-

ficients corresponding to wavefunctions Ψ_k at the end of the laser pulse interaction. $\Delta\phi_{kk'}$ is the difference between qubit phases, ϕ_k and $\phi_{k'}$, at the end of the laser pulse duration.

Another description of the dynamics occurring during the laser pulse/molecule interaction, but not used as a means for optimization, is the average population, $\bar{P}$:

$$\bar{P} = \frac{1}{N}\sum_{k=1}^{N} |\langle \Psi_k(T)|\Phi_k\rangle|^2 . \tag{4.6}$$

The average population ($\bar{P}$) describes the ability of the laser pulse to excite from an initial state to a final state as deemed by the quantum gate operation. The average population is not dependent upon the final phase of the qubits. A requirement of molecular quantum computing is *global phase alignment.*[27, 41] The final phases of each qubit after the total pulse interaction time must be the same. This ensures that the application of subsequent quantum gate operations (laser pulses) occurs without inducing a phase discrepancy and thus decreasing the effectiveness of the quantum gate. Hence, the fidelity is used as the fitness function for GA optimizations rather than the average population ($\bar{P}$). Global phase alignment is related to the second term of Equation 4.5.

4.3 Results and Discussion

This investigation was carried out in three parts in order to examine the effects on fidelity of variations to amplitude (A_j), phase (ϕ_j), number of frequency components (n) and total pulse duration (T). Each has a particular role in producing an optimal pulse shape based upon the experimental discretized pulse shaping LC-SLM. The variations to the laser pulse shaping parameters were carried out on the ACNOT$_1$, NOT$_2$ and Had$_2$ quantum logic gates and their effects on of the gate on Fidelity (F) evaluated. The three sections are as follows:

A. **Effect of total pulse duration (F vs. T)**

At a constant total pulse energy, the total pulse duration, T, was varied. The total pulse energy for each quantum gate was taken from our previous work.[32] The frequency resolution ($d\nu$) and total pulse duration (T) are related by $d\nu = \frac{2}{T}$. As a result, a qualitative relationship between the total pulse duration, T and areas of high and low fidelity can be deduced. The laser pulse included only the single transition frequency ($ACNOT_1$) or only two frequencies (NOT_2 and Had_2), depending upon the quantum gate. Binary pulse shaping (A=0 or 1, ϕ=0 or π) was utilized.

B. **Effect of laser pulse energy (F vs. A)**

The low fidelities obtained in Section 4.3.1, as detailed in the paragraph above, may be associated with pulse shapes of non-optimal total pulse energy. By determining optimal amplitudes at the excitation frequency (see Figure 4.1a; ν_0) or frequencies (see Figure 4.1b; ν_1, ν_2), the appropriate pulse shape of optimal energy can be generated. At specifically chosen values of total pulse duration, T, the number of amplitude components was varied beyond two choices (the phase variation remained at 2ϕ), from $2A$ until appropriate convergence was reached at $512A$. Thus the total pulse energy available to all frequency components can be controlled at each frequency component by amplitude variation.

C. **Effect of frequency resolution, amplitude and phase (F vs. n, A, ϕ)**

Lastly, in order to further investigate the effect of laser pulse parameters on increasing the resulting fidelity, the number of frequency components (n) was increased beyond the excitation frequency, ν_0 (see Figure 4.1a) or frequencies, ν_1 and ν_2 (see Figure 4.1b). Concurrently, the number of amplitude (A) or phase (ϕ) values was increased from only two choices to having 32 choices each (i.e., $32A$ or 32ϕ). This investigation was carried out on the pulses of optimal energy, as determined in Section 4.3.2 and detailed in the previous paragraph, of a single chosen total pulse duration for each quantum gate operation.

4.3.1 Effect of total pulse duration (F vs. T)

In order to examine the effect of the total pulse duration on the fidelity, a scan of the frequency resolution ($d\nu$) was carried out by setting the total frequency window to 500cm^{-1} and discretizing the window into odd integer values (x) for $d\nu = \dfrac{500}{x-1}$ but there was no direct optimization. Thus, the total pulse duration (T) at intervals of ΔT=0.27ps for 5.34ps$\leq T \leq$ 66.71ps was sampled. The laser pulse energies for each quantum gate were constant and chosen based upon the TL-pulse energies from Table 2.2. For these simulations, laser pulses were constructed from all combinations of amplitude and phase from A=0 or 1 and ϕ=0 or π for each quantum gate. The fidelity for each laser pulse at each value of $d\nu$ was calculated and then $d\nu$ was converted to the corresponding value for the total pulse duration. From this point on, references to the total pulse duration T should be considered synonymous to the frequency resolution $d\nu$. The field free case, for the NOT_2 and Had_2 gates when $\epsilon(t)$=0, is omitted since it produces a fidelity of zero due to the nature of the excitations involved (see Table 4.1). In comparison, the $ACNOT_1$ gate when $\epsilon(t)$=0 produces a maximum fidelity of F=0.25. Similar information about the relationship between the fidelity and total pulse duration could be determined experimentally by scanning through values of $d\nu$ and optimizing a laser pulse for each value when A=0 or 1 and ϕ=0 or π.

$ACNOT_1$ quantum gate

The total pulse energy was kept constant at E=10 μJ and the central frequency is ν_0=2151 cm^{-1}. Three unique laser pulses at each pulse duration T can be produced. Using the notation [A,ϕ], they are [1,π], [1,0] and the field free case [0,ϕ]. The fidelities for these three pulses as a function of pulse duration are shown in Figure 4.2. As seen in Figure 4.2, there are six locations where the fidelity is highest, though the pattern may repeat itself in time. The two laser pulses, [1,π] and [1,0], share a relationship such that the maximum fidelity alternates between each other as T is increased (see the inset of Figure 4.2),

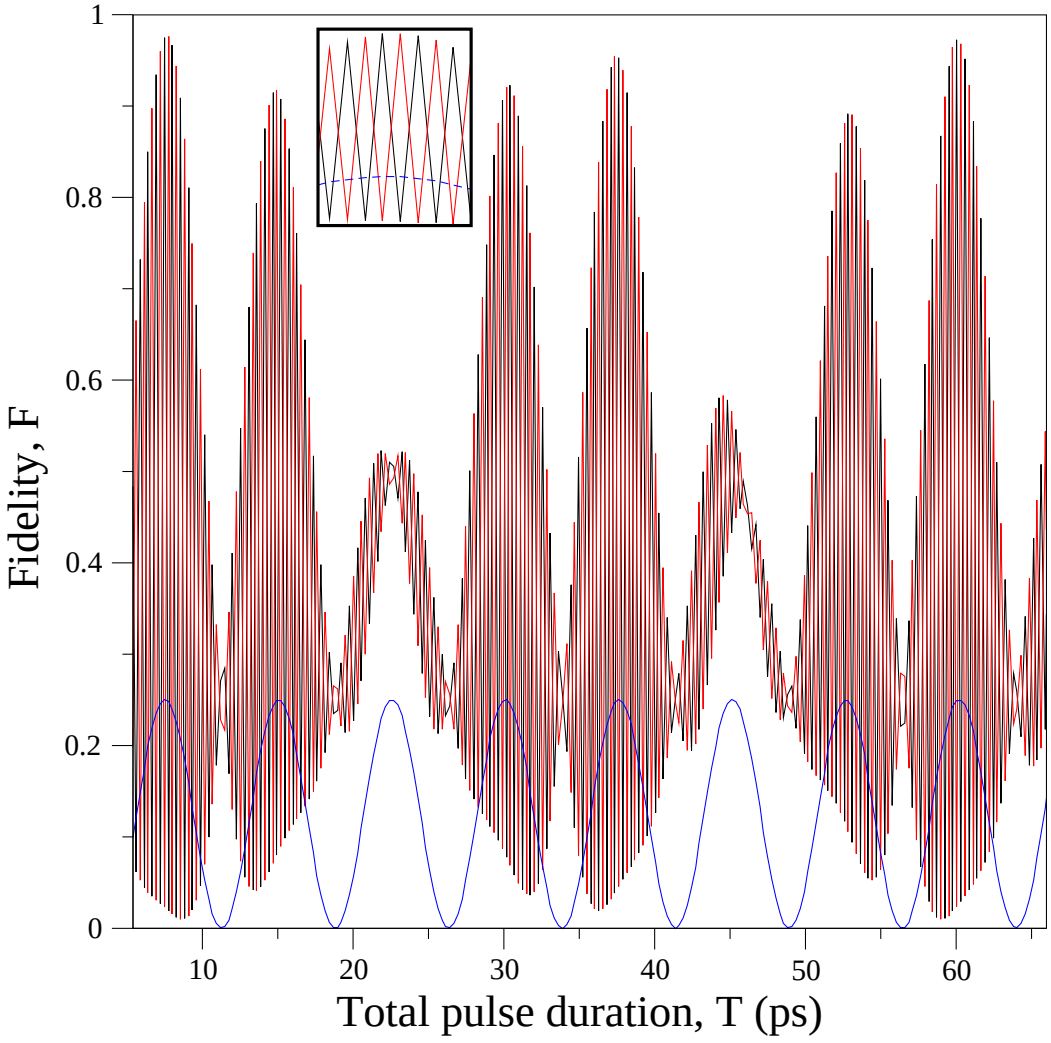

Figure 4.2: Plot of the resulting fidelities for three pulse shapes as a function of the total pulse duration T for the ACNOT$_1$ quantum gate having a total pulse energy of 10 μJ. The laser pulses, consist of 1 frequency component (n=1) at the transition frequency (2151 cm^{-1}) with a choice of amplitude $2A$ and phase 2ϕ using the notation $[A\phi]$, are $[1,\pi]$ black line, [1,0] red line and [0,0] blue line. The inset shows the alternating fidelity between $[1,\pi]$ and [1,0] for 6.5ps $\leq$T$\leq$ 8.8ps.

where the fidelities from 6.5ps $\leq T \leq$ 8.8ps are plotted. The overall pattern of maximum fidelities produced by [1,π] and [1,0] follows the trend of fidelity for the field free scenario (solid blue line), though not all cases result in a global maximum fidelity (e.g. T=22.7ps and 45.1ps). When $\epsilon(t)$=0 in the field free case (Figure 4.2; solid blue line) the excitation $|00\rangle \leftrightarrow |01\rangle$ cannot occur and thus the fidelity represents the phase alignment of qubits $|11\rangle$ and $|10\rangle$. It seems that the free evolution phase alignment of qubits $|11\rangle$ and $|10\rangle$ determines whether a high fidelity can be obtained for a specific value of $d\nu$. The exception being the unexpectedly low fidelities at T=22.7ps and 45.1ps. Analysis of the results for these two low fidelity local maxima is detailed in Section 4.3.2.

The fidelity of the free evolution of qubits $|10\rangle$ and $|11\rangle$ is described by, $F = \frac{1}{16}\left[2 + 2\cos(\Phi_{|11\rangle} - \Phi_{|10\rangle})\right]$, where $\Phi_{|q_1 q_2\rangle}$ is the final phase for qubit $|q_1 q_2\rangle$ after the pulse interaction. As seen in Figure 4.2, the maximum fidelity (peaks) occurs every $T = 7.526n$ ps. The free evolution alignment between qubits $|10\rangle$ and $|11\rangle$ is related to the energy difference between these states and occurs at a frequency of 2121 cm^{-1} (63.57ps^{-1}). This is much larger than the peak oscillation period of $\frac{1}{7.526}$=0.1329ps^{-1} just stated. However, the period observed in Figure 4.2 is simply a result of the pulse duration (frequency resolution) sampling used in the present work. When the free evolution frequency of these qubits is sampled at the pulse duration interval used in these calculations (ΔT=0.267 ps), the fidelity curve produced exactly overlaps with that of the solid blue line of Figure 4.2.

NOT$_2$ quantum gate

The total pulse energy was kept constant at E=20 μJ and with n=2 the two transition frequencies were ν_1=2121cm^{-1} and ν_2=2151cm^{-1}, with the central frequency being ν_0=2136cm^{-1}. Binary laser pulses (2A/2ϕ) were implemented. Using the notation [$A_1\phi_1$,$A_2\phi_2$], with subscripts referring to either transition frequency, a total of $(2 \times 2)^2$=16 laser pulse combinations result. Only 9 of

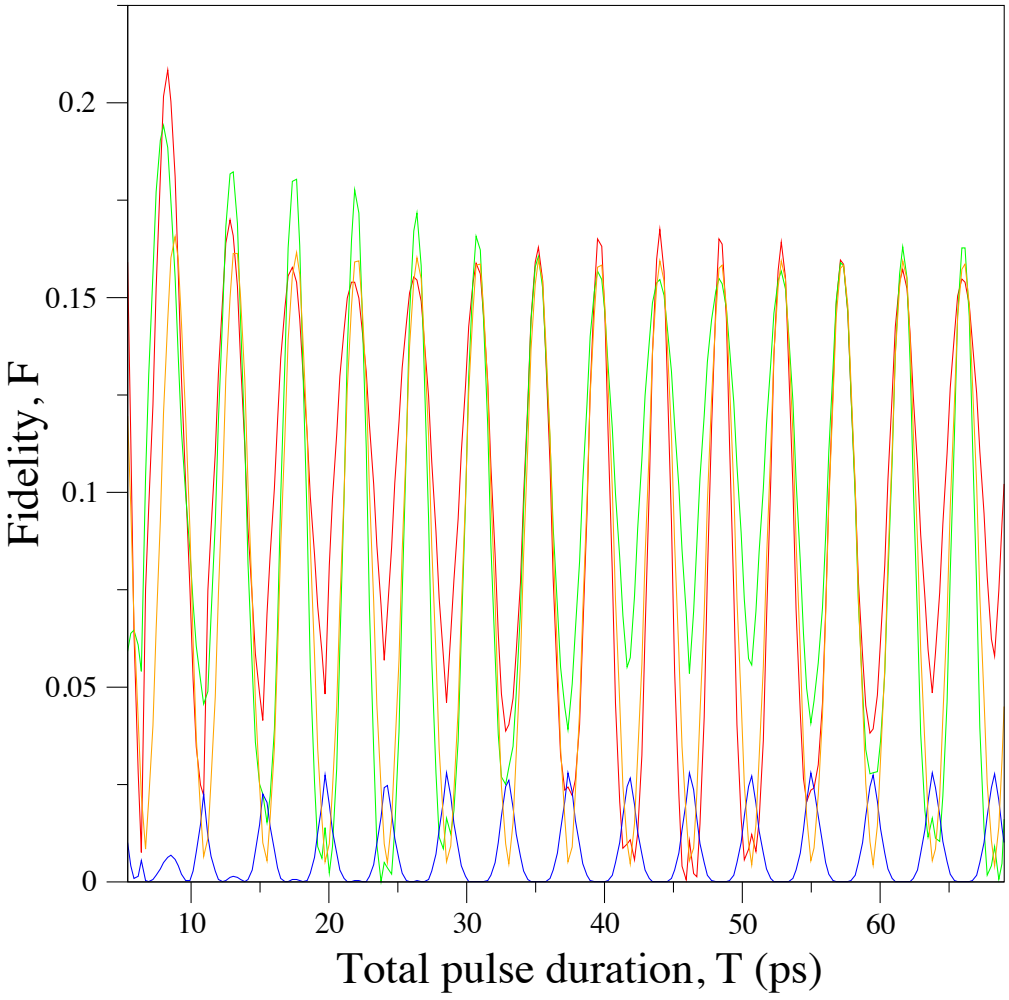

Figure 4.3: Plot of the resulting fidelities for eight pulse shapes (only 4 are unique) as a function of the total pulse duration T for the NOT_2 quantum gate having a total pulse energy of 20 μJ. The laser pulses, consisting of two frequency components (n=2) at the transition frequencies (ν_1=2121 cm^{-1},ν_2=2151 cm^{-1}) with binary pulse shaping ($2A/2\phi$) using the notation $[A_1\phi_1,A_2\phi_2]$, are $[1\pi,1\pi]$=[10, 10] red line, $[10,1\pi]$=$[1\pi,10]$ green line, $[1\pi,00]$=[10, 00] blue line and $[00,1\pi]$=[00, 10] orange line.

the combinations are unique and one of the nine combinations is the field free case; thus only 8 combinations were calculated. The resulting fidelities for the 8 unique laser pulse combinations for each value of T are shown in Figure 4.3. It is important to note that the plots in Figure 4.3 have considerably lower fidelities due to inappropriate choice of total laser pulse energy and insufficient amplitude variation beyond 2 amplitude components ($2A$). Some of the laser pulse combinations produce identical dynamics in Figure 4.3, namely: $F_{[1\pi,1\pi]}=F_{[10,10]}$ (red line), $F_{[10,1\pi]}=F_{[1\pi,10]}$ (green line), $F_{[1\pi,00]}=F_{[10,00]}$ (blue line) and $F_{[00,1\pi]}=F_{[00,10]}$ (orange line). The red, green and orange lines in Figure 4.3 seem to oscillate at approximately the same frequency while the blue line seems to be centered at their minima but with a much lower fidelity. Section 4.3.2 will show that high fidelity points do not necessarily mean 100% fidelity points.

Had$_2$ quantum gate

The total pulse energy was kept constant at E=25 μJ. Similarly to the NOT$_2$ gate, there are only 8 unique laser pulse combinations using 2 frequency components ν_1=2121cm^{-1} and ν_2=2151cm^{-1}, centered at ν_0=2136cm^{-1}. The results are shown in Figure 4.4. We refer the reader to the ACNOT$_1$ results shown in the inset of Figure 4.2, illustrating the fluctuating fidelities between pulse shapes differing in phase by π. Similar fidelity trends are observed for the results from specific laser pulse amplitude and phase combinations for the Had$_2$ quantum gate. Fidelity results of all pulse combinations for ACNOT$_1$ are plotted in Figure 4.2. However, in the case of Figure 4.4 for the Had$_2$ gate, in order to simplify the figure the fluctuations are not shown. Only the maximum fidelities between the following combinations are plotted, namely [1π,1π] and [10,10] (red line), [10,1π] and [1π,10] (green line), [1π,00] and [10,00] (blue line) and, [00,1π] and [00,10] (orange line). The black line of Figure 4.4e displays the maximum fidelity between either four possible values of Figs. 4.4a - 4.4d, at any given total pulse duration. The curves are more

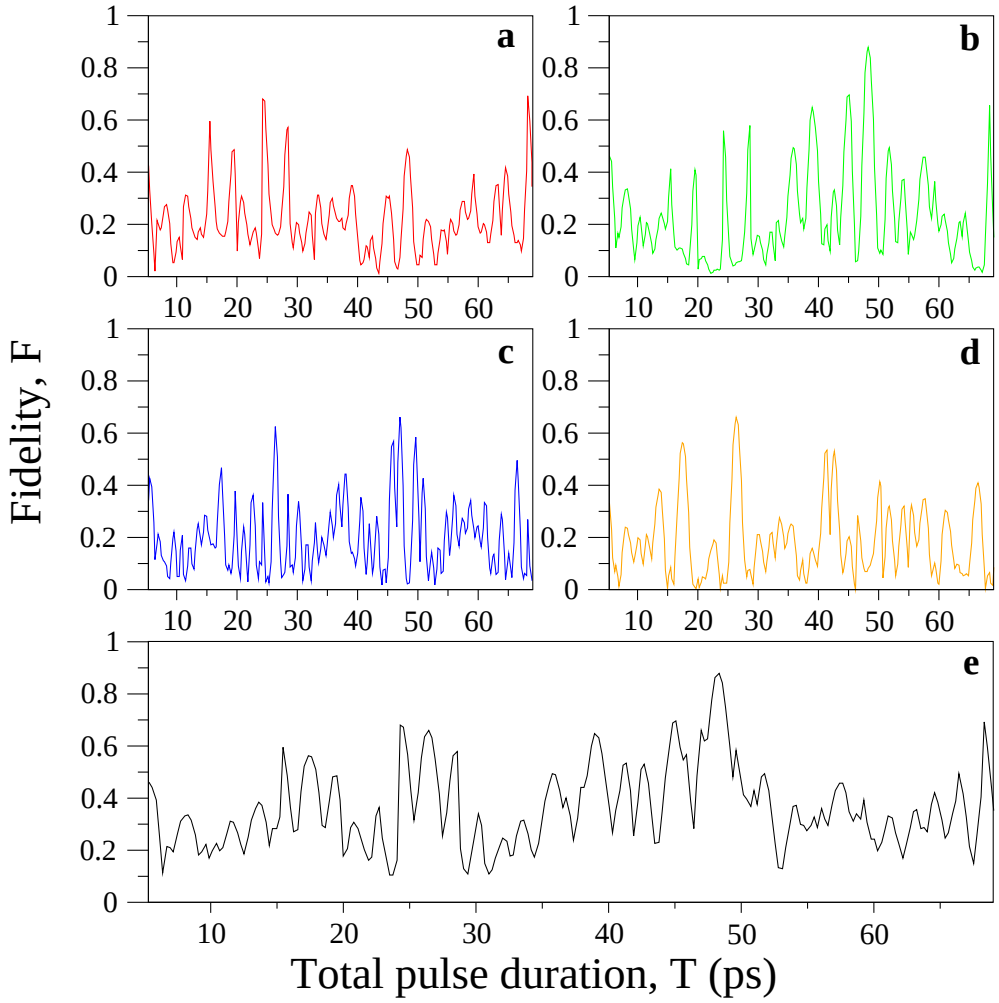

Figure 4.4: Plot of the resulting maximum fidelities for 8 pulse shapes as a function of the total pulse duration T for the Had_2 quantum gate having a total pulse energy of 25 μJ. The laser pulses, consist of 2 frequency components (n=2) at the transition frequencies (ν_1=2121 cm^{-1},ν_2=2151 cm^{-1}) with binary pulse shaping ($2A/2\phi$) using the notation [$A_1\phi_1$,$A_2\phi_2$], are: a) [1π,1π] and [10,10] red line, b) [10,1π] and [1π,10] green line, c) [1π,00] and [10,00] blue line and, d) [00,1π] and [00,10] orange line. Also plotted, in black within Figure 4.4e, are the maximum results from the previous plots of Figure 4.4a - Figure 4.4d, at any given total pulse duration.

complicated than those obtained for the $ACNOT_1$ or NOT_2 gates, likely due to the required superposition of states of the Had_2 gate. In this case there is no regular pattern, making it difficult to deduce a predictable value of T that will result in a high fidelity.

4.3.2 Effect of laser pulse energy (F vs. A)

As a first attempt to improve upon the fidelity, the optimal laser pulse energy was determined at select total pulse durations, T. These calculations could have been done for every value of T in Section 4.3.1 and would have provided a more complete picture but the optimization time requirements limited this. Using n=1 for the $ACNOT_1$ gate or n=2 for the NOT_2 and Had_2 gates, we varied the amplitude from $2A$, up to a max of $512A$, while restricting the phase to ϕ=0 or π. This can be thought of as dividing up the laser pulse energy, at specific frequency components, into a maximum of 512 segments. Moreover, by varying the amplitude what is actually being optimized is the energy associated with each transition frequency component used in the calculation. Thus the actual laser pulse energy reported will be much less than the total pulse energy since only a small fraction of the total pulse energy is carried in the frequency/frequencies used here. The laser pulse energy was increased to a value larger than used in Section 4.3.1, in order to allow more flexibility in the choice of energy. For the $ACNOT_1$ gate an energy of 30 μJ was used. For the NOT_2 and Had_2 gates, since two frequencies are needed that are not at the central peak intensity (see Figure 4.1), a value of 100 μJ is used. In general, optimizing the energy did not change the relative relationship between low and high fidelity points in Figs. 4.2 - 4.4.

$ACNOT_1$ quantum gate

Values for the total pulse duration associated with high and low fidelities were chosen from Figure 4.2, namely: 7.47ps, 11.20ps, 22.68ps and 45.10ps. The results comparing a total laser pulse energy of 10 μJ with an optimized laser

pulse energy chosen from a total pulse energy of E=30 μJ for 512A, are displayed in Table. 4.2. In this case the chosen value of E=10 μJ for all 4 cases, when using $2A$ and 2ϕ components, was able to produce the required optimal pulse energy. With a choice of 7.47ps pulse duration and using only one frequency component at the transition frequency, a 30 μJ total laser pulse energy could produce a high fidelity (here F=0.9748) when using $512A$ amplitude variations.

The pulse durations 22.68ps and 45.10ps correspond to local maxima of Figure 4.2. Analysis of the fidelity at these two points indicate that there is poor phase alignment between the qubits. For example, the optimal laser pulse in Table. 4.2 at 45.10ps produces resultant qubit phases of: $\Phi_{|00\rangle}$=-1.50 rads,$\Phi_{|01\rangle}$= -1.50 rads,$\Phi_{|10\rangle}$=-0.09 rads and $\Phi_{|11\rangle}$=-0.04 rads. It is this lack of phase alignment that produces the unexpectedly low fidelity at T=22.68ps and 45.10 ps. In comparison, analogous data for the high fidelity pulse duration T=7.47ps is $\Phi_{|00\rangle}$=-1.99 rads,$\Phi_{|01\rangle}$= -1.99 rads,$\Phi_{|10\rangle}$=-2.33 rads and $\Phi_{|11\rangle}$=-2.25 rads. The resulting phases of the qubits involved in the transition, $|00\rangle$ and $|01\rangle$, are the same because the laser pulse is symmetric (see Section 4.2.3).

Table 4.2: Comparison of resulting fidelities, pulse energies and amplitudes for laser pulses optimized for the $ACNOT_1$ gate with and without (optimal) amplitude restrictions. The amplitude used in Figure 4.2 is A=1.00 and the total pulse energy was $30\mu J$.

Total pulse duration T (ps)	**Figure 4.2 Fidelity F**	**Optimal Fidelity F**	**Figure 4.2 Pulse Energy E (μJ)**	**Optimal Pulse Energy E (μJ)**	**Optimal Amplitude A**
7.47	0.9747	0.9748	0.8388	0.8519	0.339
11.20	0.2712	0.2715	0.5592	0.5351	0.319
22.68	0.5049	0.5058	0.2763	0.2953	0.356
45.10	0.5660	0.5680	0.1390	0.1248	0.299

NOT_2 quantum gate

Values for the total pulse duration at four high fidelity points 8.27ps, 35.22ps, 44.03ps, 52.84ps and one low fidelity point 15.21ps were chosen from Figure 4.3. The results comparing a constant laser pulse energy of 20 μJ with an optimized laser pulse energy at a maximum E=100 μJ for 512A amplitude variations, are displayed in Table 4.3. It is evident, even for the low fidelity case, that the initial choice of E=20 μJ for the laser pulse energy does not produce the highest possible fidelity. Larger pulse energies were required in order to obtain larger fidelities. According to Table 4.3, a low amplitude at one of the two frequencies and a high amplitude at the other is needed to achieve optimal fidelities at a given value of T, for n=2. For example optimizing the laser pulse energy for a total pulse duration of T=8.27ps, results in an optimal amplitude of A_1=0.035 and A_2=1.00 for ν_1 and ν_2, respectively. With reference to Equation 4.3, the laser pulse with a frequency of ν_1=2121cm^{-1} has a low amplitude A_1 than the ν_2=2151cm^{-1} laser pulse with A_2=1.00. These choices of amplitudes result in high fidelities which would not have been achieved by a constant laser pulse energy with binary pulse shaping (Figure 4.3).

Table 4.3: Comparison of resulting fidelities, pulse energies and amplitudes for laser pulses optimized for the NOT_2 gate with and without (optimal) amplitude restrictions. The amplitudes, A_1/A_2, for Figure 4.3 are 1.00/1.00 and the total pulse energy was 100μJ.

Total pulse duration T (ps)	**Figure 4.3 Fidelity F**	**Optimal Fidelity F**	**Figure 4.3 Pulse Energy E (μJ)**	**Optimal Pulse Energy E (μJ)**	**Optimal Amplitude A_1/A_2**
8.27	0.2085	0.7461	2.820	7.297	0.035/1.00
15.21	0.0414	0.4256	1.571	5.203	0.376/0.949
35.22	0.1629	0.7372	0.668	1.679	0.049/0.957
44.03	0.1675	0.9994	0.534	1.281	0.051/0.908
52.84	0.1641	0.8459	0.445	0.621	0.458/0.010

Had_2 quantum gate

For the case of the $ACNOT_1$ and NOT_2 quantum gates, the choice of T at high and low fidelity points from Figure 4.2 or Figure 4.3 lead to a fairly simple regular structure. The analogous plot for the Had_2 gate (Figure 4.4) is very complex in structure, exhibiting no signs of a regular pattern. Only two total pulse durations with high fidelity points were studied from Figure 4.4, namely, 24.28ps and 48.30ps. The results comparing a constant laser pulse energy of 25 μJ with an optimized laser pulse energy at a maximum energy of 100 μJ for 512A amplitude variations, are displayed in Table 4.4. The constant 25 μJ laser pulse energy was not optimal, as seen by the large discrepancy between the fidelities. The fidelity can be significantly improved by changing the pulse energy e.g., the laser pulse optimized at T=48.30 ps attains a large fidelity (F=0.9742). The choice of optimal amplitudes is different in this case than for the NOT_2 gate since A_1 and A_2 are of similar magnitudes.

Table 4.4: Comparison of resulting fidelities, pulse energies and amplitudes for laser pulses optimized for the Had_2 gate with and without (optimal) amplitude restrictions. The amplitudes, A_1/A_2, for Figure 4.4 are 1.00/1.00 and the total pulse energy was $30\mu J$.

Total pulse duration T (ps)	**Figure 4.4 Fidelity F**	**Optimal Fidelity F**	**Figure 4.4 Pulse Energy E (μJ)**	**Optimal Pulse Energy E (μJ)**	**Optimal Amplitude A_1/A_2**
24.28	0.6810	0.8817	1.197	1.199	0.344/0.157
48.30	0.8791	0.9742	0.609	0.660	0.315/0.227

4.3.3 Effect of number of frequency components, amplitude and phase (F vs. n, A, ϕ)

From Sections 4.3.1 and 4.3.2, it is clear that the overall quantum gate fidelity is strongly dictated by the one ($ACNOT_1$) or two (NOT_2 and Had_2) transition frequency components. Here we want to consider what role additional

frequency components play in determining the overall fidelity and subsequent amplitude and phase variation on these additional frequencies. In order to do so, one of the values of the total pulse duration (T) from Section 4.3.2 for each quantum logic gate must be selected. The optimal amplitude(s) determined for this choice of pulse duration are then used as the maximum values instead of the default of 1.00. The result is an optimal amplitude (energy) at each transition frequency from which to vary the amplitude (A) and/or phase (ϕ) for increasing number of frequency components (n). For the $\mathrm{ACNOT_1}$ gate the number of frequency components varies by odd integer values according to $1 \leq n \leq 13$, so that frequency components are added to either side of the transition frequency. The $\mathrm{NOT_2}$ and $\mathrm{Had_2}$ gates vary by n=2,6 and 10, so that frequency components are added to either side of both transition frequencies (see Section 4.2.3 and Figure 4.1). Combinations of $2A$ or $32A$ and 2ϕ or 32ϕ for each number of frequency components were used to test the effect of increased amplitude or phase variation on the optimal fidelity. Also an optimization in which the energy had $32A$ amplitude variations at each value of n=10 or 13 frequency components was used as a comparison - here termed the *full* optimization. This is analogous to the energy optimization of Section 4.3.2, except in this case n=10 or n=13, resulting in a very large parameter space optimization. The results for the minimum and maximum number of frequency components studied are shown in Table 4.5. In our previous study [32], Chapter 2, we also produced GA optimized laser pulses for the $\mathrm{ACNOT_1}$, $\mathrm{NOT_2}$ and $\mathrm{Had_2}$ gates but using binary pulse shaping for n=51 frequency components at T=6.67 ps. Fidelities of F_{ACNOT_1}= 0.9729, F_{NOT_2}=0.5118 and F_{Had_2}=0.5075 were obtained using a total pulse energy of $10\mu J$, $20\mu J$ and $25\mu J$, respectively.

Table 4.5: Results of amplitude (A), phase (ϕ) and number of frequency components (n) variation at select pulse durations from Section 4.3.2 for the $ACNOT_1$, NOT_2 and Had_2 quantum gates. Also included are results from full calculations (*Full*) in which the amplitude at each frequency was flexible to vary by 32 segments between $0 \leq A \leq 1$.

		$ACNOT_1$ T=7.47 $A1$=0.339		**NOT_2** T=52.84 $A1/A2$=0.458/0.010		**Had_2** T=24.28 $A1/A2$=0.344/0.157	
n	**A/ϕ**	**Fidelity**	**Avg. Pop.**	**Fidelity**	**Avg. Pop.**	**Fidelity**	**Avg. Pop.**
1 or 2	2A/2ϕ	0.9748	0.9983	0.8459	0.9955	0.8817	0.9068
	2A/32ϕ	0.9748	0.9983	0.8459	0.9955	0.8817	0.9068
13 or 10	2A/2ϕ	0.9876	0.9947	0.8921	0.9427	0.8817	0.9068
	32A/2ϕ	0.9912	0.9956	0.9123	0.9726	0.9834	0.9873
	2A/32ϕ	0.9880	0.9949	0.9067	0.9683	0.8817	0.9068
Full 13 or 10	32A/2ϕ	0.9927	0.9948	0.9638	0.9875	0.9840	0.9847

Effect of amplitude - A

As was shown in Section 4.3.2, the use of amplitude variance allowed for laser pulse energy optimization. This produced a very large increase in the fidelity, in many instances. When $32A/2\phi$ with n=13 was used, the fidelity for the ACNOT_1 gate rose subtly from 0.9876 ($2\text{A}/2\phi$) up to F=0.9912. In the case of the Had_2 gate with $2A/2\phi$, restricting the maximum amplitudes to A_1=0.344 and A_2=0.157 limited the fidelity from increasing (constant F=0.8817) even when the number of frequency components was increased to n=13. When either n=2 or when n=13, the same laser pulse shape, consisting of only the transition frequencies, was chosen. Giving flexibility to the amplitudes ($32A/2\phi$, n=13) of the Had_2 gate allowed the fidelity to increase to 0.9834, which is very close to the full optimization fidelity of 0.9840. For the NOT_2 gate with n=13 using $32A/2\phi$, the fidelity of the optimal laser pulse, F=0.9132, is significantly less than the full optimization of 0.9638. In this case there are energies at specific frequencies that are greater than the maximum allowed by the amplitude restriction of A_1=0.458 or A_2=0.010. Increasing the amplitude variance while using these maximum values will not improve the fidelity to that of the full optimization value.

Effect of phase - ϕ

The increase of phase, beyond ϕ=0 or π, to 32ϕ has minimal effect (increase of 1.5%) or no effect on increasing the fidelity. The necessary phase condition is that the parameter space at least consists of ϕ=0 to produce positive amplitudes and ϕ=π in order to produce negative amplitudes (see Equation 4.3). An optimization for the ACNOT_1 gate with n=13 using $2A/2\phi$ produces F=0.9876, while a choice of $2A/32\phi$ gives a minor increase to F=0.9880. The population transfers between the qubits for both cases is shown in Figure 4.5, along with the amplitude and phase sequence at ν_0= 2151cm^{-1}.

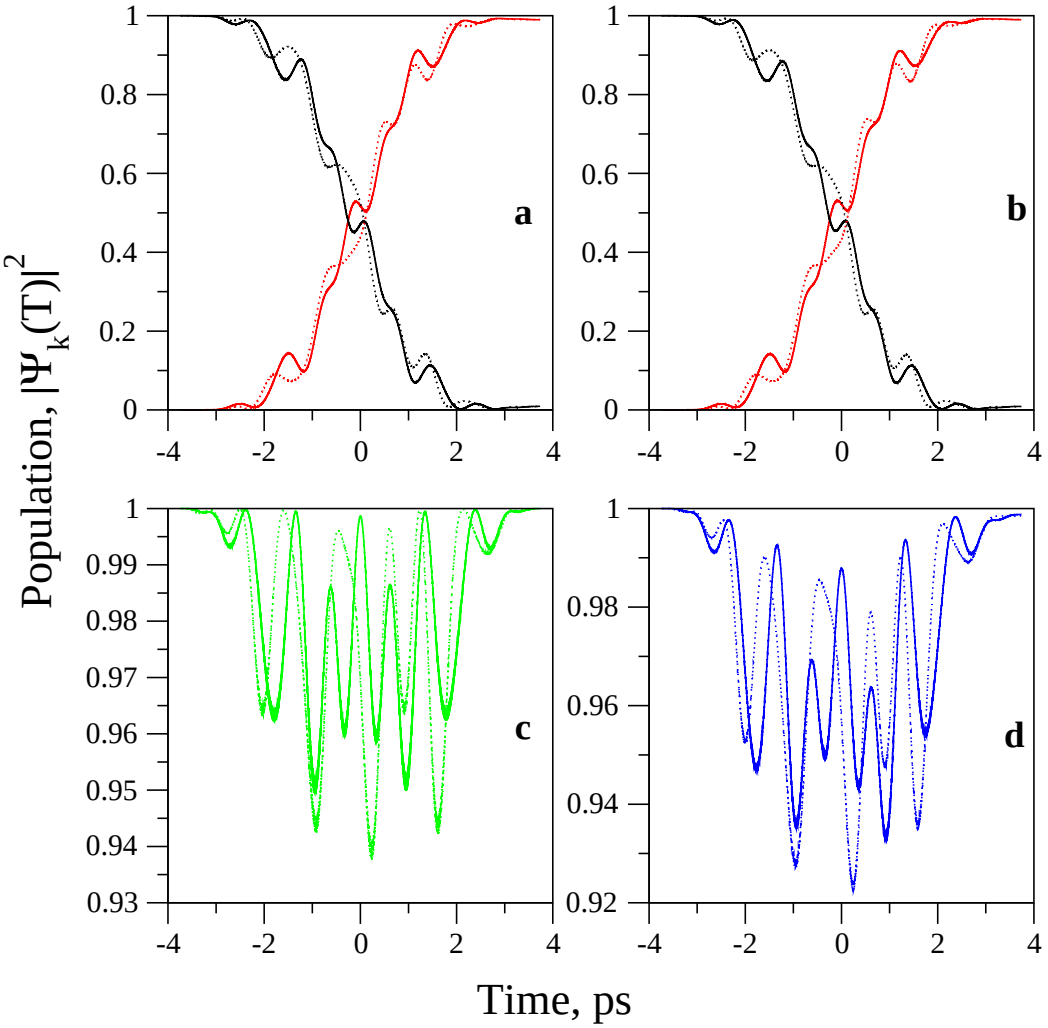

Figure 4.5: Plot of the population dynamics between qubits for the ACNOT$_1$ gate using n=13 frequency components with a total pulse energy of $30\mu J$ for $2A/2\phi$ (solid line) and for $2A/32\phi$ (dotted line). a)$|00\rangle \rightarrow |01\rangle$, b)$|01\rangle \rightarrow |00\rangle$, c)$|10\rangle \rightarrow |10\rangle$ and d)$|11\rangle \rightarrow |11\rangle$. black: $|00\rangle$, red: $|01\rangle$, green: $|10\rangle$ and blue: $|11\rangle$. The sequence of laser pulse amplitudes and phases [$A_1\phi_1$, ...,$A_{13}\phi_{13}$], with a central frequency of ν_0= 2151cm^{-1}, that produce the solid lines are [00,00,00,00,00,00,0.339 π,00,00,0.339 0, 0.339 π,0.339 π,0.339 π] and the dotted lines are [00,00,00,00,00,00,0.339 π,00,00,0.339 $\frac{1}{2}\pi$, 0.339 $\frac{19}{16}\pi$,0.339 $\frac{1}{2}\pi$,0.339 $\frac{31}{16}\pi$].

Effect of number of frequency components - n

The effect of adding additional frequency components is dependent upon the ability for the amplitude and/or phase to increase the fidelity. The addition of further frequency components beyond the transition frequency/frequencies causes a small increase in fidelity; the majority of the fidelity coming from the transition frequency/frequencies themselves. The former statement occurs for the Had_2 gate in which the fidelity has reached a maximum of 0.8817 and no further increase is accomplished by increasing the number of frequency components. The fidelity increases to 0.9834 once the amplitudes are allowed more flexibility by using $32A$ amplitude variations. The latter can be noted for the ACNOT_1 gate in which an already high fidelity (F=0.9748) when using only n=1 at the transition frequency and $2A/2\phi$, increases in fidelity only moderately when the number of frequency components is increased.

4.3.4 Qubit population dynamics

To illustrate the nature of the qubit excitations, the population dynamics for selected quantum gates are plotted. For the ACNOT_1 gate there is a comparison between the T=7.47ps single frequency using n=1 with $2A/2\phi$ optimization (F=0.9748) and to the full T=7.47ps using n=13 with $32A/2\phi$ optimization (F=0.9927). The comparison for the NOT_2 gate is between two high fidelity points for different pulse durations, namely: 44.03ps using n=1 with $2A/2\phi$ optimization (F=0.9994) and 52.84ps using n=10 with $32A/2\phi$ optimization (F=0.9123). Lastly, a comparison is made between the Had_2 gate when T=24.28ps using n=10 with $32A/2\phi$ (F=0.9834) and T=48.30ps using n=1 with $2A/2\phi$ (F=0.9742).

ACNOT_1 quantum gate

Figure 4.6 illustrates the resulting population dynamics for laser pulses optimized using T=7.47ps with the single transition frequency 2151cm^{-1} (n=1) and $2A/2\phi$ components, and also T=7.47ps at 2151cm^{-1} but with multiple

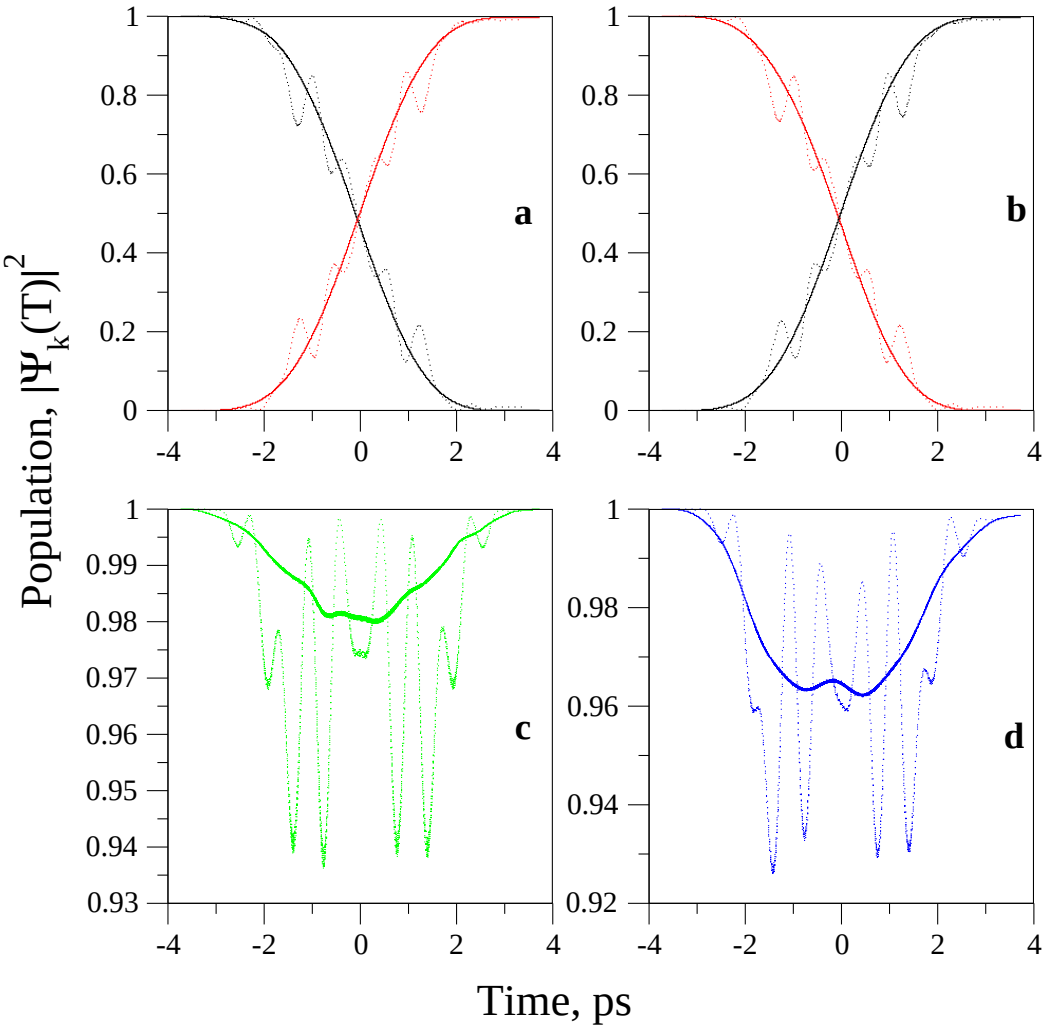

Figure 4.6: Resulting population dynamics for the four qubit transformations of the ACNOT$_1$ quantum gate of pulse duration T=7.47ps when using n=1 with $2A/2\phi$ (solid lines) and using n=13 with $32A/2\phi$ (dotted lines). a)$|00\rangle \rightarrow |01\rangle$, b)$|01\rangle \rightarrow |00\rangle$, c)$|10\rangle \rightarrow |10\rangle$ and d)$|11\rangle \rightarrow |11\rangle$. black: $|00\rangle$, red: $|01\rangle$, green: $|10\rangle$ and blue: $|11\rangle$.

frequency components (n=13) and $32A/2\phi$. In Figure 4.6a and Figure 4.6b the qubit transition $|00\rangle \leftrightarrow |01\rangle$ (black and red, respectively) is shown. For the case of n=1 (solid line) the transition seems to be a half-cycle Rabi oscillation. When an optimization is carried out for n=13 (solid line) the population dynamics seem to be a more complicated form of Rabi oscillation. For the $|10\rangle \rightarrow |10\rangle$ (Figure 4.6c) and $|11\rangle \rightarrow |11\rangle$ (Figure 4.6d) qubit transitions, requiring only a phase change to ensure global phase alignment, there is a small amount of intermediate population exchange between nearby qubits. Specifically, in both cases, a small exchange was observed for qubit $|10\rangle$ with $|11\rangle$ and $|10\rangle$, and $|11\rangle$ with $|01\rangle$ and $|10\rangle$. The majority of the fidelity for the ACNOT_1 gate under these conditions is attributed to the central frequency and optimal pulse energy. Further fidelity increases are attributed to variations in frequency components and amplitude, in order to bring the fidelity near 100%.

NOT_2 quantum gate

The population dynamics for optimized laser pulses with T=44.03ps using n=1 with $2A/2\phi$ and an optimized laser pulse with T=52.84ps using n=10 with $32A/2\phi$ are shown in Figure 4.7. Figure 4.7a and Figure 4.7b illustrate that for T=44.03 (solid line) the $|00\rangle \leftrightarrow |01\rangle$ transition proceeds through a $\frac{3}{2}$ Rabi cycle and the $|10\rangle \leftrightarrow |11\rangle$ transition through a $\frac{1}{2}$ Rabi cycle. The Rabi cycle pathways are switched when the total pulse duration is T=52.84. It is also possible to enforce the transitions to be both $\frac{1}{2}$ Rabi cycles. For T=52.84ps, n=2 and E=100 μJ, the initial maximum amplitudes were selected as: A_1=0.125 (64A, 2ϕ) and A_2=1.00 (512A, 2ϕ). The amplitude restriction is enforced on A_1 since we know from Table 4.5 the optimal value for A_2 will be low (0.010). The anticipated $\frac{1}{2}$ Rabi cycle was produced for both NOT_2 gate transitions and resulted in A_1=0.0516, A_2=0.098 and F=0.8024. A larger fidelity was found when A_1 was not restricted (F=0.8459; Table 4.5) and thus the transitions which both consist of $\frac{1}{2}$ Rabi cycles were not optimally chosen

by the GA.

Had_2 quantum gate

Lastly, the population dynamics for optimized laser pulses with T=24.28ps using n=10 with $32A/2\phi$ and T=48.30ps using n=1 with $2A/2\phi$ are shown in Figure 4.8. This figure illustrates that the T=48.30ps optimized laser pulse causes all qubit transitions to proceed through a $\frac{3}{4}$ Rabi cycle. When the laser pulse optimized is 24.28ps, the resulting optimized laser pulse produces relatively complex population dynamics, requiring many intermediate exchanges of population between qubit pairs and other rovibrational states of the Had_2 gate. This being attributed to having more frequency components (n=10).

4.4 Conclusion

A number of experimental pulse shaping parameters and their affect on the fidelities of laser pulses shaped to represent the $ACNOT_1$, NOT_2 and Had_2 quantum logic gates, were studied. Pulse shaping occurs in the frequency domain using a discretized spectrum with independent control of amplitude and phase dependent frequencies, similar to current LC-SLM setups. The parameters that were varied are (i) the frequency resolution ($d\nu$) or synonymously the pulse duration (T), (ii) the number of frequency components (n), (iii) the number of amplitude components (A_j) and (iv) the number of phase components (ϕ_j). A time domain analytic form for the discretized frequency spectrum was also formulated.

Initially, an exploration of the pulse duration was carried out for each quantum gate using laser pulses with with $2A$ and 2ϕ variation of A=0 or 1 and ϕ=0 or π. The resulting plots showed a simple relationship between the fidelity and pulse duration for the $ACNOT_1$ and NOT_2 gates. The plot obtained for the Had_2 gate showed a complex relationship. The trends observed for the $ACNOT_1$ gate fidelities at chosen pulse durations was attributed to the

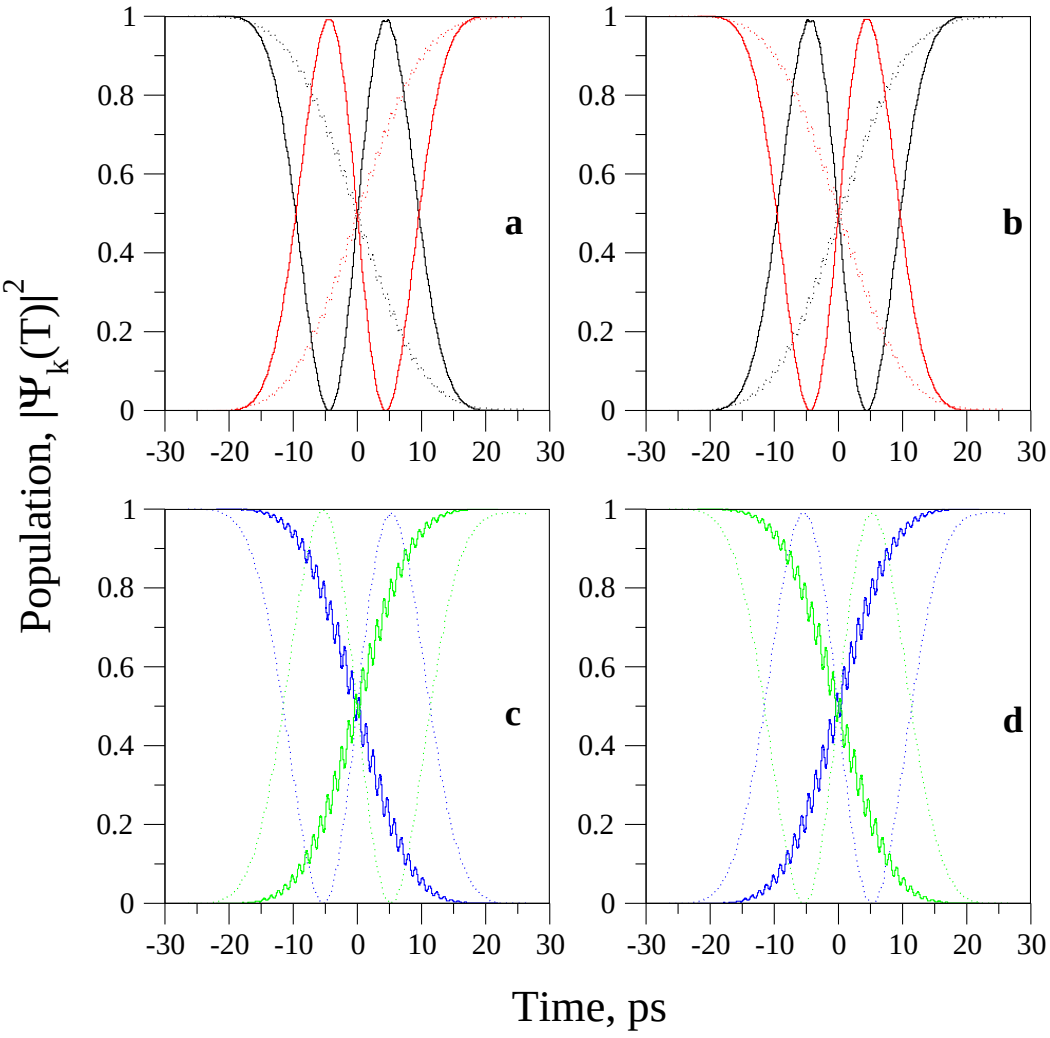

Figure 4.7: Resulting population dynamics for the four qubit transformations of the NOT_2 quantum gate when using a pulse of length T=44.03ps, n=2 and $2A/2\phi$ (solid lines), and using a pulse of length T=52.84ps, n=10 and $32A/2\phi$ (dotted lines). a)$|00\rangle \rightarrow |01\rangle$, b)$|01\rangle \rightarrow |00\rangle$, c)$|10\rangle \rightarrow |11\rangle$ and d)$|11\rangle \rightarrow |10\rangle$. black: $|00\rangle$, red: $|01\rangle$, green: $|10\rangle$ and blue: $|11\rangle$.

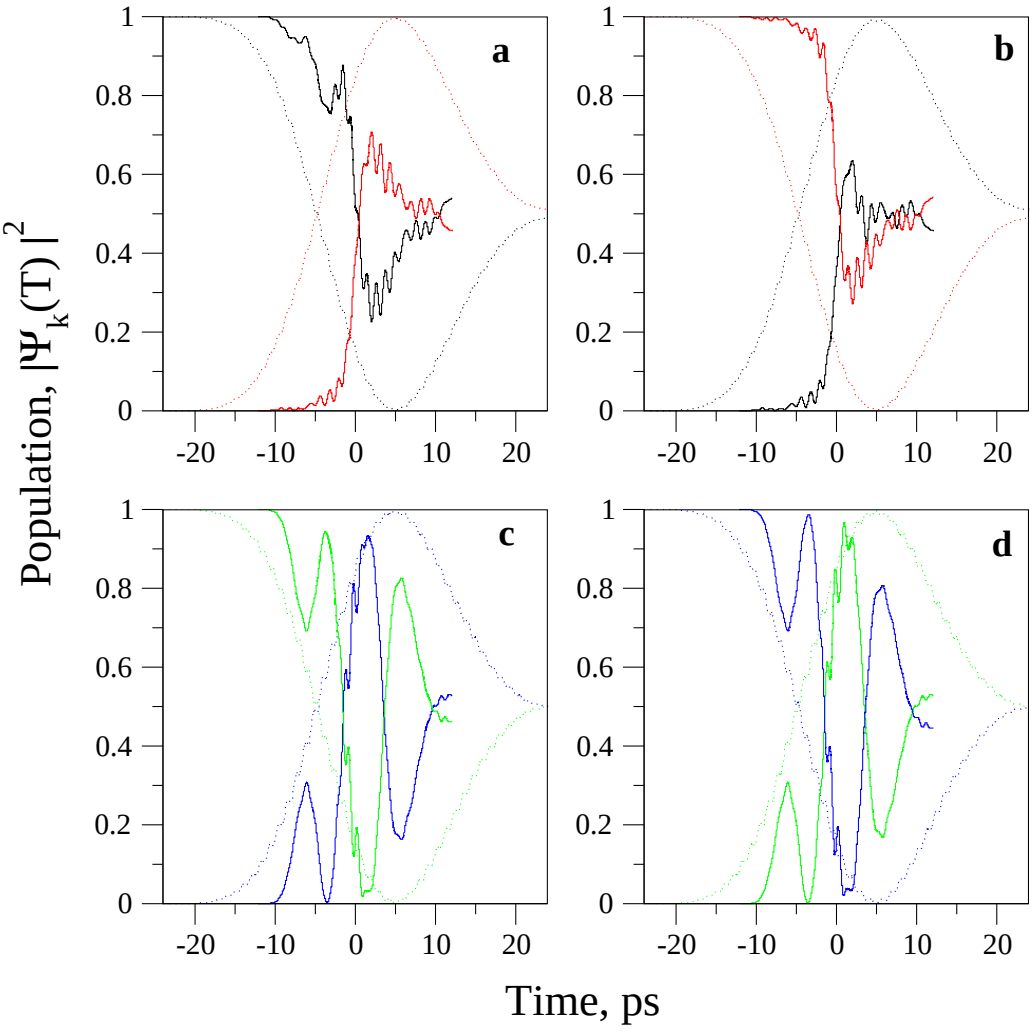

Figure 4.8: Resulting population dynamics for the four qubit transformations of the Had_2 quantum gate when using a pulse of length T=24.28ps, n=10 and $32A/2\phi$ (solid lines), and using a pulse of length T=48.30ps, n=2 and $2A/2\phi$ (dotted lines). a)$|00\rangle \leftrightarrow \frac{1}{\sqrt{2}}(|00\rangle + |01\rangle)$, b)$|01\rangle \leftrightarrow \frac{1}{\sqrt{2}}(|00\rangle - |01\rangle)$, c)$|10\rangle \leftrightarrow \frac{1}{\sqrt{2}}(|10\rangle + |11\rangle)$ and d)$|11\rangle \leftrightarrow \frac{1}{\sqrt{2}}(|10\rangle - |11\rangle)$. black: $|00\rangle$, red: $|01\rangle$, green: $|10\rangle$ and blue: $|11\rangle$.

difference in the natural evolution of the rovibrational state qubits $|10\rangle$ and $|11\rangle$.

In order to determine the optimal laser pulse energy at the qubit transition frequency/frequencies for each quantum logic gate shaped laser pulse, the amplitudes were varied by $512A$, while keeping the phase at 2ϕ (0 or π), for select values of pulse duration. The optimal amplitude chosen for each pulse duration at $30\mu J$ for the $ACNOT_1$ gate was already very near the previous choice of 1.0 for a $10\mu J$ pulse, so the fidelities did not change substantially. Two transition frequencies were required for the NOT_2 and Had_2 gates, and the resulting amplitudes were of differing magnitudes indicating that one transition requires more energy than the other. A substantial increase in the fidelity was observed in these cases since the previous optimizations used non-optimal laser pulse energies.

Lastly, we investigated the affect of increasing the number of frequency components on quantum gate fidelities. Laser pulses of one pulse duration each were shaped with 13 frequencies ($ACNOT_1$) or 10 frequencies (NOT_2 and Had_2) each with $2A/2\phi$, $32A/2\phi$ and $2A/32\phi$ amplitude and phase combinations. A *full* optimization of 13 or 10 frequencies and $32A/2\phi$ was calculated, but without optimizing the transition frequency energy and allowing the amplitudes to have more energy flexibility per frequency component. Again, amplitude variation played a major role in improving the fidelities and in some cases caused an improvement of 10%. Surprisingly, phase variation at most caused an increase of only 1.5%. The *full* optimization was very close to the results of $32A/2\phi$, except in the case of the NOT_2 gate, likely due to the necessity of large variations in energy per frequency component.

Overall, it was determined that the majority of the quantum gate fidelity resides in the transition frequency/frequencies and more so determining an optimal energy associated with them. Addition of further frequency components can cause some incremental increases in the fidelity. The variation of phase seemed to provide no significant improvement upon the fidelity. High fidelity

control of rovibrational state qubits for quantum gate operation through a shaped laser pulse also seems to be influenced by the natural evolution of the qubits.

4.5 Appendix A - Derivation of the analytic form of the laser pulse

We begin the derivation of an analytic form of the laser pulse, by starting with the simple condition of the discretized frequency domain laser pulse, $f(\nu)$, consisting of a single frequency component centered at ν_j with a resolution, $d\nu$,

$$f(\nu) = \begin{cases} \epsilon(\nu_j), & \nu_j - \frac{d\nu}{2} \leq \nu \leq \nu_j + \frac{d\nu}{2} \\ 0 & \text{otherwise} \end{cases} \tag{4.7}$$

Since there is only one frequency component, everywhere else outside of the frequency resolution is satisfied by $f(\nu)$=0. This would be the condition of Figure 4.1a if only the central frequency, ν_0, were considered. A Fourier transform of this frequency domain laser pulse $f(\nu)$, produces the resulting time domain laser pulse, $F(t)$,

$$F(t) = \int_{\nu_j - \frac{d\nu}{2}}^{\nu_j + \frac{d\nu}{2}} f(\nu) e^{i2\pi\nu t}\, d\nu. \tag{4.8}$$

Substituting in the Fourier transform, our initial case of a single frequency laser pulse, produces the following,

$$\begin{aligned} F(t) &= \epsilon(\nu_j) \int_{\nu_j - \frac{d\nu}{2}}^{\nu_j + \frac{d\nu}{2}} e^{i2\pi\nu t}\, d\nu \\ &= \epsilon(\nu_j) \left(\frac{e^{i2\pi t d\nu/2} - e^{-i2\pi t d\nu/2}}{i2\pi t} \right) e^{i2\pi\nu_j t} \\ &= \epsilon(\nu_j) \frac{\sin(\pi t d\nu)}{\pi t} e^{i2\pi\nu_j t}. \end{aligned} \tag{4.9}$$

The resulting equation can be written in terms of a sinc function,

$$F(t) = d\nu\epsilon(\nu_j)\text{sinc}(\pi t d\nu) e^{i2\pi\nu_j t}, \quad \text{sinc}(x) = \frac{\sin(x)}{x}. \tag{4.10}$$

Substituting explicitly the frequency domain laser pulse intensity, $\epsilon(\nu_j)$, used in this case, one obtains

$$\begin{aligned} F(t) &= d\nu\epsilon_0\sqrt{A_j}e^{-2\ln 2\left(\frac{\nu_j-\nu_0}{\Delta\nu}\right)^2}e^{i\phi_j}\mathrm{sinc}(\pi td\nu)e^{i2\pi\nu_j t} \\ &= d\nu\epsilon_0\sqrt{A_j}e^{-2\ln 2\left(\frac{\nu_j-\nu_0}{\Delta\nu}\right)^2}\mathrm{sinc}(\pi td\nu)e^{i(2\pi\nu_j t+\phi_j)}. \end{aligned} \tag{4.11}$$

The laser pulse is a real quantity, such that

$$\Re\left[F(t)\right] = d\nu\epsilon_0\sqrt{A_j}e^{-2\ln 2\left(\frac{\nu_j-\nu_0}{\Delta\nu}\right)^2}\mathrm{sinc}(\pi td\nu)\cos\left(2\pi\nu_j t+\phi_j\right). \tag{4.12}$$

The resulting single frequency laser pulse produced from a discretized frequency spectrum is

$$\Re\left[F(t)\right] = A'_j\mathrm{sinc}(\pi td\nu)\cos\left(2\pi\nu_j t+\phi_j\right), \quad A'_j = d\nu\epsilon_0\sqrt{A_j}e^{-2\ln 2\left(\frac{\nu_j-\nu_0}{\Delta\nu}\right)^2} \tag{4.13}$$

The above formalism for a single frequency component from a discretized spectrum, can be extended to a frequency spectrum, $\epsilon(\nu)$, of n frequency components. The Fourier transform of a discretized frequency spectrum of n frequency components is the sum of the Fourier transform at each individual discretized frequency, j. Thus the general form of the time domain laser pulse, $\epsilon(t)$, with the discretized form described by Equation 4.2 is,

$$\epsilon(t) = \mathrm{sinc}(\pi td\nu)\sum_{j=0}^{n} A'_j\cos\left(2\pi\nu_j t+\phi_j\right), \tag{4.14}$$

where,

$$A'_j = d\nu\epsilon_0\sqrt{A_j}e^{-2\ln 2\left(\frac{\nu_j-\nu_0}{\Delta\nu}\right)^2}.$$

Bibliography

[1] L. Vandersypen, M. Steffen, G. Breyta, C. Yannoni, M. Sherwood, I. Chuang, Nature **414**, 883 (2001)

[2] J. Jones, M. Mosca, J. Chem. Phys. **109**, 1648 (1998)

[3] I. Chuang, L. Vandersypen, X. Zhou, D. Leung, S. Lloyd, Nature **393**, 143 (1998)

[4] C. Sackett, D. Kielpinski, B. King, C. Langer, V. Meyer, C. Myatt, M. Rowe, Q. Turchette, W. Itano, D. Wineland, I. Monroe, Nature **404**, 256 (2000)

[5] S. Gulde, M. Riebe, G. Lancaster, C. Becher, J. Eschner, H. Haffner, F. Schmidt-Kaler, I. Chuang, R. Blatt, Nature **421**, 48 (2003)

[6] H. Nagerl, D. Leibfried, H. Rohde, G. Thalhammer, J. Eschner, F. Schmidt-Kaler, R. Blatt, Phys. Rev. A **60**, 145 (1999)

[7] D. Demille, Phys. Rev. Lett. **88**, 67901 (2002)

[8] L. Carr, D. Demille, R. Krems, J. Ye, New J. Phys. **11**, 055049 (2009)

[9] C. Tesch, R. de Vivie-Riedle, Phys. Rev. Lett. **89**, 157901 (2002)

[10] T. Baumert, T. Brixner, V. Seyfried, M. Strehle, G. Gerber, App. Phys. B **65**, 779 (1997)

[11] R. Judson, H. Rabitz, Phys. Rev. Lett. **68**, 1500 (1992)

[12] B. Amstrup, G. J. Toth, G. Szabo, H. Rabitz, A. Loerincz, J. Phys. Chem. **99**, 5206 (1995)

[13] J. Vala, Z. Amitay, B. Zhang, S. Leone, R. Kosloff, Phys. Rev. A **66**, 62316 (2002)

[14] K. Hosaka, H. Shimada, H. Chiba, H. Katsuki, Y. Teranishi, Y. Ohtsuki, K. Ohmori, Phys. Rev. Lett. **104**, 180501 (2010)

[15] K. Mishima, K. Yamashita, Chem. Phys. **367**, 63 (2010)

[16] J. L. Chen, C. M. Ling, C. C. Hwang, Y. H. Ho, J. Chem. Phys. **134**, 134103 (2011)

[17] K. Shioya, K. Mishima, K. Yamashita, Mol. Phys. **105**, 1283 (2007)

[18] M. Tsubouchi, T. Momose, Phys. Rev. A **77**, 052326 (2008)

[19] Z. Bihary, D. R. Glenn, D. A. Lidar, V. A. Apkarian, Chem. Phys. Lett. **360**, 459 (2002)

[20] Y. Ohtsuki, Chem. Phys. Lett. **404**, 126 (2005)

[21] W. Z. Cao, L. J. Tian, H. J. Jiang, C. Li, Int. J. Quant. Info. **6**, 1223 (2008)

[22] C. Menzel-Jones, M. Shapiro, Phys. Rev. A **75**, 052308 (2007)

[23] K. Mishima, , K. Tokumo, K. Yamashita, Chem. Phys. **343**, 61 (2008)

[24] K. Mishima, K. Yamashita., Chem. Phys. **361**, 106 (2009)

[25] D. Sugny, L. Bomble, T. Ribeyre, O. Dulieu, M. Desouter-Lecomte, Phys. Rev. A **80**, 042325 (2009)

[26] M. Zhao, D. Babikov, J. Chem. Phys. **125**, 024105 (2006)

[27] D. Babikov, J. Chem. Phys. **121**, 7577 (2004)

[28] E. A. Shapiro, I. Khavkine, M. Spanner, M. Y. Ivanov, Phys. Rev. A **67**, 013406 (2003)

[29] Y. Teranishi, Y. Ohtsuki, K. Hosaka, H. Chiba, H. Katsuki, K. Ohmori, J. Chem. Phys. **124**, 114110 (2006)

[30] Y. Ohtsuki, New J. Phys. **12**, 045002 (2010)

[31] R. R. Zaari, A. Brown, J. Chem. Phys. **135**, 044317 (2011)

[32] R. R. Zaari, A. Brown., J. Chem. Phys. **132**, 014307 (2010)

[33] A. P. Peirce, M. A. Dahleh, H. Rabitz, Phys. Rev. A **37**, 4950 (1988)

[34] W. Zhu, J. Botina, H. Rabitz, J. Chem. Phys. **108**, 1953 (1998)

[35] M. Schroeder, A. Brown, New J. Phys. **11**, 105031 (2009)

[36] M. Lapert, R. Tehini, G. Turinici, D. Sugny, Phys. Rev. A **79**, 063411 (2009)

[37] C. Gollub, M. Kowalewski, R. de Vivie-Riedle, Phys. Rev. Lett. **101**, 073002 (2008)

[38] A. Mantz, J. Maillard, W. Roh, K. Roa, J. Mol. Spectrosc. **57**, 155 (1975)

[39] D. Goorvitch, C. Chackerian, Astro. J. Supp. Ser. **91**, 483 (1994)

[40] D. L. Carroll, Genetic Algorithm driver **v1.7.0** (2004).

[41] C. M. Tesch, R. de Vivie-Riedle, J. Chem. Phys. **121**, 12158 (2004)

Chapter 5

Conclusions

5.1 Summary and Discussion of Results

Using shaped laser pulses to control the rovibrational state qubits of diatomic molecules for the purposes of quantum computing, though plausible, requires more insight and investigation. The molecular systems described in this thesis satisfy essential criteria as proposed by DiVincenzo and Loss, for a quantum computer candidate (see Section 1.2.7), yet minimal experimental progress has resulted. The aim of this thesis was to investigate the inherent rovibrational state structure of diatomic molecules and experimental parameters present within current pulse shaping apparatus that may determine the feasibility of these systems as quantum computing platforms. Minimal emphasis was placed on the importance of the GA parameter search space. If the parameter space contains symmetries or redundancies and is too large, then the GA has difficulty in finding an optimal solution in a reasonable number of generations. Besides the need to understand the dynamics involved, we needed to approach the problem systematically since one cannot simply select all frequency components at a maximum number of amplitude and phase variation, and be confident of the optimal solution deduced by the GA. An analytic solution for the laser pulse was also formulated (see Appendix 4.5). The consequences of amplitude and phase variation in the frequency domain, along with adjustments to the number of frequency components, can now be seen explicitly in

the time domain via the analytical expression, Equation 4.5.

The choice of which rovibrational states to utilize as qubits is important (see Chapter 2). Binary shaped laser pulses provided greater fidelities compared to a similar study on the rovibrational states of CO [1], when we chose qubits resulting in 1-photon transitions. Relatively large fidelities ($> 80\%$) were achieved using binary shaped laser pulses for the ACNOT and CNOT gates on the rovibrational states of CO. As illustrated in Fig. 2.1 there are many possible choices for sets of qubits that are comprised of rovibrational states connected by 1-photon transitions. Other choices of qubits would still have similar frequency differences between excitations since the transition types, $\Delta\nu{=}\pm1$ and $\Delta J{=}\pm1$, remain the same and thus an alternate choice of qubits would likely produce similar results.

The choice of diatomic molecule is relevant and affects the ability to shape laser pulses to perform the ACNOT_1 and NOT_2 quantum gate operations on rovibrational qubits (see Chapter 3). This was the case when restricted to a constant total laser pulse energy and frequency resolution (total pulse duration) with binary pulse shaping of 51 frequency components. The results of Chapter 4 suggest that if instead the laser pulse shaping parameters were less restrictive and further optimized then perhaps there would be no dependence on the choice of diatomic molecule. The GA results were shown to be qualitatively similar to other optimization methods such as OCT (see Chapter 3), suggesting that the pulse restrictions were not dictating the resulting fidelities and it is by deduction that the rovibrational state arrangement (i.e., choice of diatomic molecule) plays a role in producing large fidelities.

The effect of the frequency resolution, or analogously the total pulse duration, on the quantum gate fidelities was studied for shaped laser pulses of constant total energy with amplitude and phase variability of A=0 or 1 and $\phi{=}0$ or π at the qubit transition frequencies required for the quantum gate operation (see Section 4.3.1). The results showed regions of total pulse duration exhibiting both large and small fidelities. In the case of the ACNOT_1 gate

the fidelity was determined to be dependent upon the difference in the natural rovibrational state evolution between qubits $|10\rangle$ and $|11\rangle$, and the oscillatory trends were attributed to the interval at which the total pulse duration was sampled. The frequency resolution used in this case is less than the frequency required to resolve qubit excitations for CO (i.e., $d\nu < 11.4\text{cm}^{-1}$). Thus the appropriate choice of frequency resolution, or more appropriately the total pulse duration, determines largely if the free evolution of the qubits will contribute to the phase alignment and not whether the transitions are resolved. Future work could combine the study of amplitude optimization of total pulse energy (see Section 4.3.2) with variability in total pulse duration.

The effect of total laser pulse energy on quantum gate fidelities was studied for laser pulses of large but constant total energy with amplitude and phase variability $512A$ and 2ϕ (0 or π) at only the excitation frequencies (see Section 4.3.2). Results suggested a large fidelity dependence on the energy at each excitation frequency component. The dependence of energy at particular frequencies is in direct relationship to the number of optimized amplitude components (A). When the total laser pulse energy and number of amplitude components is sufficiently large, then there is enough flexibility for the optimal energy per frequency component to be chosen by the GA.

The effect of laser pulse variability in amplitude (A), phase (ϕ) and the number of frequency components (n) on quantum gate fidelities was studied (see Section 4.3.3). This was examined for laser pulses of constant total energy with amplitude and phase variability of $32A$ and 32ϕ between $0 \leq A \leq 1$ and $0 \leq \phi \leq 2\pi$ with the maximum number of frequency components of n=10 or 13. The variability in amplitude affects the energies per frequency component, as described previously, and thus is important towards obtaining large fidelities. The data suggests that increasing the number of frequency components can increase the fidelity and in some cases by at least 10%. The majority of the increase in fidelity being the result of including frequency components at and surrounding the qubit transition frequencies involved in the quantum

gate operation. Interestingly, phase variation did not appreciably affect the fidelities. Moreover, the subsequent calculations with phase variation beyond 2ϕ (i.e., more than 0 or π), posed optimization problems for the GA. Including variability in phase not only increases the parameter space the GA must search, but perhaps creates redundant noise due to the small phase dependent fluctuations in fidelity.

Overall, the primary experimental conditions, as pertaining to laser pulse shaping, that dictate whether large fidelities can be obtained are (i) the energy per frequency component and (ii) the frequency resolution (total pulse duration). Both should be used along with a sufficient number of frequency components, in order to attempt to obtain a maximum fidelity.

With respect to the fidelity function (see Eq. 1.2) used in this thesis and all other analogous GA optimizations towards quantum computation, there is an associated weight attributed to average population control and global phase alignment. This also applies to global phase alignment within OCT using an auxiliary wavefunction Ψ_5, as detailed in Section 3.2.3. The fidelity function used in the GA optimizations can be written in the form similar to Equation 4.5,

$$F = \frac{1}{4}\bar{P} + \frac{3}{4}\sum_{i\neq j}^{6} r_i r_j \cos(\Delta\Phi_{ij}), \tag{5.1}$$

where, for simplicity, the time-dependent coefficients describing final state wavefunctions are written in complex notation and are assumed to be (1,0). The number of qubit transformations is N=4, r_i describes the magnitudes of the time-dependent coefficients corresponding to wavefunctions Ψ_i at the end of the laser pulse interaction, $\Delta\Phi_{ij}$ is the difference between qubit phases, Φ_i and Φ_j, at the end of the laser pulse duration and $\bar{P}$ is the average population. Using the current fidelity function assigns a weight for the average population of 25% and subsequently the weight associated with global phase alignment is 75%. Within OCT, the addition of an extra wavefunction Ψ_5 in order to incorporate global phase alignment within the objective function, means that

average population has a weight of 80% and global phase alignment is only 20%. What effect the weightings have on optimization, specifically for laser pulse shaping, has yet to be determined. Further investigations on the effect of these weights may suggest limitations of the current fidelity function or insight into a more appropriate one.

5.2 Current Direction

In the present study only four rovibrational state qubits were selected to perform 2-qubit operations. A quantum simulator could outperform classical simulations with only 150 qubits.[2] A *universal* quantum computer as studied in this thesis, in order to perform a practical algorithm in comparison to what can be accomplished on a classical computer, would need thousands or even millions of qubits.[3, 4] Thus scalability, or increasing the number of qubits, for the universal diatomic quantum computer system studied in this thesis would pose a large challenge. In our case the number of qubits (n) or rovibrational states of a diatomic molecules scales by a factor of 2^n. This rapidly increasing number of rovibrational states compels a change of thought in the implementation posed in the study, where scalability is an issue. Instead of using the entire diatomic rovibrational structure as the qubits, it was suggested by Demille [5] that only two rotational states of a chain of coupled polar diatomic molecules trapped in an optical lattice be used. Specifically, the two lowest energy rotational states (J=0 and J=1) of each polar diatomic would be used as each qubit and thus scalability is accomplished by increasing the number of trapped diatomic molecules. The diatomic molecules can interact with each other due to electric dipole-dipole coupling and thus 2-qubit operations can be carried out between qubits. An electric field gradient is applied across the length of the diatomic molecular chain, creating specific differences between rotational state energies of each diatomic molecule and thus allowing for independent control of each molecule. Also, an excitation between rotational

states J=0 and J=1 creates a change of sign in the net electric dipole moment and thus a change in orientation of the polar diatomic molecule along the chain. Soon thereafter, an experiment by Sage et al. [6] demonstrated the preparation of RbCs in its lowest energy vibrational state (ν=0) with a narrow distribution of rotational states. Then further still, Ni et al. [7] were able to completely cool ^{40}K^{87}Rb molecules into the rovibrational ground state (ν=0, J=0). Recently, Chotia et al. [8] demonstrated not only the cooling of ^{40}K^{87}Rb molecules into their rovibrational ground state, but also the placement of these diatomic molecules within a 3-D optical lattice with lifetimes of up to 25 s.

The system of polar diatomic molecules trapped in an optical lattice as a quantum computer candidate is also of theoretical interest. The theoretical work specific to this field includes modelling the system with 1 or 2 polar diatomic molecules using optimized laser pulses to represent quantum logic gates, determining the applicability of some chosen polar diatomic molecules as practical species for the current setup and examining factors or conditions relating to the qubits and dipole-dipole coupling [9–19]. Mishima and Yamashita [9] investigated the use of the two lowest energy rovibrational states of dipole-dipole coupled NaCl-NaCl, NaBr-NaBr and NaCl-NaBr as qubits, without a static electric field and using OCT to optimize laser pulses relevant to the Deutsch-Jozsa algorithm. Pellegrini et al. [10] recently investigated the use of the two lowest energy rovibrational states of ^{41}K^{85}Rb to map 8 qubits when in the presence of a magnetic field using OCT to optimize laser pulses relevant to two quantum algorithms (0 and 1 adder, and Grover's algorithm). They also applied their theoretical setup to the two lowest energy rovibrational states of each ^{41}K^{87}Rb dipole-dipole coupled molecules (four qubits total) in the presence of a magnetic and electric field to shape laser pulse using OCT for the Grover's algorithm. Another analogous study was carried out by Bomble et al. [11] using two dipole-dipole coupled NaCs diatomic molecules in a static electric field to investigate the Deutsch-Jozsa algorithm (2 qubits) and 0 and 1 adder (8 qubits). Due to the relatively large electric and magnetic dipole

moments of polar diatomic CrRb, Pavlović et al. [12] suggested it as a relevant molecule for optical lattice/quantum computing studies. Alternatively, there have also been studies investigating the formation of LiH [13], LiCs [14, 15] and also a general photoassociative procedure for preparing diatomic molecules into their lowest rovibrational state [16]. A method for switching "on/off" the dipole moment was introduced by Yelin et al. [17], allowing for high coupling between qubit being operated on. The technique was applied to diatomic species CO and NF in which a 2-qubit phase gate was applied to two dipole-dipole coupled molecules [18]. Entanglement of qubits is a necessary requirement of quantum computation and its magnitude at specific distances and configurations between electric dipole moments was studied.[19]

Our aim at investigating the application of diatomic control using shaped laser pulses towards quantum computing was successful. We highlighted several laser pulse shaping factors for increasing the effectiveness of resulting quantum logic gates, as well as alluding to issues concerning the use of diatomic rovibrational states as qubits. The work presented in this thesis may be relevant to the aforementioned application of polar diatomic molecules trapped in an optical lattice, but the implementation of a quantum computer is far from complete. The potential advantages of a quantum computer proves to provide constant motivation, yet many of the criteria listed by DiVincenzo and Loss [3] which are essential for the implementation of a quantum computer have yet to be fully realized. Even though a future era of general purpose quantum computing is far off, the journey will provide added benefits such as greater experience at controlling complex quantum phenomena, and the development of new materials and sensors [20].

Bibliography

[1] M. Tsubouchi, T. Momose, Phys. Rev. A **77**, 052326 (2008)

[2] A. Aspuru-Guzik, P. Walther, Nat. Phys. **8**, 285 (2012)

[3] D. P. DiVincenzo, D. Loss, Superlattices Microstruct. **23**, 419 (1998)

[4] D. Kielpinski, C. Monroe, D. J. Wineland, Nature **417**, 709 (2002)

[5] D. Demille, Phys. Rev. Lett. **88**, 067901 (2002)

[6] J. M. Sage, S. Sainis, T. Bergeman, D. DeMille, Phys. Rev. Lett. **94**, 203001 (2005)

[7] K. -K. Ni, S. Ospelkaus, M. H. G. de Miranda, A. Pe'er, B. Neyenhuis, J. J. Zirbel, S. Kotochigova, P. S. Julienne, D. S. Jin, J. Ye, Science **322**, 231 (2008)

[8] A. Chotia, B. Neyenhuis, S. Moses, B. Yan, J. Covey, M. Foss-Feig, A. Rey, D. Jin, J. Ye, Phys. Rev. Lett. **108**, 080405 (2012)

[9] K. Mishima, K. Yamashita., Chem. Phys. **361**, 106 (2009)

[10] P. Pellegrini, S. Vranckx, M. Desouter-Lecomte, Phys. Chem. Chem. Phys. **13**, 18864 (2011)

[11] L. Bomble, P. Pellegrini, P. Ghesquière, M. Desouter-Lecomte, Phys. Rev. A **82**, 062323 (2010)

[12] Z. Pavlović, H. R. Sadeghpour, R. Côté, B. O. Roos, Phys. Rev. A **81**, 052706 (2010)

[13] R. Côté, E. Juarros, K. Kirby, Phys. Rev. A **81**, 060704 (2010)

[14] J. Deiglmayr, P. Pellegrini, A. Grochola, M. Repp, R. Côté, O. Dulieu, R. Wester, M. Weidemüller, New J. Phys. **11**, 055034 (2009)

[15] J. Deiglmayr, P. Pellegrini, A. Grochola, M. Repp, R. Côté, O. Dulieu, R. Wester, M. Weidemüller, New J. Phys. **12**, 079802 (2010)

[16] E. Kuznetsova, M. Gacesa, P. Pellegrini, S. F. Yelin, R. Côté, New J. Phys. **11**, 055028 (2009)

[17] S. F. Yelin, K. Kirby, R. Côté, Phys. Rev. A **74**, 050301 (2006)

[18] E. Kuznetsova, R. Côté, K. Kirby, S. F. Yelin, Phys. Rev. A **78**, 012313 (2008)

[19] Q. Wei, S. Kais, Y.P. Chen, J. Chem. Phys. **132**, 121104 (2010)

[20] T. D. Ladd, F. Jelezko, R. Laflamme, Y. Nakamura, C. Monroe, J. L. O'Brien, Nature **464**, 45 (2010)